Approximate analytical coefficient of restitution formulation for single bead impact with external load, using nonlinear visco-elastic models

Abhishek Chatterjee, Guillaume James, Bernard Brogliato

▶ **To cite this version:**

Abhishek Chatterjee, Guillaume James, Bernard Brogliato. Approximate analytical coefficient of restitution formulation for single bead impact with external load, using nonlinear visco-elastic models. [Research Report] INRIA Grenoble - Rhone-Alpes. 2021, pp.1-50. hal-03462750

HAL Id: hal-03462750
https://inria.hal.science/hal-03462750v1

Submitted on 2 Dec 2021

HAL is a multi-disciplinary open access archive for the deposit and dissemination of scientific research documents, whether they are published or not. The documents may come from teaching and research institutions in France or abroad, or from public or private research centers.

L'archive ouverte pluridisciplinaire **HAL**, est destinée au dépôt et à la diffusion de documents scientifiques de niveau recherche, publiés ou non, émanant des établissements d'enseignement et de recherche français ou étrangers, des laboratoires publics ou privés.

Approximate analytical coefficient of restitution formulation for single bead impact with external load, using nonlinear visco-elastic models

Abhishek Chatterjee[†]
abhishek.chatterjee@inria.fr

Guillaume James[†]
guillaume.james@inria.fr

Bernard Brogliato[†]
bernard.brogliato@inria.fr

[†] Univ. Grenoble Alpes, INRIA, CNRS Grenoble INP, LJK, Grenoble, 38000, France

December 2, 2021

Abstract

This work is largely concerned with the calculation of an approximate coefficient of restitution (CoR) associated with nonlinear spring/dashpot models, when a constant external load acts upon the colliding body. Some of the main applications concern well known visco-elastic models such as *Kuwabara-Kono*, *Simon-Hunt-Crosseley*, *Tsuji-Tanaka-Ishida*, etc, however the proposed approach to a very wide class of nonlinear visco-elastic contact models. It is shown that suitable expansions allow to derive a computable expression which provides accurate predictions in a valuable range of external loads and viscosity coefficients.

1 Introduction

Impacts in multibody systems are highly nonlinear phenomena whose modelling has attracted numerous researchers since a long time [1, 2, 3, 4], see the preface in [5] for a short historical summary. There are several ways to classify impact models within gross classes, as:

1. Single impacts, *i.e.*, a single collision occurs without any overlap with foregoing or next collisions.
2. Multiple impacts, *i.e.*, several collisions occur simultaneously in the system.

or as [6]:

1. Algebraic (zero-order) models which assume instantaneous collisions between perfectly rigid bodies, and relate post- and pre-impact velocities through a so-called restitution rule.
2. First-order dynamics following the Routh and the Darboux-Keller approaches, where the normal contact force impulse is used as a new time-scale.
3. Second-order dynamics which rely on compliant models of lumped flexibilities and dampings (linear or nonlinear spring-dashpot rheological models), through assemblies of various basic components: elastic, visco-elastic, frictional, fractional elastic, visco-plastic, *etc.*

In a Lagrangian framework, simultaneity of collisions means that the boundary of the admissible domain in the configuration space, is attained at a co-dimension ≥ 2 submanifold [5, Definition 6.1]. When contact compliance is taken into account, a multiple impact occurs each time several collisions overlap. In this work only single impacts are studied. Each of the above gross classes for single impacts can be refined into subclasses. One major issue is the modelling of kinetic energy dissipation. Tangential dissipation is usually modelled using extensions of set-valued Coulomb's friction. As far as normal effects are concerned, several approaches have been proposed so far to take dissipation into account (here we restrict ourselves to single impacts):

1. linear viscosity (damping),
2. nonlinear damping as in the well-known Simon-Hunt-Crossley, Kuwabara-Kono, Tsuji-Tanaka-Ishida models or the Lankarani-Nikravesh approach [7, 8][5, section 2.2.2] [9],
3. phenomenological parameters like coefficients of restitution (CoR) for the zero and first-order dynamics models, the most popular ones being kinematic (Newton), kinetic (Poisson) and energetic CoRs.
4. varying stiffnesses in compression and expansion phases (the bistiffness Crook's approach [10] [5, section 4.2.1.2]) [11],
5. plasticity effects (à la Johnson [12, 13, 14] [5, section 4.2.1.1]), Masin, Persoz and viscoelasto-plastic assemblies with set-valued frictional elements [15, 16, 17],
6. adhesive effects with Dugdale or Lennard-Jones potentials [18] [5, section 4.2.2], body bulk vibrations (see [1, Chapter III] [13, Chapter 11] [5, section 4.2.4] for references) *etc.*

In addition, it should be remarked that these models and parameters, are not independent, nor used independently one from each other. For instance it is known that parameters like CoRs in algebraic restitution rules are related [5, section 4.3.3.1], and this is also the case for first-order Darboux-Keller impact dynamics [19, 20, 21, 22] [5, sections 4.3.5.3 and 4.3.6]. Also CoR may be used in rheological models to tune the dissipation parameters as in the Lankarani-Nikravesh approach and its many extensions and variants, see [7, 8] [5, Chapter 2]. Another research direction, consists of determining the equivalent CoR to compliant rheological models: the obtained CoR can be used in algebraic models, hence introducing useful informations in the CoR (dependence on pre-impact velocity, on bodies' masses, contact equivalent stiffness, contact equivalent viscous friction, plasticity parameters, contact area, *etc*), while keeping an overall rigid-body instantaneous collisions framework. This is usually not a straighforward task, and it has been the object of many investigations for all types of models, linear spring/dashpots, nonlinear Hertz-plastic piecewise-smooth models [12] [5, section 4.2.1.1] [13], and for nonlinear spring-dashpot Simon-Hunt-Crossley and Kuwabara-Kono models. A common feature of (almost) all the models and analyses in the literature, is that it is assumed, as a fundamental basic assumption, that all the forces which are applied on the colliding bodies at the impact time, are negligible compared to the impact forces. Then exact or approximate expressions for the CoR can been derived. This is the case in particular for the Simon-Hunt-Crossley (SHC) [23, 24] and the Kuwabara-Kono (KK) [25] models, which are widely used in applications. Very few studies have analysed the same problem, taking into account the effect of an external load on the impacting bodies (*i.e.*, calling into question the fundamental assumption). Among these we may cite [26, 27, 28], which all conclude about the importance of considering external loads in certain circumstances. One of the main goals in this work is to study the effect of gravity or constant external force on the computed values of CoR, for the Kuwabara-Kono model, hereby extending the fundamental results in [29, 30, 31]. The Kuwabara-Kono model stems from continuum mechanics [32, 33, 34] and therefore occupies a particular place in the class of rheological compliant spring-dashpot models. The provided theory applies, however, to different viscous nonlinearities than SHC and KK. Approximate expressions for the CoR are given, and are shown through extensive numerical calculations to fit very well with the exact numerical solution, for large range of external loads.

The report is organised as follows: the basic model is introduced in section 2. The algorithm for the exact computation of the CoR through the integration of the dynamics is presented in section 3. Section 4 is devoted to the calculation of approximate expressions for the CoR: Section 4.1 deals with the case of small equivalent external load, section 4.2 deals with large external loads (and impacts with sticking), the accuracy of the approximation is improved in section 4.3 by taking into account high-order terms in the expansions, finally section 4.4 presents the case of any external loads (small or large). A recapitulatory section 5 summarizes the main steps which are needed to calculate the CoR approximations. Conclusions are in section 6, and useful developments and calculations can be found in Appendices A, B, C, and D.

2 Nonlinear Visco-Elastic Impact Model

Consider a system consisting of a single bead impacting the ground, as shown in Fig. 1. The mass of the bead is m and the stiffness constant is k. The external load induced on the bead is given by the parameter

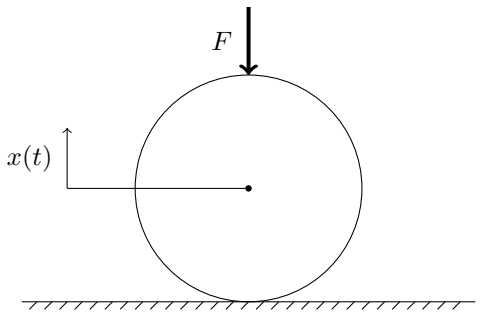

Figure 1: Single bead impacting ground, with external load

F, such that $F > 0$ produces a compressive (downward) force on the bead according to Fig. 1. The external load F is considered to be constant, which is a realistic assumption given that impact duration is typically very small. The displacement of the center of the bead in reference to the undeformed position is denoted by $x(t)$, such that the bead is in contact when $x(t) \leq 0$ and free when $x(t) > 0$. Then, based on a general visco-elastic model, the equation of motion of the bead is given by

$$m\ddot{x} = k\left[(-x)_+^{\alpha} + \gamma_0 \frac{d}{dt}(-x)_+^{\beta}\right] - mg - F \tag{1}$$

where $x_+ = \max(x, 0)$. The initial conditions for (1) are $x(0) = 0$ and $\frac{dx}{dt}(0) = -v_0$ with $v_0 > 0$. The parameters, $\alpha \geq 0$, $\beta \geq 0$ and $\gamma_0 \geq 0$ characterize the contact force behaviour: α is associated with the stiffness, whereas β and γ_0 control the dissipation during the impact. Nevertheless, for $\alpha < 1$ or $\beta < 1$, the uniqueness of the solution to the initial value problem associated with (1) is not established [35]. Hence, we make the following assumption in this study,

Assumption 1. *$\alpha \geq 1$ and $\beta \geq 1$*

If the parameters values are chosen to be $\alpha = \beta = \frac{3}{2}$, the visco-elastic model in (1) is known as the Kuwabara-Kono model [25], similarly if $\alpha = 3/2$ and $\beta = 5/2$, the Simon-Hunt-Crossley model [23, 24] is obtained. In this work we will pay particular attention to these cases. The dynamics of (1) can be re-scaled with respect to the time and length scales:

$$T = \left(\tfrac{m}{k}\right)^{\frac{1}{\alpha+1}} v_0^{\frac{1-\alpha}{\alpha+1}} \qquad \text{and} \quad \delta = v_0 T$$

by setting $x(t) = -\delta u(\tau)$ with $\tau = \frac{t}{T}$. Then the scaled dynamics is given by,

$$\frac{d^2u}{d\tau^2} + \gamma \frac{d}{d\tau}\left(u_+^{\beta}\right) + u_+^{\alpha} = \tilde{g} \tag{2}$$

where,

$$\gamma = \gamma_0 v_0^{\frac{2\beta}{\alpha+1}-1}\left(\tfrac{k}{m}\right)^{1-\frac{\beta}{\alpha+1}} \qquad \text{and} \quad \tilde{g} = \left(g + \tfrac{F}{m}\right)\tfrac{T^2}{\delta} = \left(\tfrac{m}{k}\right)^{\frac{1}{\alpha+1}} v_0^{\frac{-2\alpha}{\alpha+1}}\left(g + \tfrac{F}{m}\right)$$

The initial conditions for the scaled equations of motion in (2) are $u(0) = 0$ and $\frac{du}{d\tau}(0) = 1$. As we can see, the new scaling parameters γ and $\tilde{g}$ depend on v_0 and F. The dependence of these new scaling parameters to the actual physical quantities are demonstrated in Fig. 2, with an example of an impact under gravity and no external force exerted on the system ($g = 9.8$ m/s^2 and $F = 0$ N). Figure 2(a) shows the relationship between γ and v_0, where we can see that the value of γ increases for higher values of initial velocity, v_0. Similarly, Fig. 2(b) plots the $\tilde{g}$ with respect to the constant external force, F, for different values of v_0. Here we see that the external force F balances the gravitational constant $g = 9.8$ m/s^2 at a specific value, $F = -1.5092$ N, for all initial velocities v_0. The values for mass, $m = 1.54 \times 10^{-1}$ kg and the stiffness constant, $k = 3.6138 \times 10^{10}$ N/m$^{3/2}$ are based on the experimental result of the steel ball impact properties reported in [25], given $\alpha = \beta = 3/2$. The value of $\gamma_0 = 1.5237 \times 10^{-6}$ is is related to the CoR value for steel ball, $e = 0.893$ reported in [25], and is calculated according to an approximation

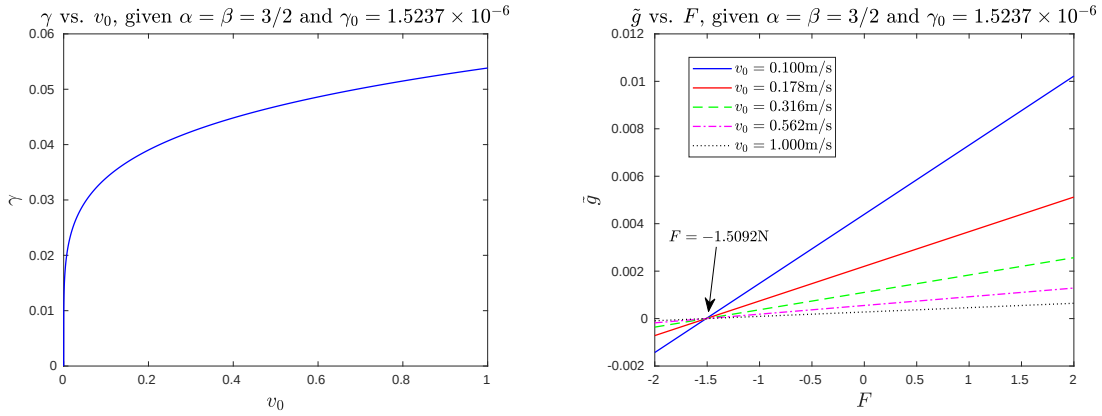

Figure 2: Values of the dimensionless scaling parameters, γ and $\tilde{g}$ with respect to changes in (a) initial velocity, v_0 and (b) external force F. The gravitational constant is $g = 9.8\text{m/s}^2$. Values for mass, $m = 1.54 \times 10^{-1}\text{kg}$ and spring constant, $k = 3.6138 \times 10^{10}\text{N/m}^{3/2}$, are based on the experimental result on steel balls in [25]. $\alpha = \beta = 3/2$ and the value of $\gamma_0 = 1.5237 \times 10^{-6}$ is calculated using the CoR, $e = 0.893$ reported in [25], according to the method mentioned in [36].

mentioned in [36]. The parameter values explain the value $F = -1.5092$ N at $\tilde{g} = 0$ intercept in Fig. 2(b), since $F = -mg = -1.54 \times 10^{-1}$ kg $\times$ 9.8 m/s^2 $= -1.5092$ N. Also we observe,that an increase in the value of the initial velocity, v_0 diminishes the effects of external load, i.e., $g + F/m$, on $\tilde{g}$.

Let us assume that the impact terminates at $\tau = T_f$ with $T_f > 0$. The impact takes place for $\tau \in (0, T_f)$, so the scaled displacement $u(\tau)$ is positive while $\tau \in (0, T_f)$ and $u(T_f) = 0$ at impact termination. The CoR for the impact can be expressed in terms of the scaled velocities as,

$$e = -\frac{\frac{du}{d\tau}(T_f)}{\frac{du}{d\tau}(0)} = -\frac{du}{d\tau}(T_f) \tag{3}$$

Thus, the CoR for a given impact can be numerically evaluated by integrating the ordinary differential equation for the scaled dynamics given in (2) until $\tau = T_f$. The ultimate goal of this work is to obtain an analytical approximation for the CoR, for arbitrary parameter values (α,β,γ, and $\tilde{g}$). Nevertheless, in order to study the validity of analytical approximate CoR, we would always need to establish a reference on the "true" values of CoR. In this study, the values of CoR obtained through numerical integration of (2) are considered the "true" CoR values, and are treated as a reference to study the validity of the approximations later. The next section discusses the method used for numerically integrating (2) in this study.

3 Calculation of the CoR by Numerical Integration

The term $\frac{d}{d\tau}\left(u_+^\beta\right) = \beta u_+^{\beta-1}\frac{du}{d\tau}$ in (2) is not Lipschitz continuous, and therefore can lead to difficulty with the numerical integration. As discussed in [35, 36], these numerical issues can be circumvented with an appropriate choice of the dynamical variable. Hence, here we will consider the same change of variable, and rewrite (2) in terms of a new *generalized velocity* parameter w:

$$\begin{aligned} \frac{du}{d\tau} &= w - \gamma u_+^\beta \\ \frac{dw}{d\tau} &= -u_+^\alpha + \tilde{g} \end{aligned} \tag{4}$$

The state variables in (4) are $\mathbf{Y} = \begin{bmatrix} u & w \end{bmatrix}^T$, such that the system in (4) can be concisely expressed as : $\dot{\mathbf{Y}} = \mathbf{F}(\mathbf{Y})$ with the initial conditions $\mathbf{Y}(0) = \begin{bmatrix} 0 & 1 \end{bmatrix}^T$, which has to be numerically integrated till $\tau = T_f$

to obtain the CoR as $e = -\frac{du}{d\tau}(T_f)$. However, since the value of T_f is not a priori known, one would need to continue the numerical integration until the impact termination conditions are met. The impact termination can take place when the bead detaches at some T_f, such that $u(T_f) = 0$ and $\frac{du}{d\tau}(T_f) < 0$. Alternatively, the bead may converge to the equilibrium point without detachment, i.e., the bead doesn't rebound and sticks to the ground. The parameters values (α, β, γ and $\tilde{g}$) dictate whether the bead will detach or not, for a given impact.

The equilibrium point of (2), by setting $\left(\frac{d^2u}{d\tau^2} = \frac{du}{d\tau} = 0\right)$, is at $\bar{u} = \tilde{g}^{\frac{1}{\alpha}}$. We can determine the characteristics of the convergence towards equilibrium by linearizing (2) about the equilibrium point. If we consider the value of $u > 0$ in the neighbourhood of $\bar{u}$, as $u = \bar{u} + v$ for a small $v \to 0$, the dynamical equations linearized around $v = 0$ read

$$\frac{d^2v}{d\tau^2} + \underbrace{\gamma\beta\tilde{g}^{\frac{\beta-1}{\alpha}}}_{2\xi\omega_n}\frac{dv}{d\tau} + \underbrace{\alpha\tilde{g}^{\frac{\alpha-1}{\alpha}}}_{\omega_n^2}v = 0.$$

The damping ratio ξ, and the natural frequency ω_n, for the linearized second-oder dynamics around the equilibrium point are expressed as,

$$\xi = \frac{\gamma\beta}{2\sqrt{\alpha}}\tilde{g}^{\frac{2\beta-\alpha-1}{2\alpha}} \quad \text{and} \quad \omega_n = \sqrt{\alpha}\,\tilde{g}^{\frac{\alpha-1}{2\alpha}}.$$

We know that the condition for an underdamped response is $0 < \xi < 1$, which leads to the equivalent inequality,

$$\gamma < \frac{2\sqrt{\alpha}}{\beta}\tilde{g}^{\frac{\alpha+1-2\beta}{2\alpha}}.$$

Thus, for any given value-pair of (α, β), there exists a constraint on the values of γ and $\tilde{g}$ that must be satisfied for an underdamped response. As an example, if we consider the Kuwabara-Kono model ($\alpha = \beta = 3/2$), the constraint on the parameter γ and $\tilde{g}$ is given by,

$$\gamma < 2\sqrt{\tfrac{2}{3}}\tilde{g}^{-\frac{1}{6}} \quad \text{or} \quad \tilde{g} < \tfrac{512}{27\gamma^6}.$$

In this work, the numerical simulations will be mainly performed in the underdamped regime. If the bead does not rebound, the velocity $\frac{du}{d\tau}$ will converge to zero with oscillations, while $u(\tau)$ will always remain positive. Hence, time-integration will stop when $u(T_f) \leq \bar{u}$ and $\frac{du}{d\tau}(T_f) = 0$, where $\bar{u} = \tilde{g}^{\frac{1}{\alpha}}$ is the equilibrium point. On the other hand, the bead will rebound if $u(T_f) = 0$ and $\frac{du}{d\tau}(T_f) < 0$ for some $T_f > 0$. Consequently, in the underdamped regime, time integration will stop at $t = T_f > 0$ where $u(T_f)u'(T_f) = 0$ and $u(T_f) \leq \tilde{g}^{\frac{1}{\alpha}}$.

The numerical integration is performed in three separate intervals (a pseudo-code for this numerical scheme is presented in Algorithm 1.):

1 Starting from initial conditions, the system of equations (4) is integrated until τ_0, such that $u'(\tau_0) = 0$. *This stops the integration at maximum compression, which guarantees that system enters the restitution phase, before the final termination.*

2 Next starting with the system states at τ_0, the system of equations (4) is numerically integrated until τ_1, such that $u(\tau_1) - \tilde{g}^{\frac{1}{\alpha}} = 0$. *After starting from the maximal compression, stopping the integration at τ_1, such that $u(\tau_1) = \tilde{g}^{\frac{1}{\alpha}}$ and $u'(\tau_1) \leq 0$, guarantees that $u(T_f) \leq \tilde{g}^{\frac{1}{\alpha}}$ and $u'(T_f) \leq 0$.*

3 Lastly, starting with the system states at τ_1, the system of equations (4) is integrated until a final time τ_2, such that $u(\tau_2)u'(\tau_2) = 0$. *This condition finally stops the integration to yield $u(T_f) = u(\tau_2) \leq \tilde{g}^{\frac{1}{\alpha}}$ and $u'(T_f) = u'(\tau_2) \leq 0$.*

In addition, time integration is stopped if $\|(u - \bar{u}, u')\|_\infty < \varepsilon$, for some small threshold ε (we fix $\varepsilon = 10^{-8}$), leading to $e = 0$.

Figure 3 shows an example of the evolution of u and $\frac{du}{d\tau}$, corresponding to the parameter values: $\alpha = 3/2$, $\beta = 3/2$, $\gamma = 0.006$ and $\tilde{g} = 0.1$, as obtained by numerically integrating (4). As one may notice from Fig. 3, in this example the bead detaches at the end of an impact, since the scaled displacement $u(\tau)$ becomes zero at the end of the impact. Fig. 4 shows the evolution of $u(\tau)$ and $\frac{du}{d\tau}$, for the parameters: $\alpha = 3/2$, $\beta = 3/2$, $\gamma = 0.06$ and $\tilde{g} = 4$. In this case, the time-integration terminates when $\frac{du}{d\tau} = 0$ and $0 < u(\tau) < \tilde{g}^{\frac{1}{\alpha}}$. Note that the CoR value shown in Fig. 4(a) is $e = 0$.

Algorithm 1 Numerical Integration Scheme

Set: $\mathbf{Y}_0 \leftarrow \mathbf{Y}(0)$, where $\mathbf{Y}(0) = \begin{bmatrix} u(0) & w(0) \end{bmatrix}^T$
while $u'(\tau) = w(\tau) - \gamma u_+^{\beta}(\tau) > 0$ **do**
  Integrate: $\dot{\mathbf{Y}}(\tau) = \mathbf{F}(\mathbf{Y}(\tau))$, with initial condition $\mathbf{Y}_0$
  Update: τ, $\mathbf{Y}(\tau)$
end while
Set: $\mathbf{Y}_0 \leftarrow \mathbf{Y}(\tau)$
while $u - \tilde{g}^{\frac{1}{\alpha}} > 0$ **do**
  Integrate: $\dot{\mathbf{Y}}(\tau) = \mathbf{F}(\mathbf{Y}(\tau))$, with initial condition $\mathbf{Y}_0$
  Update: τ, $\mathbf{Y}(\tau)$
end while
Set: $\mathbf{Y}_0 \leftarrow \mathbf{Y}(\tau)$
while $u(\tau)u'(\tau) = u(\tau)\left[w(\tau) - \gamma u_+^{\beta}(\tau)\right] < 0$ **do**
  Integrate: $\dot{\mathbf{Y}}(\tau) = \mathbf{F}(\mathbf{Y}(\tau))$, with initial condition $\mathbf{Y}_0$
  Update: τ, $\mathbf{Y}(\tau)$
end while

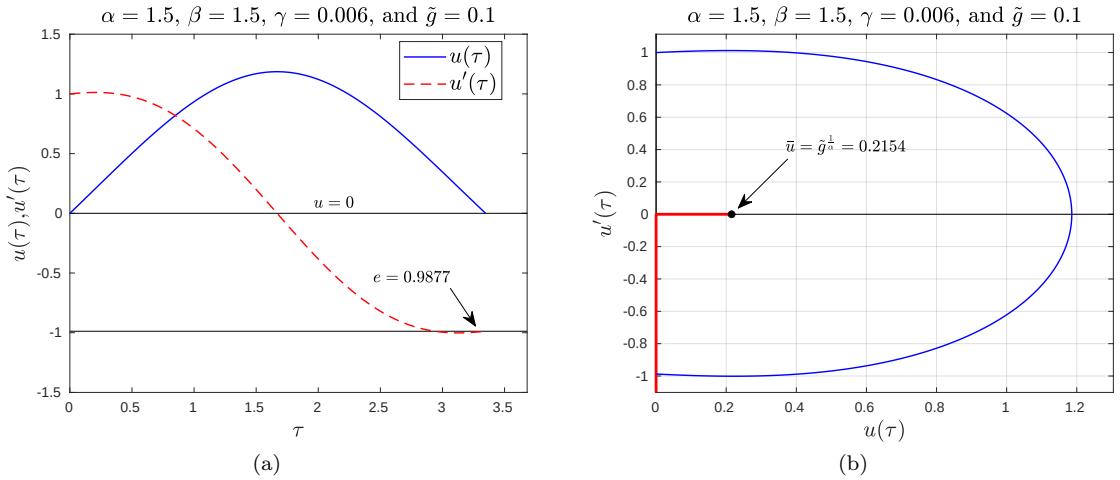

Figure 3: Numerical integration of scaled dynamics for the parameters $\alpha = \beta = \frac{3}{2}$, $\gamma = 0.006$ and $\tilde{g} = 0.1$: (a) Responses of $u(\tau)$ and $u'(\tau)$, and (b) Phase-space plot of $(u(\tau), u'(\tau))$ (the stopping condition is shown in red)

4 Analytical CoR Approximated Expression

The numerical integration scheme for CoR computation, discussed in the previous section, is mainly presented for the purpose of establishing a reference for the analytical CoR approximations that will be presented in this section. In order to obtain an analytical CoR approximation, let us begin by transforming the scaled equations of motion (2), in terms of e.

Firstly, multiplying equation (2) by $\frac{du}{d\tau}$ gives,

$$\frac{d}{d\tau}\left[\frac{1}{2}\left(\frac{du}{d\tau}\right)^2\right] + \gamma\beta\left(\frac{du}{d\tau}\right)^2 (u)^{\beta-1} + \frac{d}{d\tau}\left(\frac{u^{\alpha+1}}{\alpha+1}\right) = \tilde{g}\frac{du}{d\tau} \tag{5}$$

which if integrated from $\tau = 0$ to $\tau = T_f$, yields.

$$e^2 = 1 - 2\gamma\beta\int_0^{T_f}\left(\frac{du}{d\tau}\right)^2 u^{\beta-1} d\tau \tag{6}$$

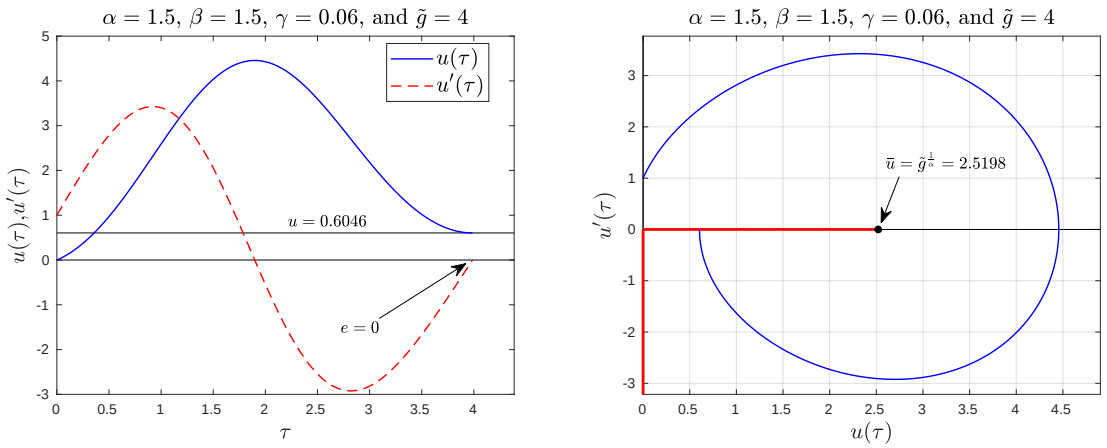

Figure 4: Numerical integration of scaled dynamics for the parameters $\alpha = \beta = \frac{3}{2}$, $\gamma = 0.06$ and $\tilde{g} = 4$: (a) Responses of $u(\tau)$ and $u'(\tau)$, and (c) Phase-space plot of $(u(\tau), u'(\tau))$ (the stopping condition in shown in red)

Let us now consider that the scaled displacement and time of detachment corresponding to the non-dissipative case ($\gamma = 0$) are $u_0(\tau)$ and T_0, respectively. Therefore, the scaled displacement and time of detachment corresponding to the dissipative case, with very small γ values ($0 \leq \gamma \ll 1$) can be expanded as : $u(\tau) = u_0(\tau) + \mathcal{O}(\gamma)$ and $T_f = T_0 + \mathcal{O}(\gamma)$. Therefore, using equation (2) we get,

$$\frac{d^2u_0}{d\tau^2} + u_0^{\alpha} = \tilde{g} \quad \text{where,} \quad u_0(0) = 0, \quad \frac{du_0}{d\tau}(0) = 1, \quad u_0(T_0) = 0 \quad \text{and,} \quad \frac{du_0}{d\tau}(T_0) = -1 \tag{7}$$

Similarly, (6) can be rewritten in terms of u_0 and rearranged as,

$$e^2 = 1 - 2\gamma\beta \int_0^{T_0} \left(\frac{du_0}{d\tau}\right)^2 {u_0}^{\beta-1} d\tau + \text{H.O.T.} \tag{8}$$

Also, noting that for small γ the value of e is close to one, which implies that the value of the second term, ϵ in equation (8) of the form: $e^2 = 1 - \epsilon$, should be close to zero. Therefore, using the expansion $(1-\epsilon)^{\frac{1}{2}} = 1 - \frac{\epsilon}{2} + \mathcal{O}(\epsilon^2)$, an expression for e can be obtained as,

$$e = 1 - \gamma\beta \int_0^{T_0} \left(\frac{du_0}{d\tau}\right)^2 {u_0}^{\beta-1} d\tau + \text{H.O.T.} \tag{9}$$

In the non-dissipative case, using the symmetry of the force time-history over the impact duration, one finds that $\tau = \frac{T_0}{2}$ corresponds to the time of maximal compression and $u_0\left(\frac{T_0}{2} + \tau\right) = u_0\left(\frac{T_0}{2} - \tau\right)$, which allows for (9) to be rewritten as,

$$e = 1 - 2\gamma\beta \int_0^{\frac{T_0}{2}} \left(\frac{du_0}{d\tau}\right)^2 {u_0}^{\beta-1} d\tau + \text{H.O.T.} \tag{10}$$

Also, multiplying (7) by $\frac{du_0}{d\tau}$ and integrating from $\tau = 0$ yields,

$$\frac{1}{2}\left[\left(\frac{du_0}{d\tau}(\tau)\right)^2 - 1\right] + \frac{u_0(\tau)^{\alpha+1}}{\alpha+1} = \tilde{g}u_0(\tau)$$

which can be used to solve for $\frac{du_0}{d\tau}$,

$$\frac{du_0}{d\tau} = \left[1 + 2\left(\tilde{g}u_0(\tau) - \frac{u_0(\tau)^{\alpha+1}}{\alpha+1}\right)\right]^{\frac{1}{2}} \tag{11}$$

Thus we can express $d\tau$ in terms of du_0,

$$d\tau = \left[1 + 2\left(\tilde{g}u_0 - \frac{{u_0}^{\alpha+1}}{\alpha+1}\right)\right]^{-\frac{1}{2}} du_0 \tag{12}$$

At the maximum compression, $\frac{du_0}{d\tau} = 0$ and therefore, the displacement given by $u_M = u_0\left(\frac{T_0}{2}\right)$ can be obtained using (11),

$$\left[1 + 2\left(\tilde{g}u_M - \frac{u_M^{\alpha+1}}{\alpha+1}\right)\right]^{\frac{1}{2}} = 0 \qquad \Rightarrow \quad \frac{1}{\alpha+1}{u_M}^{\alpha+1} - \tilde{g}u_M = \frac{1}{2} \tag{13}$$

Based on (13), we can observe that the solution of the displacement at the maximum compression, u_M depends on $\tilde{g}$. Thus, in the development that follows, we will treat u_M, as a function of $\tilde{g}$, $u_M = u_M(\tilde{g})$.

Hence, substituting (11) in (10) and then performing a change of the integration variable ($\tau \to u_0$), using the expression of $d\tau$ in (12), as well as setting $u_0(\frac{T_0}{2}) = u_M(\tilde{g})$ for the upper-bound, we can rewrite the expression for e as,

$$e = 1 - 2\,\gamma\,\beta\,\mathcal{I}(\tilde{g}) + \text{H.O.T.} \tag{14}$$

with

$$\mathcal{I}(\tilde{g}) = \int_0^{u_M(\tilde{g})} \left[1 + 2\left(\tilde{g}u_0 - \frac{{u_0}^{\alpha+1}}{\alpha+1}\right)\right]^{\frac{1}{2}} {u_0}^{\beta-1} du_0. \tag{15}$$

The exact closed-form solution cannot be obtained for the integral, however in the following sections we will consider a number of approximations that would ultimately yield an analytical solution for the CoR.

4.1 Approximation for small $\tilde{g}$

We begin by considering approximations of e, for small $\tilde{g}$ ($\tilde{g} \approx 0$). In order to do this, we will perform a first-order Taylor expansion of (14) about $\tilde{g} = 0$,

$$e = 1 - 2\gamma\beta\mathcal{I}(0) - 2\gamma\beta\tilde{g}\frac{d\mathcal{I}}{d\tilde{g}}(0) + \text{H.O.T.} \tag{16}$$

Therefore, now we need to obtain expressions for $\mathcal{I}(0)$ and $\frac{d\mathcal{I}}{d\tilde{g}}(0)$. In order to do this, let us first consider the derivative of $\mathcal{I}(\tilde{g})$,

$$\frac{d\mathcal{I}}{d\tilde{g}}(\tilde{g}) = \frac{d}{d\tilde{g}}\int_0^{u_M(\tilde{g})} h(\tilde{g}, u_0) du_0 \tag{17}$$

where,

$$h(\tilde{g}, u_0) = \left[1 + 2\left(\tilde{g}u_0 - \frac{{u_0}^{\alpha+1}}{\alpha+1}\right)\right]^{\frac{1}{2}} {u_0}^{\beta-1}$$

Using Leibniz integral rule, we may rewrite (17) as,

$$\frac{d\mathcal{I}}{d\tilde{g}}(\tilde{g}) = h\left(\tilde{g}, u_M(\tilde{g})\right) \cdot \frac{du_M}{d\tilde{g}}(\tilde{g}) + \int_0^{u_M(\tilde{g})} \frac{\partial h}{\partial \tilde{g}}(\tilde{g}, u_0) du_0$$

The term $h\left(\tilde{g}, u_M(\tilde{g})\right)$ can be evaluated using (13) to be,

$$h\left(\tilde{g}, u_M(\tilde{g})\right) = \left[1 + 2\left(\tilde{g}u_M - \frac{{u_M}^{\alpha+1}}{\alpha+1}\right)\right]^{\frac{1}{2}} {u_M}^{\beta-1} = [0]^{\frac{1}{2}} {u_M}^{\beta-1} = 0 \tag{18}$$

Hence (4.1) is given by,

$$\frac{d\mathcal{I}}{d\tilde{g}}(\tilde{g}) = \int_0^{u_M(\tilde{g})} \frac{\partial h}{\partial \tilde{g}}\left(\tilde{g}, u_0\right) du_0 = \int_0^{u_M(\tilde{g})} \left[1 + 2\left(\tilde{g}u_0 - \frac{u_0^{\alpha+1}}{\alpha+1}\right)\right]^{-\frac{1}{2}} u_0^{\beta} du_0 \tag{19}$$

We note from (19), that the coefficient of $\frac{du_M}{d\tilde{g}}$ in (4.1), given by $h\left(\tilde{g}, u_M(\tilde{g})\right)$ vanishes. Therefore, we can conclude that a zeroth-order approximation of $u_M(0)$ would be sufficient to evaluate the values of $\mathcal{I}(0)$ and $\frac{d\mathcal{I}}{d\tilde{g}}(0)$ in (16). Using (13) the zeroth-order approximation of $u_M(0)$ is given by

$$u_M(0) = u_M^* = \left(\frac{\alpha+1}{2}\right)^{\frac{1}{\alpha+1}} \tag{20}$$

Thus, evaluating the expressions for $\mathcal{I}(0)$ and $\frac{d\mathcal{I}}{d\tilde{g}}(0)$ using (20) and substituting them into (16), we obtain,

$$e = 1 - 2\gamma\beta \int_0^{u_M^*} \left[1 - 2\frac{{u_0}^{\alpha+1}}{\alpha+1}\right]^{\frac{1}{2}} {u_0}^{\beta-1} du_0 - 2\gamma\beta \int_0^{u_M^*} \left[1 - 2\frac{{u_0}^{\alpha+1}}{\alpha+1}\right]^{-\frac{1}{2}} {u_0}^{\beta} du_0 + \text{H.O.T.} \tag{21}$$

which may be rewritten as,

$$e = 1 - \gamma C_0 - \gamma\, \tilde{g} C_1 + \text{H.O.T.} \tag{22}$$

where,

$$C_0 = 2\beta \int_0^{u_M^*} \left[1 - 2\frac{{u_0}^{\alpha+1}}{\alpha+1}\right]^{\frac{1}{2}} {u_0}^{\beta-1} du_0 \quad \text{and} \quad C_1 = 2\beta \int_0^{u_M^*} \left[1 - 2\frac{{u_0}^{\alpha+1}}{\alpha+1}\right]^{-\frac{1}{2}} {u_0}^{\beta} du_0$$

We can notice that the definite integrals C_0 and C_1 can be rewritten in the form of *Euler's Beta Function* $\mathrm{B}(z,w) = \int_0^1 t^{z-1}(1-t)^{w-1} dt$, with $w, z > 0$. In this work, the Euler's Beta function would be used several times to approximate integrals, therefore here we will define a more general expression for the Beta function that can be readily used to approximate integrals,

Definition 1. *If the scalars $x, y, \rho, \lambda \in \mathbb{R}$, with $\rho, \lambda > 0$ and $x, y > -1$, then the following relationship holds,*

$$\int_0^{(1/\rho)^{1/\lambda}} t^x \left(1 - \rho t^\lambda\right)^y dt = \frac{1}{\lambda \rho^{(x+1)/\lambda}} \mathrm{B}\left(\frac{x+1}{\lambda}, y+1\right)$$

where B *is Euler's Beta function.*

The upper-bounds of the integrals C_0 and C_1 in (22) is u_M^*. According to (20) the maximum compression u_M^* is given by $u_M^* = \left(\frac{\alpha+1}{2}\right)^{\frac{1}{\alpha+1}}$. Therefore, Def. 1 can be used to express C_0 and C_1 in terms if Euler's Beta function,

$$C_0 = \beta\left(\frac{\alpha+1}{2}\right)^{\frac{\beta-\alpha-1}{\alpha+1}} \mathrm{B}\left(\frac{\beta}{\alpha+1}, \frac{3}{2}\right) \quad \text{and} \quad C_1 = \beta\left(\frac{\alpha+1}{2}\right)^{\frac{\beta-\alpha}{\alpha+1}} \mathrm{B}\left(\frac{\beta+1}{\alpha+1}, \frac{1}{2}\right)$$

Thus, having obtained the first-order analytical approximation of e in (22) for small $\tilde{g}$ values, we will now study the validity of this approximation against numerically integrated results of e. Figures 5, 6, and 7 compares the CoR values computed using the approximation in (22) and the values obtained through numerical integration of (4). In these figures the numerically integrated values of CoR are labelled as *Num. Integ.*, and the values obtained using the approximation in (22) is labeled *Small $\tilde{g}$ Approx.*. Figure 5 shows the result corresponding to the parameter values $\alpha = \beta = 3/2$, and $\gamma = 0.0001$, with $\tilde{g}$ varying in the range $[0, 10]$ in Fig. 5(a) and in the range $[0, 1]$ in Fig. 5(b). Fig. 5(b) also includes a zoomed-in plot near the value $\tilde{g} = \tilde{g}_0$. $\tilde{g}_0$ is the value of $\tilde{g}$ computed using some physical parameters from the study [37], to show the realistic range of the value of $\tilde{g}$. The value of $\tilde{g}_0 = 5.1224 \times 10^4$ is computed using the parameters:$m = 2.05 \times 10^{-3}$kg, $k = 9.858 \times 10^9 \mathrm{N/m}^{\frac{3}{2}}$, $\alpha = \beta = 3/2$, $g = 9.8$ m/s^2, and $F = 0$ N. These parameters represent the value of $\tilde{g}$, when a steel bead of 8mm diameter impacts under gravity. We note that the error between the numerically integrated value of CoR and the approximation using (22) is very small, i.e. 8.6615×10^{-8}. Therefore, we can conclude that the approximation (22) can perform well for $\gamma = 0.0001$, when the net external forces is in the same order of magnitude as the force due to gravitational acceleration. Results for other values of γ, namely $\gamma = 0.001$ and $\gamma = 0.01$, are also evaluated in Fig. 6 and Fig. 7. Figures 6(a) and 6(b) compares the CoR values within the ranges $\tilde{g} \in [0, 10]$ and $\tilde{g} \in [0, 1]$, respectively with $\gamma = 0.001$, and similarly

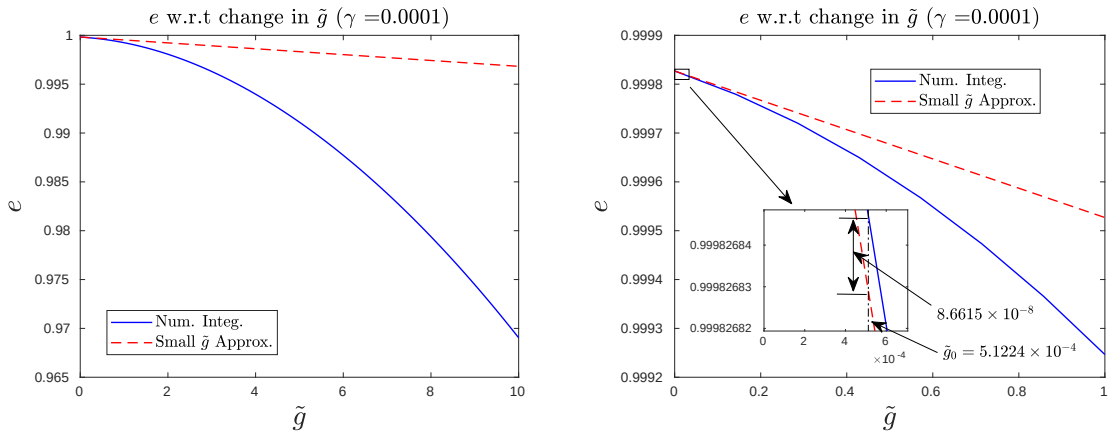

(a) (b)

Figure 5: Change in CoR with respect to (a) $\tilde{g} \in [0, 10]$ and (b) $\tilde{g} \in [0, 1]$, and also contains a zoomed-in plot that shows the value of $\tilde{g}_0$ (which is the value of $\tilde{g}$ calculated using the parameters in [37], for $g = 9.8$ m/s^2 and $F = 0$ N), with $\alpha = \frac{3}{2}$, $\beta = \frac{3}{2}$, and $\gamma = 0.0001$. The numerically integrated values of CoR are labeled as *Num. Integ.* and the values obtained using the approximation (22) are labeled *Small $\tilde{g}$ Approx.*

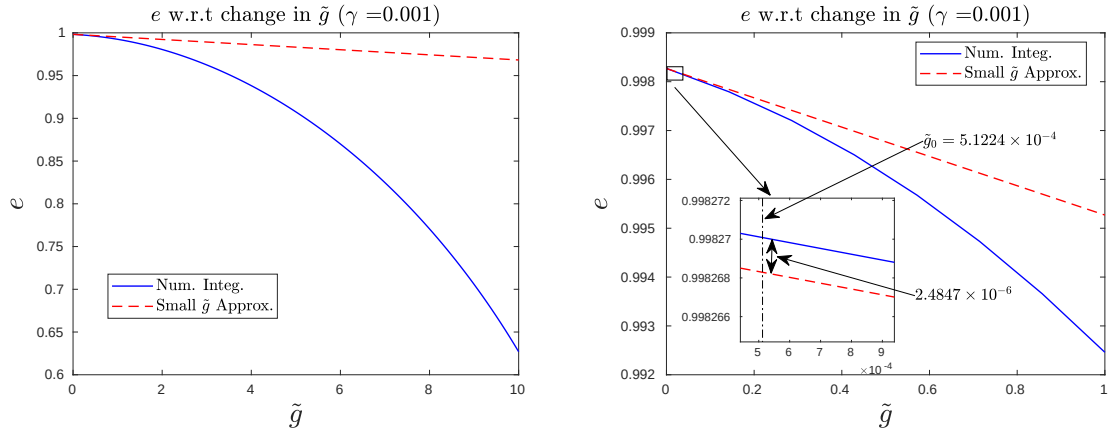

(a) (b)

Figure 6: Change in CoR with respect to (a) $\tilde{g} \in [0, 10]$, (b) $\tilde{g} \in [0, 1]$, and also contains a a zoomed-in plot that shows the value of $\tilde{g}_0$ (which is the value of $\tilde{g}$ calculated using the parameters in [37], for $g = 9.8$ m/s^2 and $F = 0$ N), with $\alpha = \frac{3}{2}$, $\beta = \frac{3}{2}$, and $\gamma = 0.001$. The numerically integrated values of CoR are labeled as *Num. Integ.* and the values obtained using the approximation (22) are labeled *Small $\tilde{g}$ Approx.*

Fig. 7(a) and Fig. 7(b) compares the CoR values in the ranges of $\tilde{g} \in [0, 10]$ and $\tilde{g} \in [0, 1]$, with $\gamma = 0.01$. Fig. 6(b) and Fig. 7(b) also includes zoomed-in plots to show the errors in CoR near the value of $\tilde{g}_0$, which is independent to γ. Again we note that the approximate CoR using (22) works well for small enough value of $\tilde{g}$. Although, it appears that the approximation (22) works well when the $\tilde{g}$ value is in the same order of magnitude as the value of $\tilde{g}_0$, one needs a better approximation for larger values of $\tilde{g}$. Also in Fig. 5, Fig. 6, and Fig. 7, the numerically calculated CoR becomes zero for high $\tilde{g}$, corresponding to the bead impacting with no detachment. The linear approximation (22) is unable to represent this no-detachment case. Additionally, we observe that the $\tilde{g}$ value beyond which the the impacting bead doesn't detach decreases as γ increases. Therefore, in order to further understand the connection between the value of γ and the value of $\tilde{g}$ beyond which the bead doesn't detach, next we will consider the problem of approximating CoR for large $\tilde{g}$. Appendix A derives a CoR approximation corresponding to large $\tilde{g}$, and also establishes an

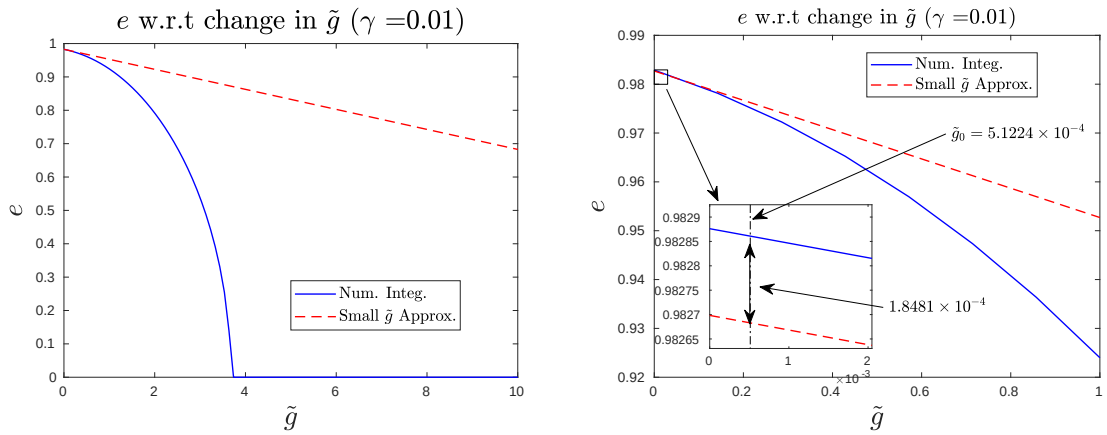

Figure 7: Change in CoR with respect to (a) $\tilde{g} \in [0, 10]$, (b) $\tilde{g} \in [0, 1]$, and also contains a zoomed-plot that shows the value of $\tilde{g}_0$ (which is the value of $\tilde{g}$ calculated using the parameters in [37], for $g = 9.8$ m/s^2 and $F = 0$ N), with $\alpha = \frac{3}{2}$, $\beta = \frac{3}{2}$, and $\gamma = 0.01$. The numerically integrated values of CoR are labeled as *Num. Integ.* and the values obtained using the approximation (22) are labeled *Small $\tilde{g}$ Approx.*

approximate relationship between the value of γ and the smallest value of $\tilde{g}$, beyond which the bead doesn't detach following the impact. The following section summarizes the main results of this approximation.

4.2 Approximation for large $\tilde{g}$ and no-rebound condition

As seen in the previous section, it is relatively straightforward to derive an analytical approximation of CoR for small values of $\tilde{g}$. The results shown in Fig. 5, Fig. 6, and Fig. 7 show that these approximations work well when the value of $\tilde{g}$ is small, but are highly inaccurate as $\tilde{g}$ becomes large. Therefore a different of CoR approximation for large $\tilde{g}$ is needed. This section presents the main results related to large $\tilde{g}$ approximation of CoR; the complete derivation of the results in this section is presented in Appendix A.

Considering a large $\tilde{g}$, the squared CoR expansion in (6), can be approximated as (See Appendix A),

$$e^2 = 1 - 2\gamma C \tilde{g}^{\left(\frac{\beta}{\alpha}+\frac{1}{2\alpha}+\frac{1}{2}\right)} \quad \text{with} \quad C = 2\sqrt{2}\frac{\beta}{\alpha}(\alpha+1)^{\left(\frac{\beta}{\alpha}+\frac{1}{2\alpha}\right)}\mathrm{B}\left(\frac{\beta+1/2}{\alpha}, \frac{3}{2}\right) \tag{23}$$

Hence, using (23), the CoR corresponding to large values of $\tilde{g}$ can be approximated as $e = \sqrt{e_+^2}$, where $e_+^2 = \max(e^2, 0)$. The value of $\tilde{g}$ is considered large if $\tilde{g} \approx \frac{{u_M}^\alpha}{\alpha+1}$, which follows from the derivation in Appendix A. It is evident from (23), that the CoR e decreases as $\tilde{g}$ increases. We know that when $\tilde{g}$ becomes very large the bead does not detach after impact. The smallest value of $\tilde{g}$, after which the bead doesn't detach, can be determined by solving for $e = 0$, using (23), as described in the proposition below.

Proposition 1. *For $\alpha, \beta \geq 1$ and small $\gamma > 0$, there exists $\tilde{g}_c \gg 1$ satisfying*

$$\tilde{g}_c^{\left(\frac{\beta}{\alpha}+\frac{1}{2\alpha}+\frac{1}{2}\right)} \approx \frac{1}{2\gamma C} \quad \text{where,} \quad C = 2\sqrt{2}\frac{\beta}{\alpha}(\alpha+1)^{\left(\frac{\beta}{\alpha}+\frac{1}{2\alpha}\right)}\mathrm{B}\left(\frac{\beta+\frac{1}{2}}{\alpha}, \frac{3}{2}\right) \tag{24}$$

such that $e = 0$ for $\tilde{g} = \tilde{g}_c$ and $e > 0$ when $1 \ll \tilde{g} < \tilde{g}_c$.

Proof. See Appendix A □

Using (24), one can determine the smallest value of $\tilde{g}$, i.e. $\tilde{g}_c \equiv \tilde{g}$, beyond which the CoR will remain zero. Alternatively, for a given value of $\tilde{g}$, (24) can also be used to determine the smallest value of γ, i.e. γ_c, such that $e = 0$ for all $\gamma > \gamma_c$. In case of Kuwabara-Kono model ($\alpha = \beta = 3/2$), $\tilde{g}_c$ can be determined by first calculating $C = 5\sqrt{2}\frac{5}{2}^{1/3}\mathrm{B}\,(4/3, 3/2) = 4.403986$ which yields the expression $\tilde{g}_c = \frac{0.30522}{\gamma^{6/11}}$.

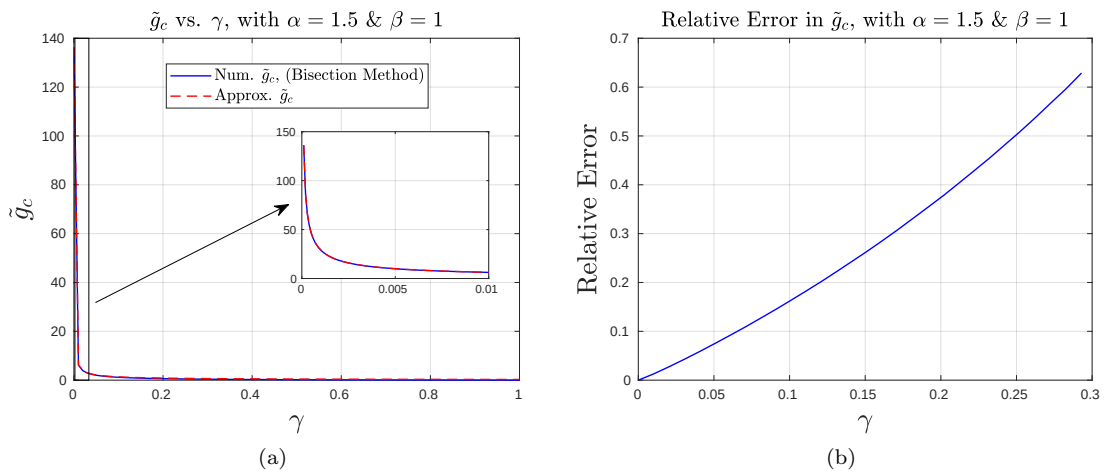

Figure 8: Plots comparing the $\tilde{g}_c$ approximation with numerically computed $\tilde{g}_c$ value using the Bisection Method, given $\alpha = 3/2$ & $\beta = 1$ (*Hertz stiffness & linear damping*). (a) $\tilde{g}_c$ vs. γ, where the plot labeled *Num. $\tilde{g}_c$ (Bisection Method)* refer to the numerical values and the plot labeled *Approx. $\tilde{g}_c$* refer to the approximate analytical value obtained using (24), (b) Relative error of the $\tilde{g}_c$ between the analytical approximations and the numerically computed values, over the range of $\gamma \in [0, 0.3]$.

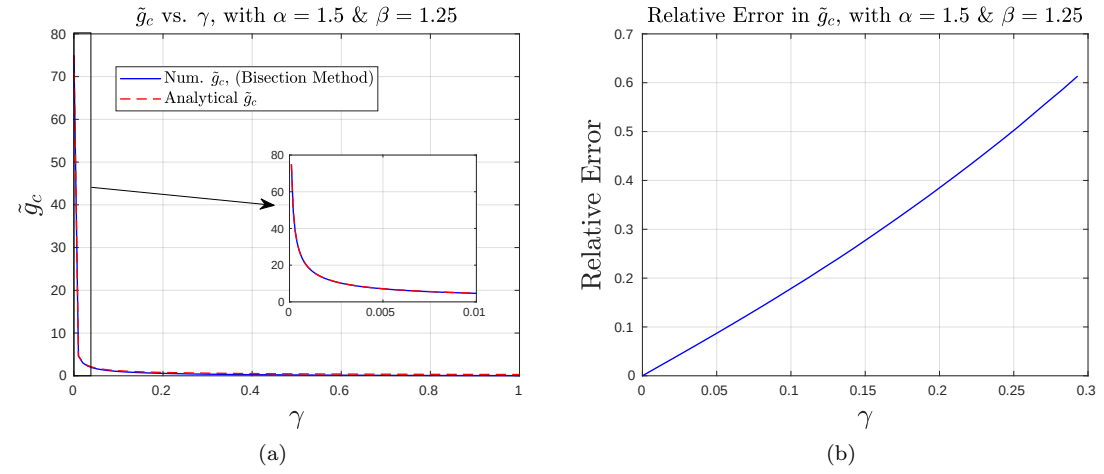

Figure 9: Plots comparing the $\tilde{g}_c$ approximation with numerically computed $\tilde{g}_c$ value using the Bisection Method, given $\alpha = 3/2$ & $\beta = 5/4$ (*Tsuji-Tanaka-Ishida model*). (a) $\tilde{g}_c$ vs. γ, where the plot labeled *Num. $\tilde{g}_c$ (Bisection Method)* refer to the numerical values and the plot labeled *Approx. $\tilde{g}_c$* refer to the approximate analytical value obtained using (24), (b) Relative error of the $\tilde{g}_c$ between the analytical approximations and the numerically computed values, over the range of $\gamma \in [0, 0.3]$.

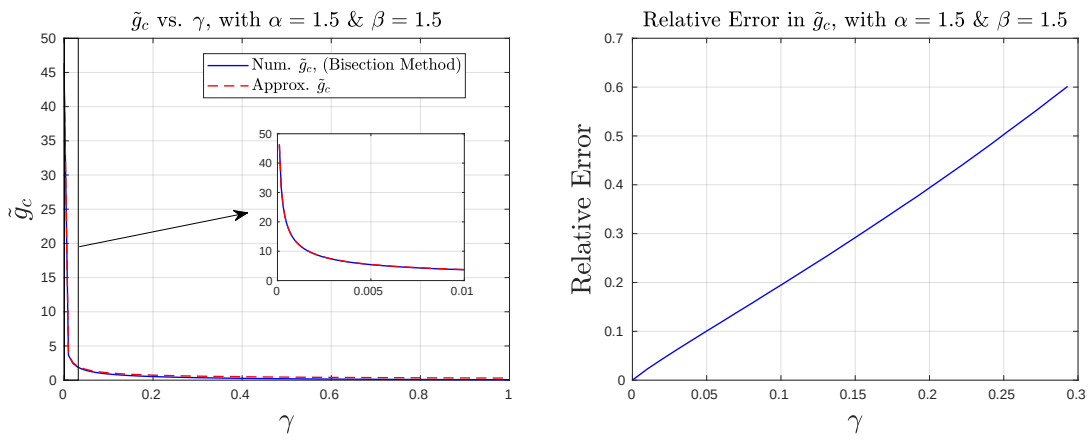

(a) (b)

Figure 10: Plots comparing the $\tilde{g}_c$ approximation with numerically computed $\tilde{g}_c$ value using the Bisection Method, given $\alpha = \beta = 3/2$ (*Kuwabara-Kono model*). (a) $\tilde{g}_c$ vs. γ, where the plot labeled *Num. $\tilde{g}_c$ (Bisection Method)* refer to the numerical values and the plot labeled *Approx. $\tilde{g}_c$* refer to the approximate analytical value obtained using (24), (b) Relative error of the $\tilde{g}_c$ between the analytical approximations and the numerically computed values, over the range of $\gamma \in [0, 0.3]$.

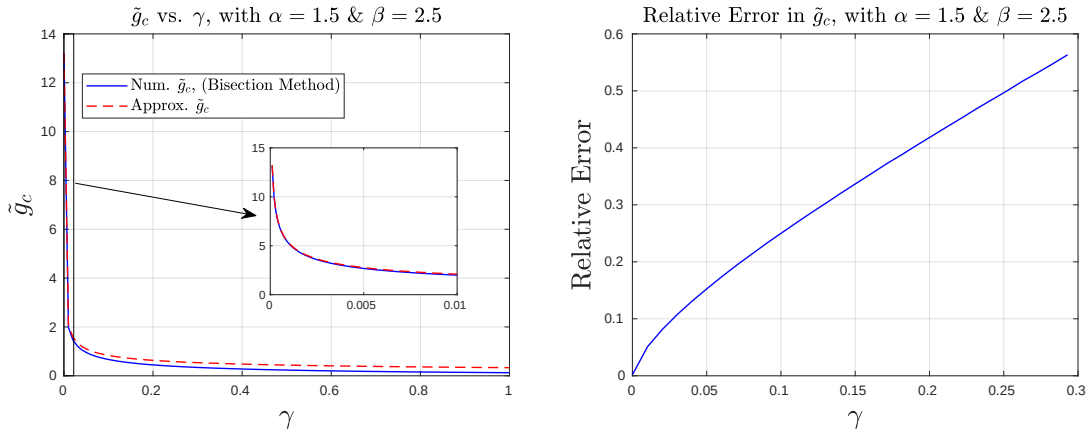

(a) (b)

Figure 11: Plots comparing the $\tilde{g}_c$ approximation with numerically computed $\tilde{g}_c$ value using the Bisection Method, given $\alpha = 3/2$ & $\beta = 5/2$ (*Hunt-Crossley model*). (a) $\tilde{g}_c$ vs. γ, where the plot labeled *Num. $\tilde{g}_c$ (Bisection Method)* refer to the numerical values and the plot labeled *Approx. $\tilde{g}_c$* refer to the approximate analytical value obtained using (24), (b) Relative error of the $\tilde{g}_c$ between the analytical approximations and the numerically computed values, over the range of $\gamma \in [0, 0.3]$.

The condition (24) can work for any value of α and β. Figures 8, 9 10, and 11 show four different cases, with constant $\alpha = 3/2$, but β value is changed in each figure. Figure 8 shows the dependence of γ on $\tilde{g}_c$, when $\alpha = 3/2$ and $\beta = 1$ (which correspond to the visco-elastic model defined by *Hertz stiffness & linear damping*). Figure 8(a) shows the value of $\tilde{g}_c$ as a function of $\gamma \in (0, 1]$. It also includes the zoomed-in plots of $\tilde{g}_c$ with $\gamma \in (0, 0.01]$. The plots labeled *Num. $\tilde{g}_c$ (Bisection Method)* are the results obtained using a numerical scheme, whereas the plots with the label *Approx. $\tilde{g}_c$* correspond to the results obtained using the $\tilde{g}_c$ approximation given in (24). The numerical results, corresponding to the label *Num. $\tilde{g}_c$ (Bisection Method)*, is obtained by using the Bisection method to calculate the value of $\tilde{g}_c$ such that $e = 0$, for a given value of $\gamma \in (0, 1]$. The values of e needed for the bisection method implementation is computed via numerical integration of (4), to yield numerically accurate values for $\tilde{g}_c$. We can see from Fig. 8 that analytical approximation of $\tilde{g}_c$ closely matches the numerically computed values of $\tilde{g}_c$. Fig.8(b) shows the relative errors of the approximated $\tilde{g}_c$ with respect to the numerically computed values. However the range of γ values in Fig. 8(b) has been reduced to $\gamma \in [0, 0.3]$, since the relative errors for very high γ values looses meaning as $\tilde{g}_c \to 0$ for high γ values. We see that the relative errors remain small in this range. While the relative error appears to be increasing with γ, that is expected since $\tilde{g}_c$ gets smaller as γ is increased. Similar, comparisons can be carried out for other (α, β) value pairs. Figure 9, Fig. 10, and Fig. 11 present the comparisons of $\tilde{g}_c$ for *Tsuji-Tanaka-Ishida model* ($\alpha = 3/2$ & $\beta = 5/4$), *Kuwabara-Kono model* ($\alpha = \beta = 3/2$), and *Simon-Hunt-Crossley model* ($\alpha = 3/2$ & $\beta = 5/2$), respectively. In all these comparisons it is evident that the analytical approximation of $\tilde{g}_c$ in terms of γ given in (24), works well for all values of α and β. This also shows that the analytical approximation of e for very large values of $\tilde{g}$ given in (23) is also correct. However, we know that for very large $\tilde{g}$, the value of $e \to 0$, so the approximation (23) doesn't serve much purpose. It would be more interesting to have an approximation for intermediate values of $\tilde{g}$. Recall that all approximations presented till this this point, are linearly dependent to γ. In order to obtain a valid approximation in the intermediate range of $\tilde{g}$ value, it would be useful to include higher order γ terms, into the formulation for CoR. In the following section, we derive another approximation of e that includes a $\mathcal{O}(\gamma^2)$ term.

4.3 Inclusion of an $\mathcal{O}(\gamma^2)$ term

In order to make the CoR approximation valid over larger ranges of γ and $\tilde{g}$, we need to include higher-order terms in the expansion. This section deals with the inclusion of an $\mathcal{O}(\gamma^2)$ term into the CoR approximation. A CoR expansion with an $\mathcal{O}(\gamma^2)$ term will have the following general form,

$$e = 1 - \gamma C_0 - \gamma \tilde{g} C_1 - \gamma^2 C_2 + \text{H.O.T.} \tag{25}$$

where C_0 and C_1 are known and identical to the coefficients obtained in(22). The coefficient C_2 is an unknown that would contribute towards the $\mathcal{O}(\gamma^2)$ term. Here we will obtain the unknown coefficient C_2, by first using a known expansion for the Kuwabara - Kono model ($\alpha = \beta = 3/2$), with no external force ($\tilde{g} = 0$), presented by Schwager and Pöschel [31]. We will study whether the simple inclusion of the C_2 term based on the Schwager-Pöschel expansion coefficients can predict the CoR with adequate accuracy for arbitrary values of $\tilde{g}$. Later, we will also derive a more general $\mathcal{O}(\gamma^2)$ expansion of e in terms of γ, without linearizing it with respect to $\tilde{g}$, for arbitrary values of α and β.

4.3.1 Using Schwager-Pöschel CoR approximation

The CoR formulation presented by Schwager and Pöschel in [31] is a power-series solution of e, consisting of arbitrary order powers of γ, assuming no external force ($\tilde{g} = 0$). However, we are only interested in the expansion with terms up to $\mathcal{O}(\gamma^2)$, which as per [31] is given by,

$$e = 1 + c_1 \bar{\beta} v_0^{\frac{1}{5}} + c_2 \bar{\beta}^2 v_0^{\frac{2}{5}} + \text{H.O.T.} \tag{26}$$

where v_0 is the initial pre-impact velocity, and c_i are numerical coefficients derived from the solution of the displacement trajectory. $\bar{\beta} = \bar{\gamma} \bar{k}^{-\frac{3}{5}}$, where $\bar{k} = \frac{k}{m}$ and $\bar{\gamma} = \frac{3}{2} \frac{k \gamma_0}{m}$. Thus, $\bar{\beta}$ is given by,

$$\bar{\beta} = \frac{3}{2} \gamma_0 \left(\frac{k}{m} \right)^{\frac{2}{5}} \tag{27}$$

Next, considering $\gamma = \gamma_0 v_0^{\frac{2\beta}{\alpha+1}-1} \frac{k}{m}^{1-\frac{\beta}{\alpha+1}}$, which when substituted with $\alpha = \beta = \frac{3}{2}$ becomes $\gamma = \gamma_0 v_0^{\frac{1}{5}} \left(\frac{k}{m}\right)^{\frac{2}{5}}$. Thus, the expression for $\bar{\beta}$ can be rewritten as,

$$\bar{\beta} = \frac{3}{2} \gamma v_0^{-\frac{1}{5}} \tag{28}$$

Substituting this into (26) we get,

$$e = 1 + \frac{3}{2} c_1 \gamma + \frac{9}{4} c_2 \gamma^2 + \text{H.O.T.} \tag{29}$$

The authors of [31], refer to (26) or equivalently (29) as the naive formulation, since the impact termination criteria used to derive this expression is based on displacement. They also present an alternative formulation for e that is determined by evaluating when the contact force vanishes. However, since we do not use a contact force based criteria in this work, we are using the so-called naive CoR formulation from [31] to obtain the the value of C_2.

Comparing (29) with (25), we notice that the unknown coefficient C_2 in (25) can be expressed as,

$$C_2 = -\frac{9}{4} c_2 \tag{30}$$

The value of c_2, as presented in [31] is $c_2 = 0.7982665553$. Thus, the numerical value of C_2 is $C_2 = -1.7960997494$. Now, having estimated the value of C_2 in the expansion (25) with the help of the Schwager-Pöschel coefficient (corresponding to $\tilde{g} = 0$) [31], we can begin to study the effects of adding this $\mathcal{O}(\gamma^2)$ term. Figures 12(a), 12(b), 12(c), and 12(d) show how e varies with respect of γ, given fixed values of $\tilde{g} = 0$, $\tilde{g} = 0.05$, $\tilde{g} = 1$, and $\tilde{g} = 10$, respectively. The plots in Fig. 12 are presented over the range $\gamma \in [0, 0.1]$ and include close-up zoom near $\gamma \approx 0$. The corresponding absolute errors of $\mathcal{O}(\gamma)$ and $\mathcal{O}(\gamma^2)$ expansions of e, with respect to the numerical computation, are shown in Fig. 13. In these figures, *Num. Integ.* refers to the CoR results obtained via direct numerical integration of (4), *Small $\tilde{g}$ Approx.* refers to the results obtained using the first-order approximation in (22), and *SP Coeff.* refers to the results computed using the $\mathcal{O}(\gamma^2)$ approximation given in (25) with the C_2 coefficient defined in terms of (30), which is equivalent to the coefficient found in [31] corresponding to $\tilde{g} = 0$. We observe from these results that the inclusion of the Schwager-Pöschel-based $\mathcal{O}(\gamma^2)$ term improves the accuracy of e for small values of $\tilde{g}$, as can be seen from Fig. 12(a) and Fig. 12(b), and their corresponding absolute errors in Fig. 13(a) and Fig. 13(b). However, as the magnitude of $\tilde{g}$ is increased in Fig.12(c) and Fig. 12(d), and their corresponding absolute error plots in Fig. 13(c) and Fig. 13(d), we see that the Schwager-Pöschel based $\mathcal{O}(\gamma^2)$ approximation fails for large γ. The coefficient C_2 obtained in (30), uses the coefficient value c_2 form [31]. Since [31] ignores external load and gravitational acceleration, the coefficient value of c_2 doesn't hold for higher value of $\tilde{g}$. Thus, we can conclude that the coefficients in the $\mathcal{O}(\gamma^2)$ expansion in (25) can not be independent of $\tilde{g}$, if it has to remain valid for cases with high external load, or $\tilde{g}$. Hence, in the following section we derive an alternate $\mathcal{O}(\gamma^2)$ expansion of e, with coefficients dependent on $\tilde{g}$, such that the CoR approximation can remain valid for arbitrary $\tilde{g}$.

4.3.2 Using the solution for $\frac{\partial u}{\partial \gamma}$

The $\mathcal{O}(\gamma^2)$ term obtained from the Schwager-Pöschel expansion in the preceding section, is only valid for the parameter values $\alpha = \beta = 3/2$. Moreover, we noticed from Figs. 12 and 13, that the inclusion of C_2 terms does not significantly improve the results for high values of γ and $\tilde{g}$. Therefore, now we will consider an alternative approach for deriving an $\mathcal{O}(\gamma^2)$ series solution for e, that is valid for arbitrary values of $\alpha \geq 1$, $\beta \geq 1$ and $\tilde{g} \geq 0$. This approach is based on an expansion with respect to γ, that uses the solution for the variation of the displacement at zero-dissipation ($\gamma = 0$), $\frac{\partial u}{\partial \gamma}$ at $\gamma = 0$. Note that all the expansions presented up to this point were based on a small $\tilde{g}$ approximation, therefore they did not predict well the CoR solutions when $\tilde{g}$ was large. The expansion presented in this section avoids the first-order Taylor expansion with respect to $\tilde{g}$, which makes them accurate for larger values of $\tilde{g}$. Nevertheless, a consequence of not linearizing e with respect to $\tilde{g}$ is that the coefficients in the resulting series solution are not simple functions, and therefore cannot be readily evaluated and would require some further approximations which are discussed in later sections.

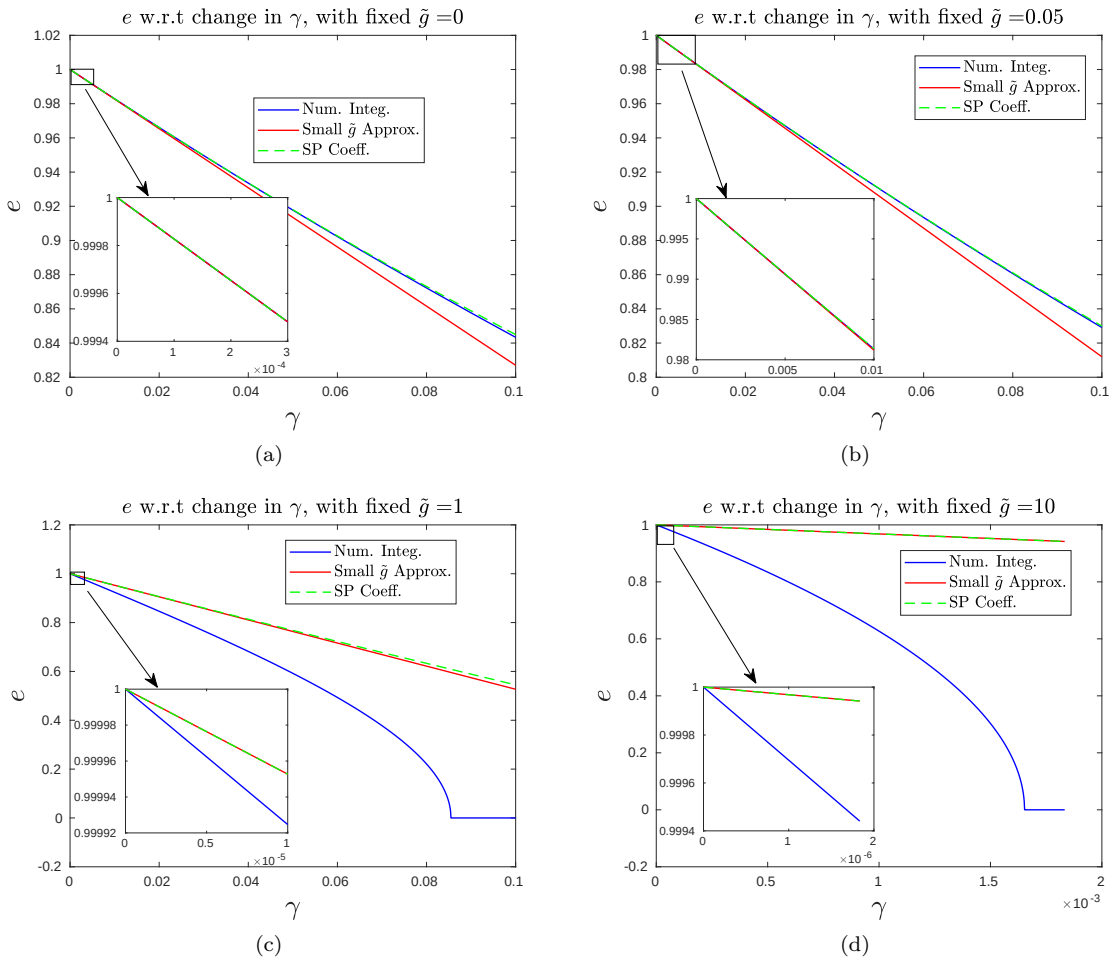

Figure 12: Comparison between the CoR values computed via numerical integration of (4) (plots labeled *Num. Integ.*), with the the $\mathcal{O}(\gamma)$ expansion in (22) (plots labeled *Small $\tilde{g}$ Approx.*), and the Schwager-Pöschel [31] coefficient based $\mathcal{O}(\gamma^2)$ expansion in (25) & (30), (plots labeled *SP Coeff.*), for varying $\tilde{g}$ values. (a) $\tilde{g} = 0$, (b) $\tilde{g} = 0.05$, (c) $\tilde{g} = 1$ and (d) $\tilde{g} = 10$. Zoomed-in plots included in the figure.

We will begin by defining u as a function of both γ and τ, of the form $u(\gamma, \tau)$ and rewriting the governing differential equation in (2) as,

$$\begin{gathered} \frac{\partial^2 u}{\partial \tau^2} + \gamma \frac{\partial u}{\partial \tau}\left(u_+^\beta\right) + u_+^\alpha = \tilde{g} \\ \text{with,} \quad u(\gamma, 0) = 0 \quad \text{and} \quad \frac{\partial u}{\partial \tau}(\gamma, 0) = 1 \quad \text{where,} \quad \tau \in [0, T_f] \end{gathered} \tag{31}$$

T_f is the impact duration with $u(\gamma, T_f) = 0$ and $\frac{\partial u}{\partial \tau}(\gamma, T_f) = -e$. Now, the task at hand, is to expand the CoR expression with respect to γ, so we consider the e^2 expression, given in (6), and rewrite it as,

$$e^2 = 1 - 2\gamma\beta\mathcal{I}(\gamma, \tilde{g}) \quad \text{where,} \quad \mathcal{I}(\gamma, \tilde{g}) = \int_0^{T_f} \left(\frac{\partial u}{\partial \tau}\right)^2 u^{\beta-1} d\tau \tag{32}$$

The integral function $\mathcal{I}(\gamma, \tilde{g})$ can be simplified, by first performing an integration by parts and then substituting (31) for $\frac{\partial^2 u}{\partial \tau^2}$ (noting that $u(\gamma, 0) = u(\gamma, T_f) = 0$),

$$\mathcal{I}(\gamma, \tilde{g}) = \int_0^{T_f} \left(\frac{\partial u}{\partial \tau}\right)^2 u^{\beta-1} d\tau = -\frac{1}{\beta} \int_0^{T_f} \frac{\partial^2 u}{\partial \tau^2} u^\beta d\tau = \frac{1}{\beta} \int_0^{T_f} u^\beta (u^\alpha - \tilde{g}) d\tau \tag{33}$$

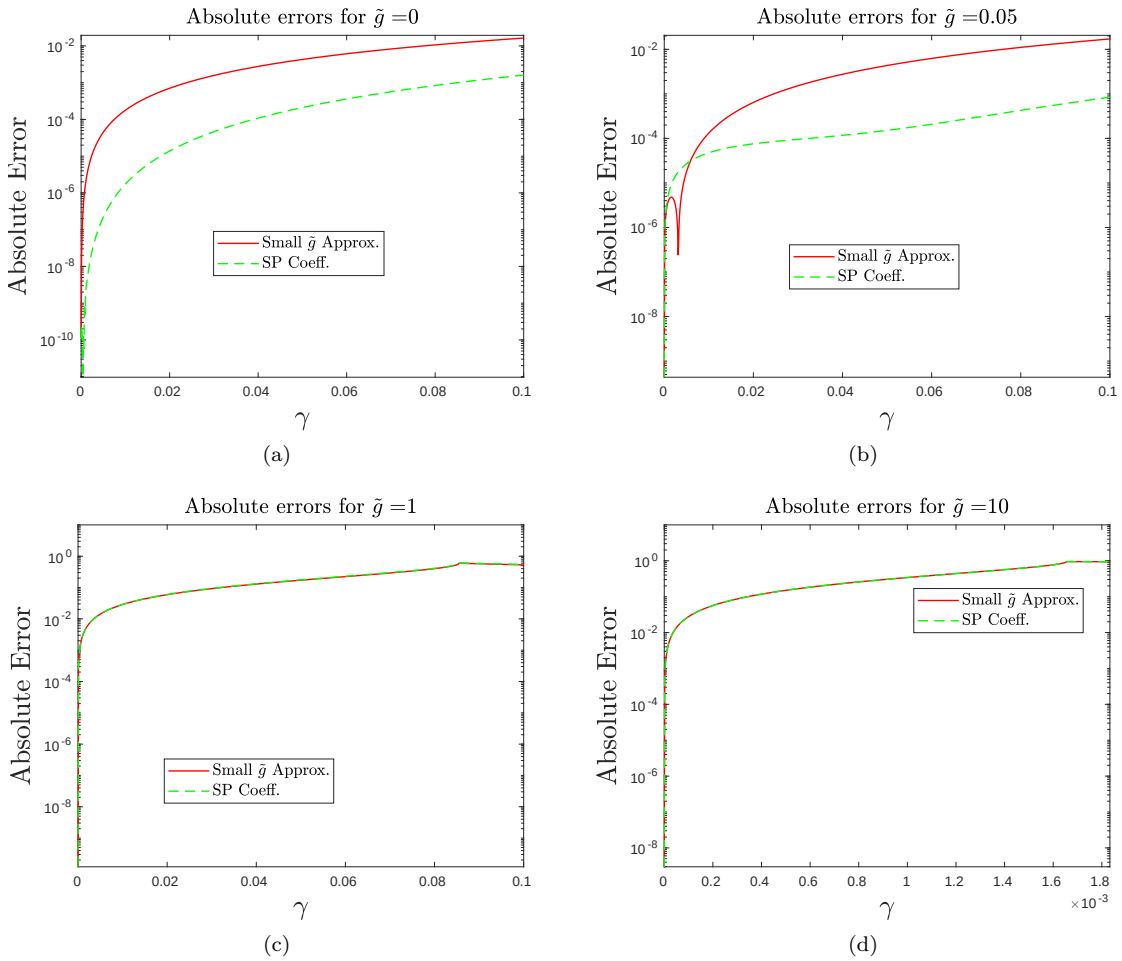

Figure 13: Absolute errors of e computed using the $\mathcal{O}(\gamma)$ expansion in (22) (plot labeled *Small $\tilde{g}$ Approx.*) and the Schwager-Poschel [31] coefficient based $\mathcal{O}(\gamma^2)$ CoR expansion (25) & (30) (plots labeled *SP Coeff.*) with respect to the CoR values computed via direct numerical integration of (4), for varying $\tilde{g}$ values. (a) $\tilde{g} = 0$, (b) $\tilde{g} = 0.05$, (c) $\tilde{g} = 1$ and (d) $\tilde{g} = 10$.

Differentiating $\mathcal{I}(\gamma, \tilde{g})$ with respect to γ using the Leibniz integral rule and then substituting $u(\gamma, T_f) = 0$ leads to,

$$\frac{\partial \mathcal{I}}{\partial \gamma}(\gamma, \tilde{g}) = \frac{1}{\beta} \int_0^{T_f} \frac{\partial u}{\partial \gamma} \left[(\beta + \alpha) u^{\beta+\alpha-1} - \tilde{g}\beta u^{\beta-1} \right] d\tau \tag{34}$$

Thus, the expansion of (32) about $\gamma \approx 0$, can be expressed in terms of (33) and (34),

$$e^2 = 1 - 2\beta \mathcal{I}(0, \tilde{g})\gamma - 2\beta \frac{\partial \mathcal{I}}{\partial \gamma}(0, \tilde{g})\gamma^2 + \mathcal{O}(\gamma^3) \tag{35}$$

However, note that $\frac{\partial \mathcal{I}}{\partial \gamma}(\gamma, \tilde{g})$ depends on the variation of the displacement solution with respect to γ, i.e., $\frac{\partial u}{\partial \gamma}$, which is unknown. Appendix B reformulates $\frac{\partial \mathcal{I}}{\partial \gamma}(\gamma, \tilde{g})$, based on a solution for $\frac{\partial u}{\partial \gamma}$ at $\gamma = 0$. This reformulation leads to an $\mathcal{O}(\gamma^2)$ expression for the CoR e, as defined below in Proposition 2.

Proposition 2. *The $\mathcal{O}(\gamma^2)$ order series solution for the coefficient of restitution, e is given by,*

$$e \approx \min\left(e_+, e_s\right), \tag{36}$$

where, $e_+^2 = \max(e^2, 0)$*, and* e^2 *is given by the expansion,*

$$e^2 = 1 - 2\beta\mathcal{I}(0,\tilde{g})\gamma + 2\beta^2\mathcal{I}(0,\tilde{g})\mathcal{Q}(0,\tilde{g})\gamma^2 \tag{37}$$

In (36), e_s *is a linearization of* e^2 *that is valid for small* $\tilde{g}$*, and is given by,*

$$e_s = \max\left(1 - \beta\mathcal{I}(0,\tilde{g})\gamma + \beta^2\mathcal{I}(0,\tilde{g})\left[\mathcal{Q}(0,\tilde{g}) - \frac{1}{2}\mathcal{I}(0,\tilde{g})\right]\gamma^2, 0\right). \tag{38}$$

The functions $\mathcal{I}(0,\tilde{g})$ *and* $\mathcal{Q}(0,\tilde{g})$ *are integrals given by,*

$$\mathcal{I}(0,\tilde{g}) = 2\int_0^{u_M}\left[1 + 2\left(\tilde{g}u_0 - \frac{u_0^{\alpha+1}}{\alpha+1}\right)\right]^{\frac{1}{2}} u_0^{\beta-1}du_0$$

and,

$$\mathcal{Q}(0,\tilde{g}) = \int_0^{u_M}\left[1 + 2\left(\tilde{g}u_0 - \frac{u_0^{\alpha+1}}{\alpha+1}\right)\right]^{-\frac{1}{2}} u_0^{\beta-1}du_0.$$

Proof. See Appendix B. □

We can check the validity of Proposition 2 for the case $\tilde{g} = 0$, by comparing the coefficient values with the ones obtained using Schwager and Pöschel's results [31]. The integrals $\mathcal{I}(0,\tilde{g})$ can be evaluated at $\tilde{g} = 0$. Therefore, we may use the value of maximum compression as, $u_M = u_M^* = \left(\frac{\alpha+1}{2}\right)^{1/(\alpha+1)}$, and then use Definition 1 to yield,

$$\begin{aligned}
\mathcal{I}(0,0) &= 2\int_0^{\left(\frac{\alpha+1}{2}\right)^{1/(\alpha+1)}}\left(1 - 2\frac{u_0^{\alpha+1}}{\alpha+1}\right)u_0^{\beta-1}du_0 \\
&= \left(\frac{\alpha+1}{2}\right)^{\frac{\beta}{\alpha+1}-1}\frac{\alpha+1}{\alpha+1+2\beta}B\left(\frac{1}{2},\frac{\beta}{\alpha+1}\right) \\
&= \left(\frac{\alpha+1}{2}\right)^{\frac{\beta}{\alpha+1}-1}\frac{\alpha+1}{\alpha+1+2\beta}\sqrt{\pi}\frac{\Gamma\left(\frac{\beta}{\alpha+1}\right)}{\Gamma\left(\frac{1}{2}+\frac{\beta}{\alpha+1}\right)}
\end{aligned} \tag{39}$$

Similarly, for the integral in $\mathcal{Q}(0,\tilde{g})$ at $\tilde{g} = 0$, we can use Definition 1, to compute $\mathcal{Q}(0,0)$, in terms of the beta function,

$$\begin{aligned}
\int_0^{T_0/2} u_0^{\beta-1}d\tau &= \int_0^{\left(\frac{\alpha+1}{2}\right)^{1/(\alpha+1)}} u_0^{\beta-1}\left(1 - 2\frac{u_0^{\alpha+1}}{\alpha+1}\right)^{-\frac{1}{2}}du_0 \\
&= \left(\frac{\alpha+1}{2}\right)^{\frac{\beta}{\alpha+1}-1}\frac{\sqrt{\pi}}{2}\frac{\Gamma\left(\frac{\beta}{\alpha+1}\right)}{\Gamma\left(\frac{1}{2}+\frac{\beta}{\alpha+1}\right)}
\end{aligned} \tag{40}$$

As defined in Proposition 2, for small $\tilde{g}$, $e = e_s$ which is given in (38). Hence, if we substitute (39) and (40) into (38), we obtain the CoR expression, given by,

$$e|_{\tilde{g}=0} = 1 - \gamma C_0 - \gamma^2 C_2 + \mathcal{O}(\gamma^3)$$

with,

$$\begin{aligned}
C_0 &= \beta\left(\frac{\alpha+1}{2}\right)^{\frac{\beta}{\alpha+1}-1}\frac{\alpha+1}{\alpha+1+2\beta}\sqrt{\pi}\frac{\Gamma\left(\frac{\beta}{\alpha+1}\right)}{\Gamma\left(\frac{1}{2}+\frac{\beta}{\alpha+1}\right)} \\
C_2 &= -\frac{\beta^3(\alpha+1)^{\frac{2\beta}{\alpha+1}-1}}{2^{\frac{2\beta}{\alpha+1}-2}(\alpha+2\beta+1)^2}\left[\mathrm{B}\left(\frac{\beta}{\alpha+1},\frac{1}{2}\right)\right]^2.
\end{aligned}$$

Evaluating C_0 and C_2 for the values $\alpha = \beta = \frac{3}{2}$, we obtain the values $C_0 = 1.7302$ and $C_2 = -1.7961$. Comparing with (29), we know that $C_0 = -\frac{3}{2}c_1$ and $C_2 = -\frac{9}{4}c_2$, where c_1 and c_2 are the coefficients presented in [31]. The values of these coefficients reported in [31] are $c_1 = -1.15448854$ and $c_2 = 0.7982665553$. So, we can checked $C_0 = -\frac{3}{2}(-1.15448854) = 1.7302$ and $C_2 = -\frac{9}{4}(0.7982665553) = -1.7961$ (which are identical to the values obtained in Sec. 4.1 and Sec. 4.3.1) to conclude that the e expansion obtained above in (38) agrees with the $\mathcal{O}(\gamma^2)$ expansion presented in [31], when $\tilde{g} = 0$. Additionally, one can also check the validity of this coefficients when $\tilde{g} \neq 0$, by numerically computing the values of the integrals $\mathcal{I}(0, \tilde{g})$ and $\mathcal{Q}(0, \tilde{g})$ and then use them to compute the e with the two approximations provided in (36), to see which approximation works better in comparison to the CoR computed via direct numerical integration of (4). Appendix B presents these comparisons, from which one can conclude that both approximations in Proposition 2 hold in their respective range of validity which depends on the values of γ and $\tilde{g}$.

4.4 Approximate CoR for arbitrary $\tilde{g}$

From the previous sections it follows that we can obtain analytical CoRs corresponding to both small and large values of $\tilde{g}$. In (24) we obtained an expression for $\tilde{g}_c$, which is the large value of $\tilde{g}$ when $e = 0$, or in other words the bead doesn't rebound. Also, we have previously noted that the inclusion of an $\mathcal{O}(\gamma^2)$ term improves the accuracy of analytical CoR. The CoR approximations in Proposition 2 that include $\mathcal{O}(\gamma^2)$ term consist of integral functions dependent on $\tilde{g}$. While we have good approximations of these integral functions when $\tilde{g} \approx 0$ and $\tilde{g} \approx \tilde{g}_c$, a valid approximation for the entire range of $\tilde{g}$ remains to be computed. So, here we will consider (37), which can be rewritten (with the notation $\mathcal{I}(0, \tilde{g}) = \mathcal{I}(\tilde{g})$) as,

$$e^2 = 1 - 2\beta\mathcal{I}(\tilde{g})\gamma + 2\beta^2\mathcal{I}(\tilde{g})Q(\tilde{g})\gamma^2 + \mathcal{O}(\gamma^3)$$

where,

$$\mathcal{I}(\tilde{g}) = 2\int_0^{u_M} \left[1 + 2\left(\tilde{g} - \frac{u_0^{\alpha+1}}{\alpha+1}\right)\right]^{\frac{1}{2}} u_0^{\beta-1} du_0 \tag{41}$$

and,

$$Q(\tilde{g}) = \int_0^{T_0/2} u_0^{\beta-1} d\tau = \int_0^{u_M} \left[1 + 2\left(\tilde{g} - \frac{u_0^{\alpha+1}}{\alpha+1}\right)\right]^{-\frac{1}{2}} u_0^{\beta-1} du_0 \tag{42}$$

The integral functions $\mathcal{I}(\tilde{g})$ and $\mathcal{Q}(\tilde{g})$ can not be explicitly evaluated for arbitrary values of $\tilde{g}$. However, we can notice that the integrands of the two integral functions is closely linked to the integrand of Euler's Beta function, such that we can evaluate these integrals exactly in terms of Euler's Beta function when $\tilde{g} = 0$. Hence, to obtain approximations of $\mathcal{I}(\tilde{g})$ and $\mathcal{Q}(\tilde{g})$, we will rely on finding an equivalent approximation for the integrands, such that the integrals could be evaluated in terms of Euler's Beta function for all values of $\tilde{g}$.

4.4.1 Approximate calculation of $\mathcal{I}(\tilde{g})$ and $\mathcal{Q}(\tilde{g})$

Before approximating $\mathcal{I}(\tilde{g})$ and $\mathcal{Q}(\tilde{g})$, we will consider a change of variable. Since we wish to obtain this interpolation for arbitrarily large $\tilde{g} \in [0, \infty]$, we will redefine it in terms of a new variable $\theta \in [0, 1]$, which is given by,

$$\frac{u_M^{\alpha+1}}{\alpha+1} = \frac{1}{2\theta} \quad \text{such that,} \quad \tilde{g}(\theta) = \left(\frac{\alpha+1}{2\theta}\right)^{\frac{-1}{\alpha+1}} \left(\frac{1}{2\theta} - \frac{1}{2}\right) \tag{43}$$

Thus, $\tilde{g}$ in terms of θ correspond to,

$$\theta = 1 \implies \tilde{g} = 0 \quad \text{and,} \quad \theta \to 0 \implies \tilde{g} \to \infty \tag{44}$$

Finally, with the substitution $u_0 = u_M x$, we may write the integrals as,

$$\mathcal{I}\left(\tilde{g}(\theta)\right) = \frac{2}{\sqrt{\theta}}\left(\frac{\alpha+1}{2\theta}\right)^{\frac{\beta}{\alpha+1}} \int_0^1 \left[\theta + (1-\theta)x - x^{\alpha+1}\right]^{\frac{1}{2}} x^{\beta-1} dx = K(\theta) J_{\alpha,\beta}(\theta) \tag{45}$$

and,

$$Q\left(\tilde{g}(\theta)\right) = \sqrt{\theta}\left(\frac{\alpha+1}{2\theta}\right)^{\frac{\beta}{\alpha+1}} \int_0^1 \left[\theta + (1-\theta)x - x^{\alpha+1}\right]^{-\frac{1}{2}} x^{\beta-1} dx = L(\theta) M_{\alpha,\beta}(\theta) \tag{46}$$

where,

$$\begin{aligned} K(\theta) &= \frac{2}{\sqrt{\theta}}\left(\frac{\alpha+1}{2\theta}\right)^{\frac{\beta}{\alpha+1}} \qquad J_{\alpha,\beta}(\theta) = \int_0^1 \left[\theta + (1-\theta)x - x^{\alpha+1}\right]^{\frac{1}{2}} x^{\beta-1} dx \\ L(\theta) &= \sqrt{\theta}\left(\frac{\alpha+1}{2\theta}\right)^{\frac{\beta}{\alpha+1}} \qquad M_{\alpha,\beta}(\theta) = \int_0^1 \left[\theta + (1-\theta)x - x^{\alpha+1}\right]^{-\frac{1}{2}} x^{\beta-1} dx \end{aligned} \tag{47}$$

The functions $K(\theta)$ and $L(\theta)$ can be computed directly given the values of α, β and θ. Whereas, the functions $J_{\alpha,\beta}(\theta)$ and $M_{\alpha,\beta}(\theta)$ are integrals that can be evaluated in terms of the Euler's Beta function when $\theta = 0$ and $\theta = 1$, but do not have a closed-form solution when $\theta \in (0,1)$. Hence, we seek an approximation for the integrals $J_{\alpha,\beta}(\theta)$ and $M_{\alpha,\beta}(\theta)$ for the all values of $\theta \in [0,1]$. In order to proceed further with such an approximation, we first note that the integrals $J_{\alpha,\beta}(\theta)$ and $M_{\alpha,\beta}(\theta)$ can be related, due the similarity in the structure of their integrands. The relationship between the two integral functions is defined below in Proposition 3, the proof for which can be found in Appendix C.

Proposition 3. *The integrals $J_{\alpha,\beta}(\theta)$ and $M_{\alpha,\beta}(\theta)$ are related according to the following relationship,*

$$J_{\alpha,\beta}(\theta) = \frac{\alpha+1}{2\beta} M_{\alpha,\alpha+\beta+1}(\theta) + \frac{\theta-1}{2\beta} M_{\alpha,\beta+1}(\theta) \tag{48}$$

Proof. See Appendix C □

Therefore, now we only need to find an approximation for $M_{\alpha,\beta}(\theta)$, and then use the approximating function to compute $J_{\alpha,\beta}(\theta)$ using (48).

In order to compute $M_{\alpha,\beta}(\theta)$ for all values of $\theta \in [0,1]$, we follow the approach of approximating the integrand of $M_{\alpha,\beta}(\theta)$, such that the integral $M_{\alpha,\beta}(\theta)$ could be represented as a summation of Beta functions with coefficients. The integrand is approximated with the help of Chebyshev polynomials of arbitrary order n, which leads to some recurrence relations that are used for the approximation of $M_{\alpha,\beta}(\theta)$. The details of this development can be found in Appendix C, and here we present the final result of this approximation in Proposition 4.

Proposition 4. *The n-th (n being an odd number) order approximation of $M_{\alpha,\beta}(\theta)$ is given by,*

$$M_{\alpha,\beta}(\theta) \simeq \sum_{j=0}^{n-1} c_j a_{j,0} \ , \quad \text{with,} \quad j \text{ even} \tag{49}$$

where coefficients $a_{j,k}$ and c_j are defined below. The coefficients c_j can be computed as,

$$\begin{cases} c_0 &= \dfrac{2}{n+1} \displaystyle\sum_{k=(n+1)/2}^{n} h_{\alpha,\theta}(x_k) \\ c_j &= \dfrac{4}{n+1} \displaystyle\sum_{k=(n+1)/2}^{n} h_{\alpha,\theta}(x_k) \cos\left(j\pi \frac{2k+1}{2n+2}\right), \qquad \text{if} \quad j \geq 2 \text{ and is even} \\ c_j &= 0, \qquad\qquad\qquad\qquad\qquad\qquad\qquad\qquad\qquad\qquad\qquad\qquad \text{if} \quad j \geq 2 \text{ and is odd} \end{cases} \tag{50}$$

where $h_{\alpha,\theta}(x)$ is a function related to the approximated and the actual integrand of $M_{\alpha,\beta}(\theta)$, and is given by,

$$h_{\alpha,\theta}(x) = \left(\frac{x^{1-\theta} - x^{\alpha+1}}{\theta + (1-\theta)x - x^{\alpha+1}}\right)^{\frac{1}{2}} \tag{51}$$

x_k are Chebyshev nodes in the range $[0,2]$ and are given by,

$$x_k = \cos\left(\pi \frac{2k+1}{2n+2}\right) + 1, \quad k \in \mathbb{N} \tag{52}$$

j \ k	0	1	2	3	4	...	$n-1$
0	$a_{0,0}$	$a_{0,1}$	$a_{0,2}$	$a_{0,3}$	$a_{0,4}$	...	$a_{0,n-1}$
1	$a_{1,0}$	$a_{1,1}$	$a_{1,2}$	$a_{1,3}$	...	$a_{1,n-2}$	
2	$a_{2,0}$	$a_{2,1}$	$a_{2,2}$	...	$a_{2,n-3}$		
3	$a_{3,0}$	$a_{3,1}$	...	$a_{3,n-4}$			
4	$a_{4,0}$	...	$a_{4,n-4}$				
⋮	⋮	⋰					
$n-1$	$a_{n-1,0}$						

Table 1: Tabular computation of $a_{i,j}$, based on the recurrence relations in (53). The values $a_{j,0}$ in column $k = 0$ (highlighted in gray), are required for the final computation of $M_{\alpha,\beta}(\theta)$.

Due to the relationship of the coefficients $a_{j,k}$ to Chebyshev polynomials, they can be calculated using recurrence relations given by,

$$\begin{aligned} a_{j+2,k} &= 2a_{j+1,k+1} - 2a_{j+1,k} - a_k \quad \text{for} \qquad j \geq 0 \\ a_{0,k} &= \tfrac{1}{\alpha+\theta} B\left(\tfrac{\beta+k-1/2+\theta/2}{\alpha+\theta}, \tfrac{1}{2}\right) \quad \text{and} \quad a_{1,k} = a_{0,k+1} - a_{0,k} \end{aligned} \tag{53}$$

Proof. See Appendix C. □

As seen in (49), the evaluation of the approximation $M_{\alpha,\beta}(\theta)$ for a given order n (n being an odd number), requires computation of the coefficients $a_{j,k}$, using the recurrence relations in (53). These calculations may be summarized via the tabular computation scheme demonstrated in Table 1.

Note that the order n for the approximation of $M_{\alpha,\beta}(\theta)$ in (49) needs to be carefully selected. While a lower order of n corresponds to large overall errors, very high order of n leads to lower aggregate errors, but high local errors due to oscillations in the response of $M_{\alpha,\beta}(\theta)$ with respect to θ. It was found that an order $n = 21$ works best for the given approximations (See Appendix C for more details). Thus the numerical results presented henceforth were computed using the order $n = 21$.

4.4.2 Numerical Results

In this section we will primarily study the validity of the $\mathcal{O}(\gamma^2)$ approximation e, as given in Proposition 2, against numerical computation of CoR, based on (4). The main goal is to study how the parameter values γ and $\tilde{g}$ affect the prediction of e using the $\mathcal{O}(\gamma^2)$ approximation. Since, the approximations can work with arbitrary values of $\alpha \geq 1$ and $\beta \geq 1$, here we will study the validity of the $\mathcal{O}(\gamma^2)$ CoR approximation in the context of four different visco-elastic models: 1) *Hertz stiffness with linear damping*, 2) *Tsuji-Tanaka-Ishida model*, 3) *Kuwabara-Kono model*, and 4) *Simon-Hunt-Crossley model*. The four figures, Fig. 14, Fig. 16, Fig. 18, and, Fig. 20, correspond to four visco-elastic models considered in this study, namely *Hertz stiffness with linear damping* ($\alpha = 3/2$ & $\beta = 1$), *Tsuji-Tanaka-Ishida model*($\alpha = 3/2$ & $\beta = 5/4$), *Kuwabara-Kono model* ($\alpha = \beta = 3/2$), and *Simon-Hunt-Crossley model* ($\alpha = 3/2$ & $\beta = 5/2$), respectively. Each of these figures consists of four sub-figures, corresponding to the values $\tilde{g} = 0$,0.05,1, and 10, that show the dependence of e with respect to γ. The plots labeled *Num. Integ.* show the results of e that are computed via numerical integration of (4). These numerically integrated results form the reference against which other approximations are compared. The figures corresponding to the value of $\tilde{g} = 0$ contain plots

labeled *Exact Coeffs.* which show the results of e computed using the $\mathcal{O}(\gamma^2)$ approximation using the exact values of $\mathcal{I}(\tilde{g})$ and $\mathcal{Q}(\tilde{g})$ using (39) and (40). In all other figures, corresponding to values of $\tilde{g} \neq 0$, the plots labeled *Num. Coeffs.* show the results of e with the $\mathcal{O}(\gamma^2)$ approximation, where the integrals $\mathcal{I}(\tilde{g})$ and $\mathcal{Q}(\tilde{g})$ are computed via numerical integration of (41) and (42). Lastly, in all figures within Fig. 14, Fig. 16, Fig. 18, and Fig. 20, there are plots labeled *Approx. Coeffs.*. These plots refer to the results of e using the $\mathcal{O}(\gamma^2)$ approximation according to (36), where the integrals are approximated as $\mathcal{I}(\tilde{g}(\theta)) = K(\theta)J_{\alpha,\beta}(\theta)$ and $\mathcal{Q}(\tilde{g}(\theta)) = L(\theta)M_{\alpha,\beta}(\theta)$, with the functions $J_{\alpha,\beta}(\theta)$ and $M_{\alpha,\beta}(\theta)$ further approximated using (48) and (49), respectively. We can see from the figures that these results closely match the results where the integrals are computed numerically. The CoR results based on Schwager-Pöschel coefficient, which we have already studied in Sec. 4.3.1, are also included in Fig. 18, corresponding to $\alpha = \beta = 3/2$ for completeness. The absolute errors associated with each approximation of e presented in Fig. 14, Fig. 16, Fig. 18, and Fig. 20, with respect to the numerically integrated CoR values are shown in Fig. 15, Fig. 17, Fig. 19, and Fig. 21. Additionally, the maximum absolute errors within certain interesting ranges of γ are also reported in Tables 2, 3, 4, and 5. The absolute error values for the various approximations presented in Fig. 15, Fig. 17, Fig. 19, Fig. 21, Tab. 2, Tab. 3, Tab. 4, and Tab. 5 are all computed with respect to the CoR values computed via numerical integration of (4), which are labeled *Num. Integ.* in Fig. 14, Fig. 16, Fig. 18, and Fig. 20. However, for some specific values of the parameters α, β, and $\tilde{g}$, the CoR has an explicit analytical solution. The proposed $\mathcal{O}(\gamma^2)$ approximations in (36), is also studied against these known analytical CoR solutions. These results are presented in Appendix D.

The general conclusion that can be drawn by studying the results in Fig. 14, Fig. 15, Fig. 16, Fig. 17, Fig. 18, Fig. 19, Fig. 20, Fig. 21, Tab. 2, Tab. 3, Tab. 4, and Tab. 5 is that the $\mathcal{O}(\gamma^2)$ approximation of e using (36) gives very accurate CoR results for small and large $\tilde{g}$, and particularly when γ is also small. Based on Fig. 15, Fig. 17, Fig. 19, and Fig. 21, we can observe that the absolute errors corresponding to small γ are very small. The order of magnitude for these errors in the small range of γ values can be read off from the set of maximum absolute error values reported in Tables 2, 3 4, and 5. The absolute error values increases with the γ value until attachment (no rebound, corresponding to $e = 0$) takes place. In particular, one can notice the large errors corresponding to higher values of γ when $\tilde{g} = 1$ in Fig. 14(c),, Fig. 16(c), Fig. 18(c), Fig. 20(c), and the corresponding maximum absolute error values for $\gamma \geq 0.02$ in Tab. 2(a), Tab. 3(a) Tab. 4(a), and Tab. 5(a). The $\mathcal{O}(\gamma^2)$ expansion of e given in (36) relies on the expansion with respect to γ about $\gamma = 0$ (associated with the non-dissipative impacts). Therefore, the absolute error of the predicted CoR based on $\mathcal{O}(\gamma^2)$ expansion with respect to the numerically integrated e, increases with γ. Also, comparing Fig. 14(c), Fig. 16(c), Fig. 18(c), and Fig. 20, we can notice the pattern that the magnitude of the absolute error at high γ also increases with the value of β. Since, the parameter β in the equation of motion (1) refers to the power on the dissipation term, it affects the amount of dissipation that takes place during the impact, and thereby its influence is also scaled by γ, which is a coefficient to the dissipation term in (1). Hence, given that the $\mathcal{O}(\gamma^2)$ expansion of e is considered about $\gamma = 0$, the error increases with the β values. In Fig. 14(d), Fig. 14(d), Fig. 18(d), and Fig. 20(d), corresponding to $\tilde{g} = 10$, we see that the prediction of e using the $\mathcal{O}(\gamma^2)$ expansion is very accurate in the range of γ values for which attachment takes place. This is to be expected since both the numerically integrated e and the analytical $\mathcal{O}(\gamma^2)$ expansion, following the threshold $e_+^2 = \max(e^2, 0)$ in (36), becomes zero. Tables 2(b), 4(b), and 5(b), which examines this range separately, reports maximum absolute error values close to machine precision, for high γ values. While the e predictions look very accurate for all γ values in Fig. 14(d), Fig. 18(d), and Fig. 20(d), a closer examination of the maximum absolute error values in Tab. 2(b), Tab. 4(b), and Tab. 5(b) reveals that, similar to all other cases of $\tilde{g}$ values, the errors increase with the value γ until the impact attaches or doesn't rebound. Another observation one can make based on the reported maximum absolute errors in the intermediate γ ranges (corresponding to the second columns) in Tab. 2(b), Tab. 4(b), and Tab. 5(b), is that the errors associated for the $\mathcal{O}(\gamma^2)$ expasion with the approximated integrals ($\mathcal{I}(\tilde{g}(\theta)) = K(\theta)J_{\alpha,\beta}(\theta)$ & $\mathcal{Q}(\tilde{g}(\theta)) = L(\theta)M_{\alpha,\beta}(\theta)$) are higher than the errors from the same expansion using numerically integrated integrals ($\mathcal{I}(\tilde{g})$ and $\mathcal{Q}(\tilde{g})$). This is a consequence of the approximations (based on Chebyshev nodes) of the integral $M_{\alpha,\beta}(\theta)$, which is very accurate at $\theta = 0$ and $\theta = 1$, and less accurate if $\theta \in (0, 1)$. Nevertheless, despite the aforementioned inaccuracies for high γ values, one notices that the absolute error values are generally small, while being very accurate for small γ and small $\tilde{g}$ values. As noted in [35, 36], the γ values calculated using the experimental values of e reported in [25] associated with various materials using the *Kuwabara-Kono model* ($\alpha = \beta = 3/2$) have a maximum order of 10^{-1}. Also from the examples based on experimental results presented in Fig. 2(b),

5(b), 6(b), and 7(b), we can see that the value of $\tilde{g}$ remains very small for a gravitational acceleration value of $g = 9.8$ m/s^2, with $F = 0$ N. Therefore, based on these physically relevant parameter values, we can conclude that the $\mathcal{O}(\gamma^2)$ approximation of e will remain very accurate for most materials within a reasonable γ range, and with an external load up to several orders of magnitude higher than the weight of the bead.

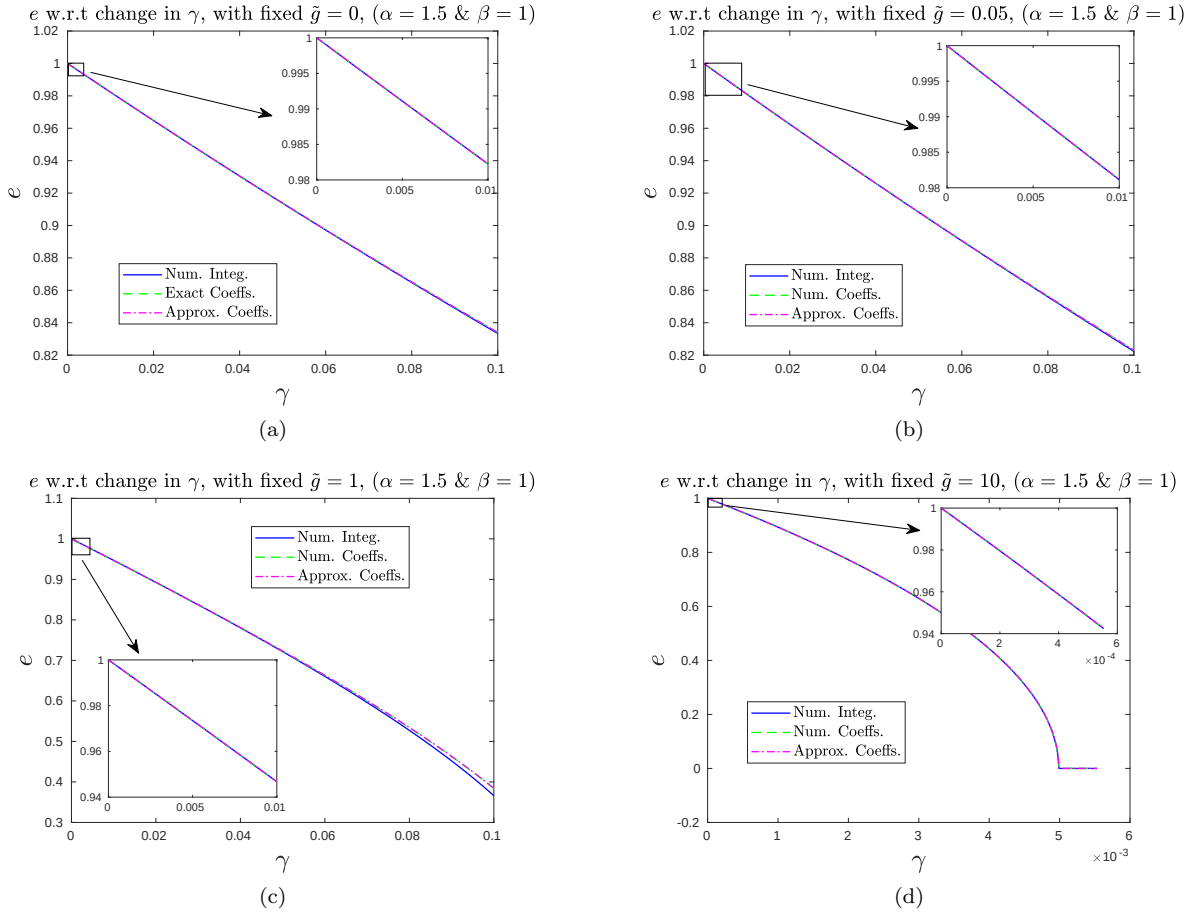

Figure 14: Comparison between the CoR values computed via numerical integration of (4), and the $\mathcal{O}(\gamma^2)$ approximations given by (36) (labeled *Num. Integ.*), using the numerically integrated functions $\mathcal{I}(\tilde{g})$ and $\mathcal{Q}(\tilde{g})$ from (41) and (42) (labeled *Num. Coeffs.*), and the approximated functions $\mathcal{I}(\tilde{g}(\theta)) = K(\theta)J_{\alpha,\beta}(\theta)$ and $\mathcal{Q}(\tilde{g}(\theta)) = L(\theta)M_{\alpha,\beta}(\theta)$ using (48) and (49) (labeled *Approx. Coeffs.*). When $\tilde{g} = 0$, the values $\mathcal{I}(0)$ and $\mathcal{Q}(0)$ are calculated using (39) and (40). Results are shown for the visco-elastic model with $\alpha = 3/2$ & $\beta = 1$ (*Hertz stiffness with linear damping*), for the cases: (a) $\tilde{g} = 0$, (b) $\tilde{g} = 0.05$, (c)$\tilde{g} = 1$, and (d) $\tilde{g} = 10$.

5 Recapitulation

This section is dedicated to present a brief summary of the method for computing the analytical approximation of the CoR for single spherical bead undergoing impact in the presence of a constant external load. The fundamental set of quantities needed for this computation is given by:

m : Mass of the spherical bead.

k : Stiffness constant used in the general nonlinear visco-elastic contact model

Types of $\mathcal{I}$ & $\mathcal{Q}$	Exact[(39),(40)]/Num.[(41),(42)]		Approx.[(48),(49)]	
$\tilde{g}$	$\gamma < 0.02$	$\gamma \geq 0.02$	$\gamma < 0.02$	$\gamma \geq 0.02$
0	5.39×10^{-6}*	6.57×10^{-4}*	5.39×10^{-6}	6.57×10^{-4}
0.05	5.63×10^{-6}	6.89×10^{-4}	1.32×10^{-5}	7.26×10^{-4}
1	6.82×10^{-5}	1.77×10^{-2}	1.32×10^{-4}	1.85×10^{-2}

(a) Max. absolute errors within different γ ranges for $\tilde{g} = 0, 0.05,$ and, 1

Type of $\mathcal{I}$ & $\mathcal{Q}$	$\gamma < 0.0011$	$0.0011 \leq \gamma \leq 0.0051$	$\gamma > 0.0051$
Num.[(41),(42)]	4.39×10^{-7}	4.25×10^{-3}	5.63×10^{-13}
Approx.[(48),(49)]	8.03×10^{-5}	1.33×10^{-2}	5.63×10^{-13}

(b) Max. absolute errors within different γ ranges for $\tilde{g} = 10$

Table 2: Maximum Absolute Errors on the $\mathcal{O}(\gamma^2)$ expansion of e using a visco-elastic model with $\alpha = 3/2$ and $\beta = 1$ (*Hertz Stiffness with linear damping*), for $\tilde{g} = 0$, 0.05, 1, and, 10, in various γ ranges. *Errors on $\mathcal{O}(\gamma^2)$ expansions of e while using the exact values of $\mathcal{I}(\tilde{g} = 0)$ and $\mathcal{Q}(\tilde{g} = 0)$, according to (39) and (40).

Types of $\mathcal{I}$ & $\mathcal{Q}$	Exact[(39),(40)]/Num.[(41),(42)]		Approx.[(48),(49)]	
$\tilde{g}$	$\gamma < 0.02$	$\gamma \geq 0.02$	$\gamma < 0.02$	$\gamma \geq 0.02$
0	9.17×10^{-6}*	1.11×10^{-3}*	9.17×10^{-6}	1.11×10^{-3}
0.05	9.88×10^{-6}	1.12×10^{-3}	1.77×10^{-5}	1.12×10^{-3}
1	1.65×10^{-4}	1.10×10^{-1}	2.40×10^{-4}	1.11×10^{-1}

(a) Max. absolute errors within different γ ranges for $\tilde{g} = 0, 0.05,$ and, 1

Types of $\mathcal{I}$ & $\mathcal{Q}$	$\gamma < 0.00063$	$0.00063 \leq \gamma \leq 0.0029$	$\gamma > 0.0029$
Num.[(41),(42)]	5.56×10^{-8}	3.32×10^{-4}	2.84×10^{-13}
Approx.[(48),(49)]	8.07×10^{-5}	1.76×10^{-2}	2.84×10^{-13}

(b) Max. absolute errors within different γ ranges for $\tilde{g} = 10$

Table 3: Maximum Absolute Errors on the $\mathcal{O}(\gamma^2)$ expansion of e using a visco-elastic model with $\alpha = 3/2$ and $\beta = 5/4$ (*Tsuji-Tanaka-Ishida model*), for $\tilde{g} = 0$, 0.05, 1, and, 10, in various γ ranges. *Errors on $\mathcal{O}(\gamma^2)$ expansions of e while using the exact values of $\mathcal{I}(\tilde{g} = 0)$ and $\mathcal{Q}(\tilde{g} = 0)$, according to (39) and (40).

Types of $\mathcal{I}$ & $\mathcal{Q}$	Exact[(39),(40)]/Num.[(41),(42)]		Approx.[(48),(49)]	
$\tilde{g}$	$\gamma < 0.02$	$\gamma \geq 0.02$	$\gamma < 0.02$	$\gamma \geq 0.02$
0	1.37×10^{-5}*	1.60×10^{-3}*	1.37×10^{-5}	1.60×10^{-3}
0.05	1.52×10^{-5}	1.78×10^{-3}	2.33×10^{-5}	1.82×10^{-3}
1	3.67×10^{-4}	2.08×10^{-1}	4.58×10^{-4}	2.09×10^{-1}

(a) Max. absolute errors within different γ ranges for $\tilde{g} = 0, 0.05,$ and, 1

Types of $\mathcal{I}$ & $\mathcal{Q}$	$\gamma < 0.000367$	$0.000367 \leq \gamma \leq 0.00169$	$\gamma > 0.00169$
Num.[(41),(42)]	1.06×10^{-7}	2.38×10^{-4}	2.84×10^{-13}
Approx.[(48),(49)]	8.11×10^{-5}	2.11×10^{-2}	2.84×10^{-13}

(b) Max. absolute errors within different γ for $\tilde{g} = 10$

Table 4: Maximum Absolute Errors on the $\mathcal{O}(\gamma^2)$ expansion of e using a visco-elastic model with $\alpha = \beta = 3/2$ (*Kuwabara-Kono model*), with $\tilde{g} = 0$, 0.05, 1, and, 10, for various γ ranges. *Errors on $\mathcal{O}(\gamma^2)$ expansions of e while using the exact values of $\mathcal{I}(\tilde{g} = 0)$ and $\mathcal{Q}(\tilde{g} = 0)$, according to (39) and (40).

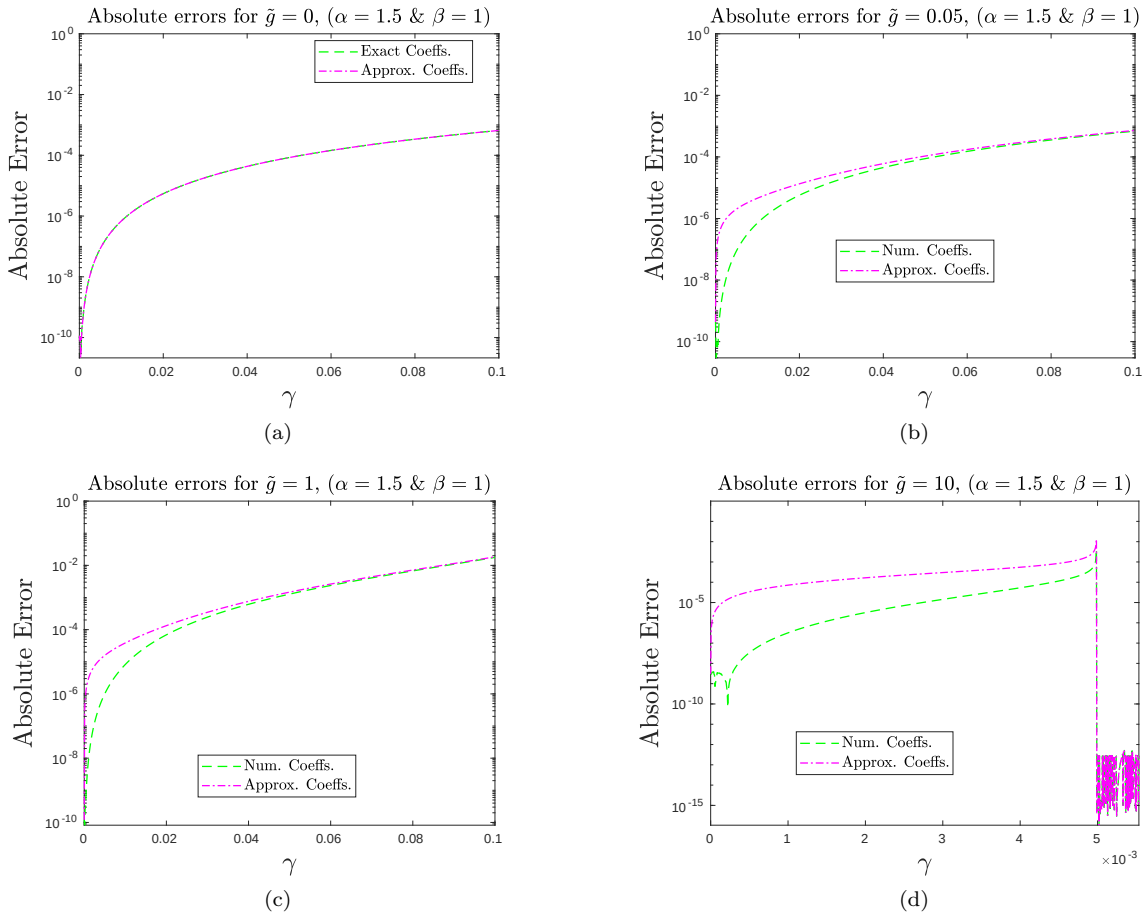

Figure 15: Absolute errors of the $\mathcal{O}(\gamma^2)$ CoR approximations (36) using the numerically integrated functions $\mathcal{I}(\tilde{g})$ and $\mathcal{Q}(\tilde{g})$ from (41) and (42) (labeled *Num. Coeffs.*), and the approximated functions $\mathcal{I}(\tilde{g}(\theta)) = K(\theta)J_{\alpha,\beta}(\theta)$ and $\mathcal{Q}(\tilde{g}(\theta)) = L(\theta)M_{\alpha,\beta}(\theta)$ from (48) and (49) (labeled *Approx. Coeffs.*). When $\tilde{g} = 0$, the results with the numerical results are replaced with the absolute error of $\mathcal{O}(\gamma^2)$ CoR computed with $\mathcal{I}(0)$ and $\mathcal{Q}(0)$ using (39) and (40) (labeled *Exact Coeffs.*).The absolute errors are computed in reference to the CoR values computed through numerical integration of (4). Results are shown for the visco-elastic model with $\alpha = 3/2$ & $\beta = 1$ (*Hertz stiffness with linear damping*), for the cases: (a) $\tilde{g} = 0$, (b) $\tilde{g} = 0.05$, (c)$\tilde{g} = 1$, and (d) $\tilde{g} = 10$.

α : Exponent parameter on the displacement (deformation), according to the general nonlinear visco-elastic contact model ($\alpha = 3/2$ for Kuwabara-Kono model).

β : Exponent parameter on the speed (deformation-rate), according to the general nonlinear visco-elastic contact model ($\beta = 3/2$ for Kuwabara-Kono model; $\beta = 5/2$ for Simon-Hunt-Crossley).

γ_0 : A coefficient to the speed (deformation-rate), according to the general nonlinear visco-elastic contact model.

F : Constant external load on the bead.

g : Gravitational acceleration constant.

v_0 : Impact velocity of the bead.

The first step is to convert the aforementioned fundamental parameters into two re-scaled parameters that are necessary for the computation of the approximate CoR. These two re-scaled parameters, $\tilde{g}$ and γ can be

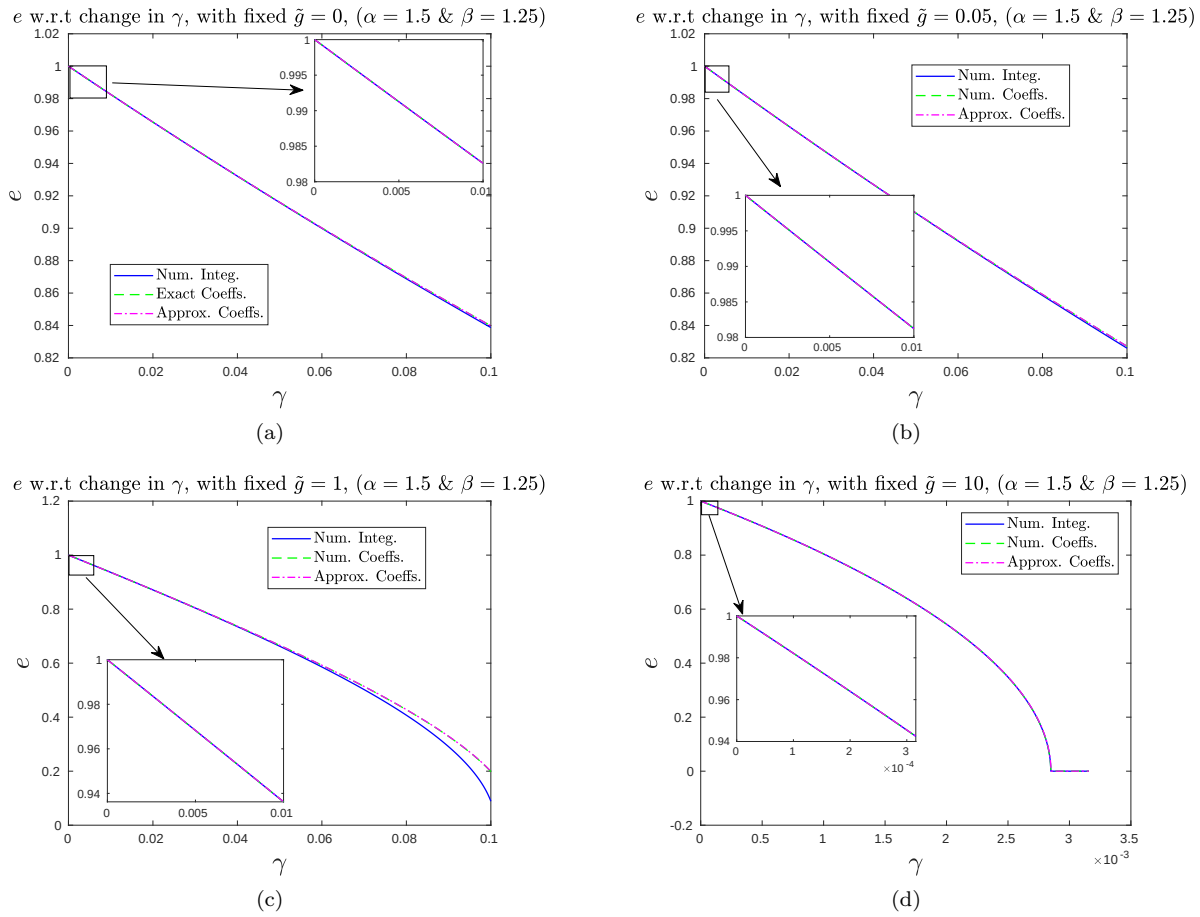

Figure 16: Comparison between the CoR values computed via numerical integration of (4), and the $\mathcal{O}(\gamma^2)$ approximations given by (36) (labeled *Num. Integ.*), using the numerically integrated functions $\mathcal{I}(\tilde{g})$ and $\mathcal{Q}(\tilde{g})$ from (41) and (42) (labeled *Num. Coeffs.*), and the approximated functions $\mathcal{I}(\tilde{g}(\theta)) = K(\theta)J_{\alpha,\beta}(\theta)$ and $\mathcal{Q}(\tilde{g}(\theta)) = L(\theta)M_{\alpha,\beta}(\theta)$ using (48) and (49) (labeled *Approx. Coeffs.*). When $\tilde{g} = 0$, the values $\mathcal{I}(0)$ and $\mathcal{Q}(0)$ are calculated using (39) and (40). Results are shown for the visco-elastic model with $\alpha = 3/2$ & $\beta = 5/4$ (*Tsuji-Tanaka-Ishida model*), for the cases: (a) $\tilde{g} = 0$, (b) $\tilde{g} = 0.05$, (c)$\tilde{g} = 1$, and (d) $\tilde{g} = 10$.

computed as:

$$\gamma = \gamma_0 v_0^{\frac{2\beta}{\alpha+1}-1} \left(\frac{k}{m}\right)^{1-\frac{\beta}{\alpha+1}}$$

$$\text{and,} \quad \tilde{g} = \left(\frac{m}{k}\right)^{\frac{1}{\alpha+1}} v_0^{\frac{-2\alpha}{\alpha+1}} \left(g + \frac{F}{m}\right)$$

After the re-scaled parameters of $\tilde{g}$ and γ are obtained, one may proceed to calculate the integrals $\mathcal{I}(\tilde{g})$ and $\mathcal{Q}(\tilde{g})$. These integrals can be calculated either numerically or analytically. Numerical integration would lead to more accurate results when $\tilde{g}$ is neither too large nor to small. However, small and large values of $\tilde{g}$ the analytical approximation is very accurate. The steps for computing the analytical approximation of $\mathcal{I}(\tilde{g})$ and $\mathcal{Q}(\tilde{g})$ are listed below:

1 Solve for $\theta \in [0, 1]$, such that $\tilde{g}(\theta) = \left(\frac{\alpha+1}{2\theta}\right)^{\frac{-1}{\alpha+1}} \left(\frac{1}{2\theta} - \frac{1}{2}\right)$. This can be obtained using the *Bisection Method*.

2 Using the value of θ directly evaluate the functions $K(\theta) = \frac{2}{\sqrt{\theta}}\left(\frac{\alpha+1}{2\theta}\right)^{\frac{\beta}{\alpha+1}}$ and $L(\theta) = \sqrt{\theta}\left(\frac{\alpha+1}{2\theta}\right)^{\frac{\beta}{\alpha+1}}$.

3 Next to evaluate the function $M_{\alpha,\beta}(\theta)$, first choose an order of approximation n (ideally $n = 21$).

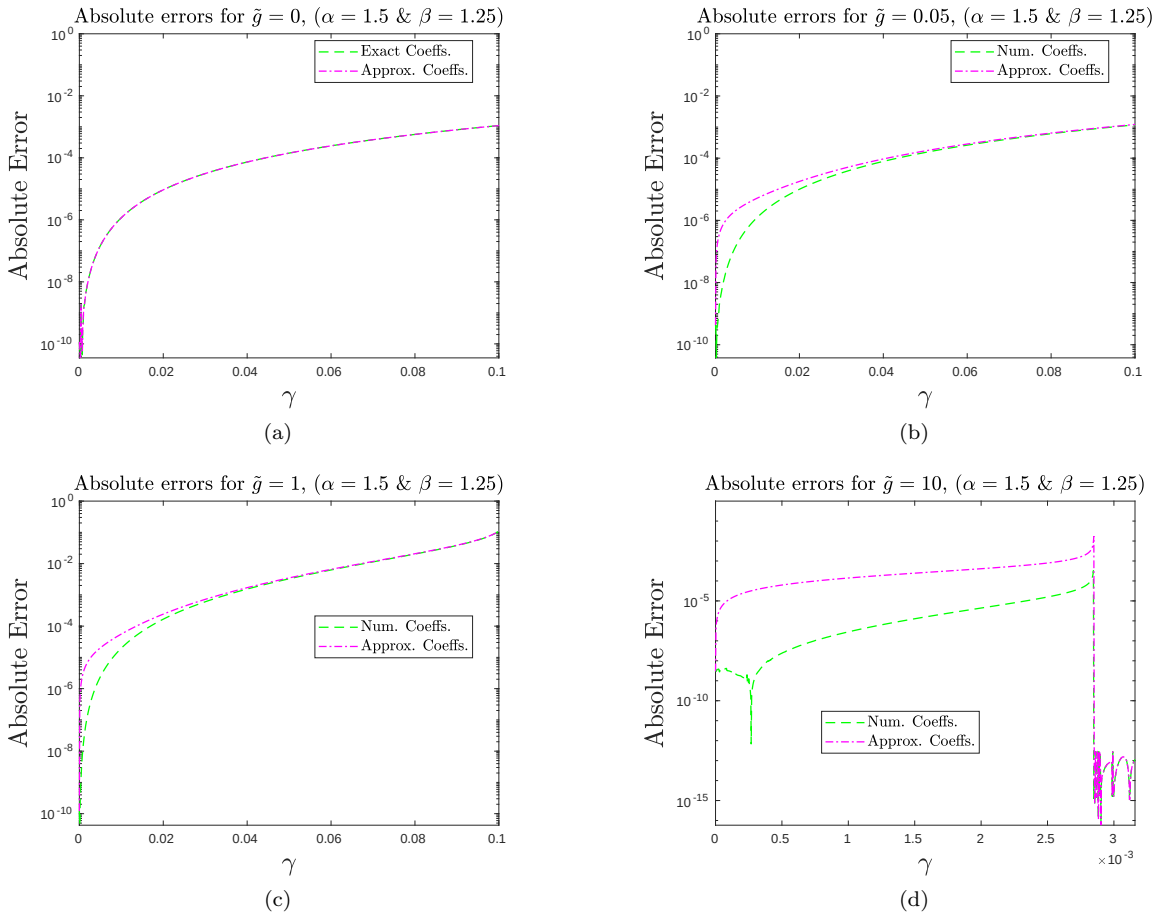

Figure 17: Absolute errors of the $\mathcal{O}(\gamma^2)$ CoR approximations (36) using the numerically integrated functions $\mathcal{I}(\tilde{g})$ and $\mathcal{Q}(\tilde{g})$ from (41) and (42) (labeled *Num. Coeffs.*), and the approximated functions $\mathcal{I}(\tilde{g}(\theta)) = K(\theta)J_{\alpha,\beta}(\theta)$ and $\mathcal{Q}(\tilde{g}(\theta)) = L(\theta)M_{\alpha,\beta}(\theta)$ from (48) and (49) (labeled *Approx. Coeffs.*). When $\tilde{g} = 0$, the results with the numerical results are replaced with the absolute error of $\mathcal{O}(\gamma^2)$ CoR computed with $\mathcal{I}(0)$ and $\mathcal{Q}(0)$ using (39) and (40) (labeled *Exact Coeffs.*).The absolute errors are computed in reference to the CoR values computed through numerical integration of (4). Results are shown for the visco-elastic model with $\alpha = 3/2$ & $\beta = 5/4$ (*Tsuji-Tanaka-Ishida model*), for the cases: (a) $\tilde{g} = 0$, (b) $\tilde{g} = 0.05$, (c)$\tilde{g} = 1$, and (d) $\tilde{g} = 10$.

Based on the choice of n the coefficients c_j and $a_{j,k}$ can be calculated using the relations in (50) and (53). Finally compute the $M_{\alpha,\beta}(\theta)$ approximation using (49).

4 Following the same procedure as in the previous step, compute $M_{\alpha,\alpha+\beta+1}(\theta)$ and $M_{\alpha,\beta+1}(\theta)$. Then use these values to compute $J_{\alpha,\beta}(\theta)$ according to (48).

5 Compute $\mathcal{I}(\tilde{g}(\theta)) = K(\theta)J_{\alpha,\beta}(\theta)$ and $\mathcal{Q}(\tilde{g}(\theta)) = L(\theta)M_{\alpha,\beta}(\theta)$, using (47).

Lastly, select the appropriate expansion from (36) to calculate the analytical approximation of e, using the values of $\mathcal{I}(\tilde{g}(\theta))$ and $\mathcal{Q}(\tilde{g}(\theta))$. The `MATLAB` implementation of the aforementioned method along with all numerical results presented in this report is available at the GitHub repository [38].

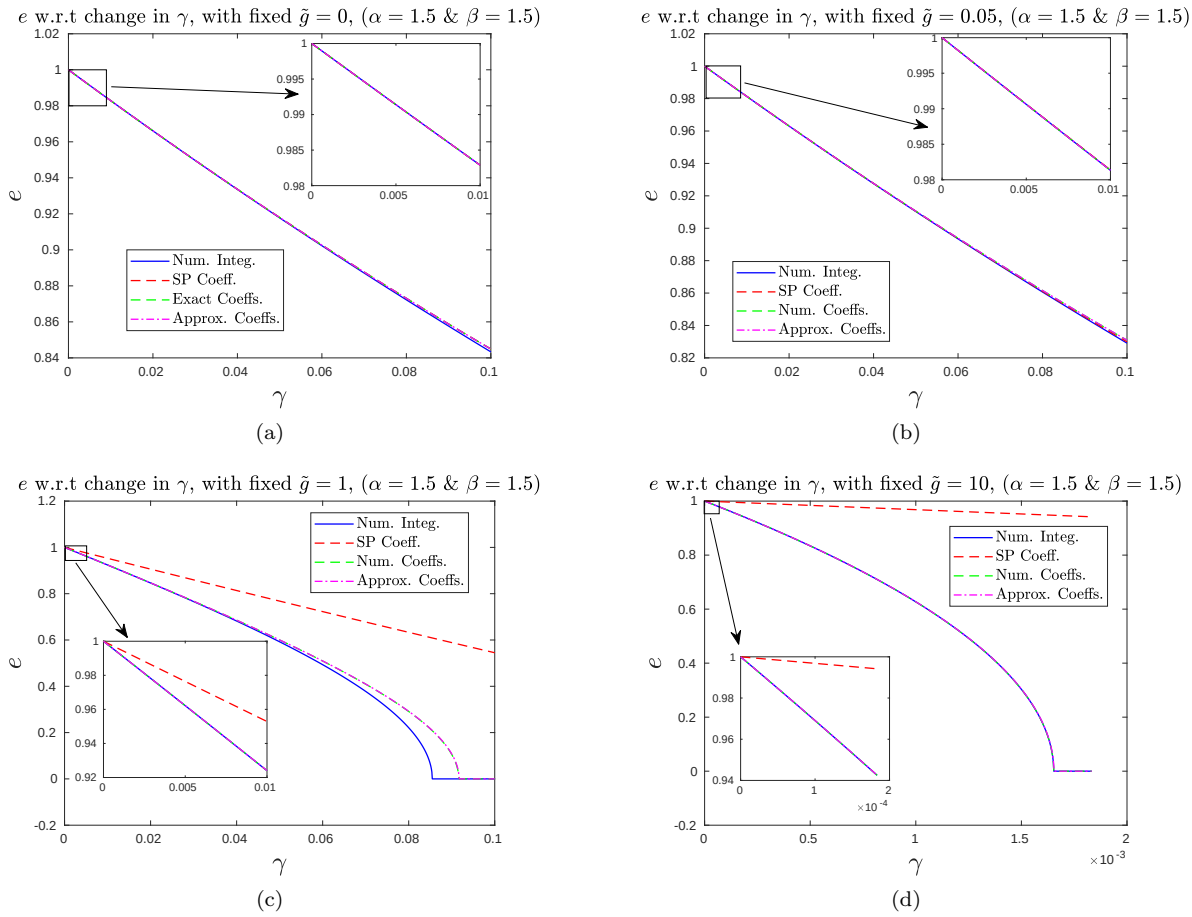

Figure 18: Comparison between the CoR values computed via numerical integration of (4), and the $\mathcal{O}(\gamma^2)$ approximations given by (36) (labeled *Num. Integ.*), using the numerically integrated functions $\mathcal{I}(\tilde{g})$ and $\mathcal{Q}(\tilde{g})$ from (41) and (42) (labeled *Num. Coeffs.*), and the approximated functions $\mathcal{I}(\tilde{g}(\theta)) = K(\theta)J_{\alpha,\beta}(\theta)$ and $\mathcal{Q}(\tilde{g}(\theta)) = L(\theta)M_{\alpha,\beta}(\theta)$ using (48) and (49) (labeled *Approx. Coeffs.*). When $\tilde{g} = 0$, the values $\mathcal{I}(0)$ and $\mathcal{Q}(0)$ are calculated using (39) and (40). Results are shown for the visco-elastic model with $\alpha = \beta = 3/2$(*Kuwabara-Kono model*), for the cases: (a) $\tilde{g} = 0$, (b) $\tilde{g} = 0.05$, (c)$\tilde{g} = 1$, and (d) $\tilde{g} = 10$. The Schwager-Pöschel coefficient based $\mathcal{O}(\gamma^2)$ approximation from (25) (30) is also included (labeled *SP Coeff.*).

6 Conclusion

The goal of this study was to derive an approximate analytical solution of Coefficient of Restitution (CoR) for a single bead impact, while considering the effects of external load. In this study, we derived several series expansions of the CoR based on a general nonlinear visco-elastic model and studied their accuracy with respect to calculations of CoR from numerical integration. First, a first-order expansion of CoR was obtained that linearly depended on a scaled parameter representing the external load and force due to gravity. We saw that this first-order approximation was only valid for small magnitudes of external loads and gravity. We then derived a second-order approximation, which while still linearly depending on gravity and external load, has a second-order dependence to the scaled parameter representing the damping (dissipation). To compute the unknown coefficient for this second-order term, we used a coefficient value from another study that assumed no external load or gravity in the derivation. The second-order CoR approximation that we obtained based on this coefficient value improved the CoR approximation for small magnitudes of small external load and gravitational force, but didn't perform well for higher forces. Hence, lastly we derived our final second-order approximation of the CoR with respect to the dissipation-dependent scaled parameter.

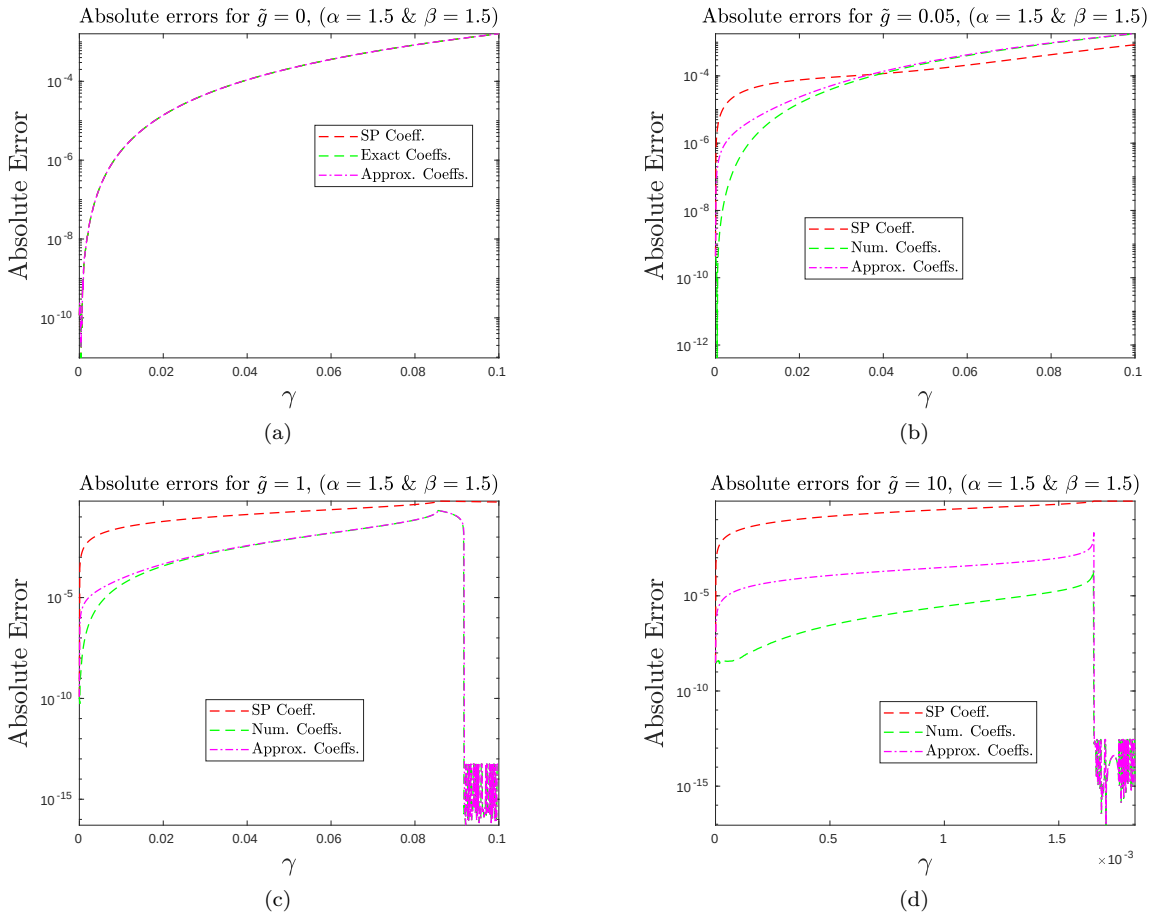

Figure 19: Absolute errors of the $\mathcal{O}(\gamma^2)$ CoR approximations (36) using the numerically integrated functions $\mathcal{I}(\tilde{g})$ and $\mathcal{Q}(\tilde{g})$ from (41) and (42) (labeled *Num. Coeffs.*), and the approximated functions $\mathcal{I}(\tilde{g}(\theta)) = K(\theta)J_{\alpha,\beta}(\theta)$ and $\mathcal{Q}(\tilde{g}(\theta)) = L(\theta)M_{\alpha,\beta}(\theta)$ from (48) and (49) (labeled *Approx. Coeffs.*). When $\tilde{g} = 0$, the results with the numerical results are replaced with the absolute error of $\mathcal{O}(\gamma^2)$ CoR computed with $\mathcal{I}(0)$ and $\mathcal{Q}(0)$ using (39) and (40) (labeled *Exact Coeffs.*).The absolute errors are computed in reference to the CoR values computed through numerical integration of (4). Results are shown for the visco-elastic model with $\alpha = \beta = 3/2$ (*Kuwabara-Kono model*), for the cases: (a) $\tilde{g} = 0$, (b) $\tilde{g} = 0.05$, (c)$\tilde{g} = 1$, and (d) $\tilde{g} = 10$.The absolute errors of Schwager-Pöschel coefficient based $\mathcal{O}(\gamma^2)$ approximation from (25) (30) are also included.

In this final second-order approximation, the coefficients obtained were functions of the applied force, hence this approximation was found to be very accurate for bot large and small magnitudes of external load and gravitational force.

A Condition for no detachment after impact for large $\tilde{g}$

The goal of this appendix is to approximate the solution of e for large $\tilde{g}$, using the expansion (8), and determine the value of $\tilde{g}_c$, such that $e = 0$, $\forall\ \tilde{g} \geq \tilde{g}_c$. Let us begin by rewriting (8) as,

$$e^2 = 1 - 2\gamma\beta\mathcal{I}(\tilde{g}) + \text{H.O.T.} \tag{54}$$

where,

$$\mathcal{I}(\tilde{g}) = \int_0^{T_0} \left(\frac{du_0}{d\tau}\right)^2 u_0^{\beta-1} d\tau \tag{55}$$

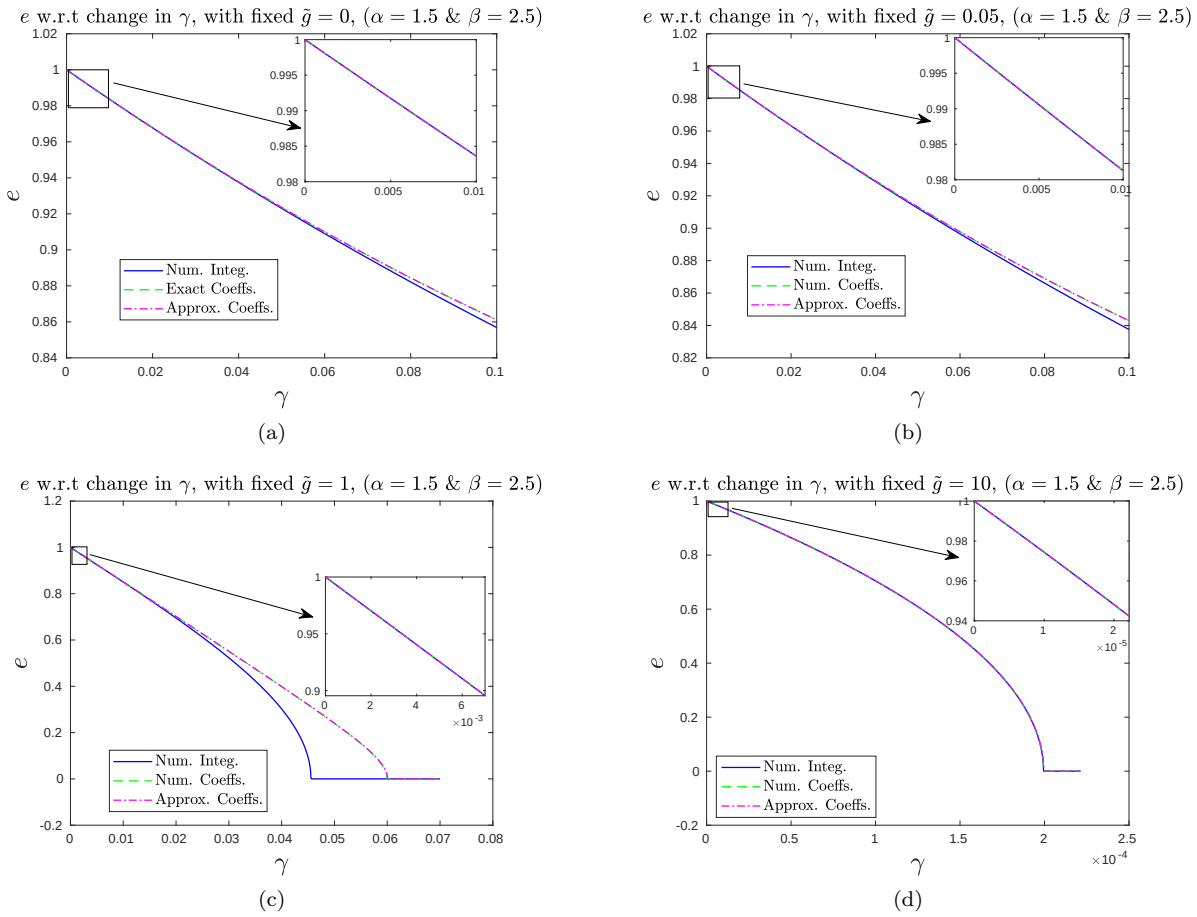

Figure 20: Comparison between the CoR values computed via numerical integration of (4), and the $\mathcal{O}(\gamma^2)$ approximations given by (36) (labeled *Num. Integ.*), using the numerically integrated functions $\mathcal{I}(\tilde{g})$ and $\mathcal{Q}(\tilde{g})$ from (41) and (42) (labeled *Num. Coeffs.*), and the approximated functions $\mathcal{I}(\tilde{g}(\theta)) = K(\theta)J_{\alpha,\beta}(\theta)$ and $\mathcal{Q}(\tilde{g}(\theta)) = L(\theta)M_{\alpha,\beta}(\theta)$ using (48) and (49) (labeled *Approx. Coeffs.*). When $\tilde{g} = 0$, the values $\mathcal{I}(0)$ and $\mathcal{Q}(0)$ are calculated using (39) and (40). Results are shown for the visco-elastic model with $\alpha = 3/2$ & $\beta = 5/2$ (*Simon-Hunt-Crossley model*), for the cases: (a) $\tilde{g} = 0$, (b) $\tilde{g} = 0.05$, (c)$\tilde{g} = 1$, and (d) $\tilde{g} = 10$.

where, T_0 corresponds to the final time at the end of the non-rebounding impact, when e reaches 0. Assuming symmetry about the maximal compression, we can rewrite the integral in (55) as,

$$\mathcal{I}(\tilde{g}) = 2\int_0^{\frac{T_0}{2}} \left(\frac{du_0}{d\tau}\right)^2 u_0^{\beta-1} d\tau \tag{56}$$

Since, we are considering the case when γ is small ($\gamma \ll 1$), the derivation of $\frac{du_0}{d\tau}$ given in (11) remains valid here, where it is given by,

$$\frac{du_0}{d\tau} = \left[1 + 2\left(\tilde{g}u_0 - \frac{{u_0}^{\alpha+1}}{\alpha+1}\right)\right]^{\frac{1}{2}}$$

The maximal deformation u_M, as shown earlier in (13), is given by the solution to the equation,

$$\frac{1}{\alpha+1}{u_M}^{\alpha+1} - \tilde{g}u_M = \frac{1}{2} \tag{57}$$

Since, here we consider a large $\tilde{g}$, (57) can be approximated as,

$$\tfrac{1}{\alpha+1}{u_M}^{\alpha+1} - \tilde{g}u_M \approx 0 \qquad \rightarrow \quad u_M = \tilde{g}^{\frac{1}{\alpha}} y \tag{58}$$

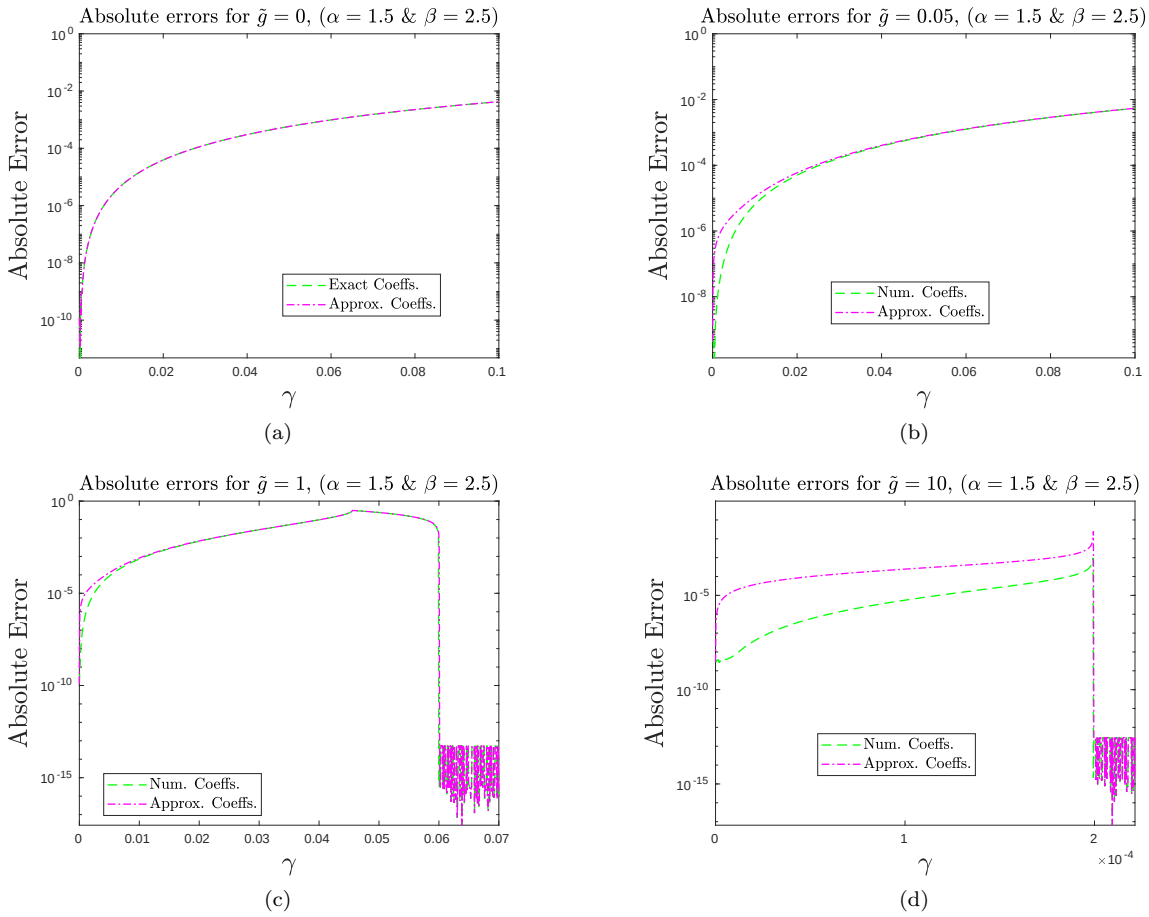

Figure 21: Absolute errors of the $\mathcal{O}(\gamma^2)$ CoR approximations (36) using the numerically integrated functions $\mathcal{I}(\tilde{g})$ and $\mathcal{Q}(\tilde{g})$ from (41) and (42) (labeled *Num. Coeffs.*), and the approximated functions $\mathcal{I}(\tilde{g}(\theta)) = K(\theta)J_{\alpha,\beta}(\theta)$ and $\mathcal{Q}(\tilde{g}(\theta)) = L(\theta)M_{\alpha,\beta}(\theta)$ from (48) and (49) (labeled *Approx. Coeffs.*). When $\tilde{g} = 0$, the results with the numerical results are replaced with the absolute error of $\mathcal{O}(\gamma^2)$ CoR computed with $\mathcal{I}(0)$ and $\mathcal{Q}(0)$ using (39) and (40) (labeled *Exact Coeffs.*).The absolute errors are computed in reference to the CoR values computed through numerical integration of (4). Results are shown for the visco-elastic model with $\alpha = 3/2$ & $\beta = 5/2$ (*Simon-Hunt-Crossley model*), for the cases: (a) $\tilde{g} = 0$, (b) $\tilde{g} = 0.05$, (c)$\tilde{g} = 1$, and (d) $\tilde{g} = 10$.

where $y = (1+\alpha)^{\frac{1}{\alpha}} + \mathcal{O}(\tilde{g}, \alpha)$ and is treated as an unknown at this point. Equation (58) intuitively approximates that the left-hand side of (57) becomes negligible, when $\tilde{g} \gg 1$; a more rigorous approximation is presented below.Next, substituting u_M from the approximation in (58) back into (57), we obtain,

$$\frac{1}{\alpha+1} y^{\alpha+1} \tilde{g}^{1+\frac{1}{\alpha}} - y\tilde{g}^{1+\frac{1}{\alpha}} = \frac{1}{2} \tag{59}$$

Now if we consider a parameter $\epsilon = \frac{1}{\tilde{g}^{1+\frac{1}{\alpha}}}$, which is very small since $\tilde{g} \gg 1$, then (59) can be rewritten as,

$$\frac{1}{\alpha+1} y^{\alpha+1} - y = \frac{\epsilon}{2} \tag{60}$$

The left-hand side of (60) depends upon the small value of ϵ, and thus validates the approximation shown earlier in (58). Since ϵ already depends on $\tilde{g}$ and α, we can rewrite the expansion of y as $y = (1+\alpha)^{\frac{1}{\alpha}} + \mathcal{O}(\epsilon)$, and also u_M as $u_M = [\tilde{g}(1+\alpha)]^{\frac{1}{\alpha}} + \mathcal{O}(\frac{1}{\tilde{g}})$. Now, considering the integral in (56), changing integration variable

Types of $\mathcal{I}$ & $\mathcal{Q}$	Exact[(39),(40)]/Num.[(41),(42)]		Approx.[(48),(49)]	
$\tilde{g}$	$\gamma < 0.02$	$\gamma \geq 0.02$	$\gamma < 0.02$	$\gamma \geq 0.02$
0	3.87×10^{-5}*	4.26×10^{-3}*	3.87×10^{-5}	4.26×10^{-3}
0.05	4.94×10^{-5}	5.39×10^{-3}	5.84×10^{-5}	5.43×10^{-3}
1	2.06×10^{-3}	3.11×10^{-1}	2.20×10^{-3}	3.11×10^{-1}

(a) Max. absolute errors within different γ ranges for $\tilde{g} = 0, 0.05,$ and, 1

Types of $\mathcal{I}$ & $\mathcal{Q}$	$\gamma < 0.00004$	$0.00004 \leq \gamma \leq 0.00020$	$\gamma > 0.00020$
Num.[(41),(42)]	3.83×10^{-7}	9.67×10^{-4}	2.84×10^{-13}
Approx.[(48),(49)]	8.57×10^{-5}	2.50×10^{-1}	2.84×10^{-13}

(b) Max. absolute errors within different γ for $\tilde{g} = 10$

Table 5: Maximum Absolute Errors on the $\mathcal{O}(\gamma^2)$ expansion of e using a visco-elastic model with $\alpha = 3/2$ and $\beta = 5/2$ (*Simon-Hunt-Crossley model*), with $\tilde{g} = 0$, 0.05, 1, and, 10, for various γ ranges. *Errors on $\mathcal{O}(\gamma^2)$ expansions of e while using the exact values of $\mathcal{I}(\tilde{g} = 0)$ and $\mathcal{Q}(\tilde{g} = 0)$, according to (39) and (40).

($\tau \to u_0$), and substituting the upper-bound as $u_0(\frac{T_0}{2}) = u_M = [\tilde{g}(1+\alpha)]^{\frac{1}{\alpha}}$, we get,

$$\mathcal{I}(\tilde{g}) = 2\int_0^{\tilde{g}^{\frac{1}{\alpha}}y} \left[1 + 2\left(\tilde{g}u_0 - \frac{{u_0}^{\alpha+1}}{\alpha+1}\right)\right]^{\frac{1}{2}} u_0^{\beta-1} du_0 \tag{61}$$

Let us now introduce a new variable y_0 and consider $u_0 = \tilde{g}^{\frac{1}{\alpha}}y_0$, which also implies $du_0 = \tilde{g}^{\frac{1}{\alpha}}dy_0$. Considering these substitution in (61) we obtain,

$$\mathcal{I}(\tilde{g}) = 2\int_0^{y} \left[1 + 2\tilde{g}^{1+\frac{1}{\alpha}}\left(y_0 - \frac{{y_0}^{\alpha+1}}{\alpha+1}\right)\right]^{\frac{1}{2}} \tilde{g}^{\frac{\beta}{\alpha}} y_0^{\beta-1} dy_0 = 2\tilde{g}^{\frac{\beta}{\alpha}+\frac{1}{2\alpha}+\frac{1}{2}} \int_0^{y} \left[\epsilon + 2\left(y_0 - \frac{y_0^{\alpha+1}}{\alpha+1}\right)\right]^{\frac{1}{2}} {y_0}^{\beta-1} dy_0 \tag{62}$$

Since, $\epsilon \approx 0$, the integral in (62) can be approximated as,

$$\mathcal{I}(\tilde{g}) = 2\sqrt{2}\tilde{g}^{\frac{\beta}{\alpha}+\frac{1}{2\alpha}+\frac{1}{2}} \int_0^{(1+\alpha)^{\frac{1}{\alpha}}} \left(1 - \frac{y_0^{\alpha}}{\alpha+1}\right)^{\frac{1}{2}} {y_0}^{\beta-\frac{1}{2}} dy_0 + \text{H.O.T.} \tag{63}$$

Now we can consider another change of variable with $t = \frac{{y_0}^{\alpha}}{\alpha+1}$, which also yields $dt = \frac{\alpha {y_0}^{\alpha-1}}{\alpha+1} dy_0$. Note that with this variable, $y_0 = y$, we get $t = \frac{y^{\alpha}}{\alpha+1} = \frac{\left[(1+\alpha)^{\frac{1}{\alpha}}\right]^{\alpha}}{\alpha+1} = 1$. Hence, after making these substitutions in (63) and simplifying, we obtain,

$$\mathcal{I}(\tilde{g}) = 2\sqrt{2}\left(\frac{\alpha+1}{\alpha}\right)(\alpha+1)^{\frac{\beta-\alpha+\frac{1}{2}}{\alpha}} \tilde{g}^{\left(\frac{\beta}{\alpha}+\frac{1}{2\alpha}+\frac{1}{2}\right)} \int_0^1 (1-t)^{\frac{1}{2}} t^{\frac{\beta-\alpha+\frac{1}{2}}{\alpha}} dt \tag{64}$$

The integral in (64), is in the form of Euler's beta function, which can be evaluated. Thus, substituting (64) into (54), and expressing the integral in terms of Euler's beta function, according to Def. 1, yields,

$$e^2 \approx 1 - 2\gamma C \tilde{g}^{\left(\frac{\beta}{\alpha}+\frac{1}{2\alpha}+\frac{1}{2}\right)} \tag{65}$$

where,

$$C = 2\sqrt{2}\frac{\beta}{\alpha}(\alpha+1)^{\left(\frac{\beta}{\alpha}+\frac{1}{2\alpha}\right)} \mathrm{B}\left(\frac{\beta+\frac{1}{2}}{\alpha}, \frac{3}{2}\right)$$

Thus, (65) presents an approximation for the expansion (54), corresponding to large $\tilde{g}$. Hence, (65) can be used to solve for $\tilde{g}_c \equiv \tilde{g}$, such that, $e = 0$,

$$\tilde{g}_c^{\left(\frac{\beta}{\alpha}+\frac{1}{2\alpha}+\frac{1}{2}\right)} \approx \frac{1}{2\gamma C} \tag{66}$$

The relationship (66), establishes a relationship between $\tilde{g}_c$ and the other parameters, namely α,β, and γ. The value of CoR remains $e = 0$ for any $\tilde{g} \geq \tilde{g}_c$.

B Order 2 expansion of e^2 around $\gamma \approx 0$

The main objective of this appendix is to formulate the quantity $\frac{\partial I}{\partial \gamma}(\gamma, \tilde{g})$ at $\gamma = 0$, which follows from the development presented in Sec. 4.2 on the $\mathcal{O}(\gamma^2)$ expansion of e^2. Let the solution of (31) for the non-dissipative case, $\gamma = 0$ be u_0, with the corresponding impact duration as T_0. We know that u_0 is *symmetric* around $\frac{T_0}{2}$ with $u_0(\frac{T_0}{2} + h) = u_0(\frac{T_0}{2} - h),\ \forall\ h \in [0, \frac{T_0}{2}]$, and from (13), that $u_M = u_0(\frac{T_0}{2})$, satisfies the constraint $\frac{1}{\alpha+1}u_M^{\alpha+1} - \tilde{g}u_M = \frac{1}{2}$. Also, we note that the scaled velocity $\frac{\partial u_0}{\partial \tau}$, is *anti-symmetric*, since $\frac{\partial u_0}{\partial \tau}(\frac{T_0}{2} + h) = -\frac{\partial u_0}{\partial \tau}(\frac{T_0}{2} - h),\ \forall\ h \in \left[0, \frac{T_0}{2}\right]$. In (35), we need to evaluate $\mathcal{I}$ and $\frac{\partial \mathcal{I}}{\partial \gamma}$ for $\gamma = 0$, so using the symmetric property we can rewrite the integral at $\gamma = 0$ as,

$$\mathcal{I}(0, \tilde{g}) = 2\int_0^{\frac{T_0}{2}} \left(\frac{\partial u_0}{\partial \tau}\right)^2 u_0^{\beta-1} d\tau \tag{67}$$

Using (11), we can rewrite the above expression as,

$$\mathcal{I}(0, \tilde{g}) = 2\int_0^{u_M} \left[1 + 2\left(\tilde{g}u_0 - \frac{u_0^{\alpha+1}}{\alpha+1}\right)\right]^{\frac{1}{2}} u_0^{\beta-1} du_0 \tag{68}$$

Similarly, when $\gamma = 0$, $\frac{\partial \mathcal{I}}{\partial \gamma}$ can be expressed as,

$$\frac{\partial \mathcal{I}}{\partial \gamma}(0, \tilde{g}) = \frac{1}{\beta}\int_0^{T_0} \frac{\partial u}{\partial \gamma}(0, \tau)\left[(\beta + \alpha)u_0^{\beta+\alpha-1} - \tilde{g}\beta u_0^{\beta-1}\right] d\tau \tag{69}$$

We need to find the expression $\frac{\partial u}{\partial \gamma}(0, \tau)$, to further evaluate (69). We may proceed towards this goal by differentiating (31) with respect to γ and then setting $\gamma = 0$,

$$\frac{\partial^2}{\partial \tau^2}\left(\frac{\partial u}{\partial \gamma}(0, \tau)\right) + \frac{\partial}{\partial \tau}(u_0^\beta) + \alpha u_0^{\alpha-1}\frac{\partial u}{\partial \gamma}(0, \tau) = 0 \tag{70}$$

Now, if we consider the variable $u_\gamma^0 = \frac{\partial u}{\partial \gamma}(0, \tau)$, we obtain a linear non-homogeneous ordinary differential equation of the form,

$$\frac{\partial^2 u_\gamma^0}{\partial \tau^2} + \alpha u_0^{\alpha-1}u_\gamma^0 + \frac{\partial}{\partial \tau}(u_0^\beta) = 0, \tag{71}$$

$$u_\gamma^0(0) = 0 \qquad \text{and} \qquad \frac{du_\gamma^0}{d\tau}(0) = 0.$$

If we consider the homogeneous part of (71), we can deduce that one of the solutions is $\frac{\partial u_0}{\partial \tau}$. We may check this by setting $\gamma = 0$ in (31) and differentiating it with respect to τ,

$$\frac{\partial^2}{\partial \tau^2}\left(\frac{\partial u_0}{\partial \tau}\right) + \alpha u_0^{\alpha-1}\left(\frac{\partial u_0}{\partial \tau}\right) = 0$$

Comparing the above equation with (71), we see that indeed $\frac{\partial u_0}{\partial \tau}$ is one of the solutions for the homogeneous ODE. Next we need to find a solution for the homogeneous system independent from $\frac{\partial u_0}{\partial \tau}$. Let this complementary solution be u_1, such that it satisfies the differential equation,

$$\frac{\partial^2 u_1}{\partial \tau^2} + \alpha u_0^{\alpha-1}u_1 = 0 \tag{72}$$

and the boundary condition,

$$\frac{\partial u_1}{\partial \tau}\left(\frac{T_0}{2}\right) = 0 \tag{73}$$

In order for u_1 to be independent of $\frac{\partial u_0}{\partial \tau}$, the Wronskian of these two solution, must be non-zero. Additionally, we note the that the differential equation in (71) does not have a dissipative term, which implies that the

Wronskian must be a constant. Thus, we may obtain the other boundary condition for the complementary solution u_1 by first setting the Wronskian to a non-zero constant and then solving for the $u_1(\frac{T_0}{2})$. The Wronskian for the complementary solutions, u_1 and $\frac{\partial u_0}{\partial \tau}$, is given by,

$$W = \begin{vmatrix} u_1 & \frac{\partial u_0}{\partial \tau} \\ \frac{\partial u_1}{\partial \tau} & \frac{\partial^2 u_0}{\partial \tau^2} \end{vmatrix} = u_1 \frac{\partial^2 u_0}{\partial \tau^2} - \frac{\partial u_0}{\partial \tau}\frac{\partial u_1}{\partial \tau} = \text{constant} \tag{74}$$

Thus, having defined the complementary solutions u_1 and $\frac{\partial u_0}{\partial \tau}$ and their associated Wronskian, W, we can define the particular solution of (71), via. the variation of parameter formulation as,

$$u_\gamma^0 = -\frac{\partial u_0}{\partial \tau}\int_0^\tau \frac{1}{W}\frac{\partial u_0^\beta}{\partial \tau}u_1 d\tau + u_1 \int_0^\tau \frac{1}{W}\frac{\partial u_0^\beta}{\partial \tau}\frac{\partial u_0}{\partial \tau}d\tau \tag{75}$$

Note that in (75), the particular solution is scaled by the reciprocal of W. Thus, we are allowed to choose any constant value for W. Here we choose the value of the Wronskian to be $W = 1$. Since, the Wronskian is a constant, now we can evaluate it at $\tau = \frac{T_0}{2}$,

$$\begin{aligned} W = W\left(\frac{T_0}{2}\right) &= u_1\left(\frac{T_0}{2}\right)\frac{\partial^2 u_0}{\partial \tau^2}\left(\frac{T_0}{2}\right) - \frac{\partial u_0}{\partial \tau}\left(\frac{T_0}{2}\right)\frac{\partial u_1}{\partial \tau}\left(\frac{T_0}{2}\right) \\ &= \left(\tilde{g} - u_M^\alpha\right) u_1\left(\frac{T_0}{2}\right) = 1 \end{aligned} \tag{76}$$

Thus, we can obtain the other boundary condition for u_1, as,

$$u_1\left(\frac{T_0}{2}\right) = \frac{1}{\tilde{g} - u_M^\alpha} \tag{77}$$

Additionally, we can also deduce the relationship,

$$\frac{\partial}{\partial \tau}\left(\frac{u_1}{\partial u_0/\partial \tau}\right) = -\frac{W}{\left(\partial u_0/\partial \tau\right)^2} = -\frac{1}{\left(\partial u_0/\partial \tau\right)^2} \tag{78}$$

Lastly, given that $W = 1$, the particular solution of u_γ^0 simplifies to,

$$u_\gamma^0 = -\frac{\partial u_0}{\partial \tau}\int_0^\tau \frac{\partial u_0^\beta}{\partial \tau}u_1 d\tau + u_1 \int_0^\tau \frac{\partial u_0^\beta}{\partial \tau}\frac{\partial u_0}{\partial \tau}d\tau \tag{79}$$

Since, the particular solution u_γ^0 is to be used in the evaluation $\frac{\partial \mathcal{I}}{\partial \gamma}(0, \tilde{g})$ in (69), which requires an integration over the domain $[0, T_0/2]$, we can further simplify (79) by considering the symmetry. We proceed by splitting u_γ^0 as,

$$u_\gamma^0 = y_a + z_a + y_s + w_a$$

where,

$$\begin{aligned} y_a &= -\frac{\partial u_0}{\partial \tau}\int_0^{T_0/2} \frac{\partial u_0^\beta}{\partial \tau}u_1 d\tau \quad \text{is anti-symmetric} \\ z_a &= -\frac{\partial u_0}{\partial \tau}\int_{T_0/2}^{\tau} \frac{\partial u_0^\beta}{\partial \tau}u_1 d\tau \quad \text{is anti-symmetric} \\ y_s &= u_1 \int_0^{T_0/2} \frac{\partial u_0^\beta}{\partial \tau}\frac{\partial u_0}{\partial \tau}d\tau \quad \text{is symmetric} \\ w_a &= u_1 \int_{T_0/2}^{\tau} \frac{\partial u_0^\beta}{\partial \tau}\frac{\partial u_0}{\partial \tau}d\tau \quad \text{is anti-symmetric} \end{aligned} \tag{80}$$

Since the function $(\beta+\alpha)u_0^{\beta+\alpha-1} - \tilde{g}\beta u_0^{\beta-1}$ is symmetric, the only non-vanishing term in (69) is given by,

$$\begin{aligned}\frac{\partial \mathcal{I}}{\partial \gamma}(0,\tilde{g}) &= \frac{1}{\beta}\int_0^{T_0} y_s\left[(\beta+\alpha)u_0^{\beta+\alpha-1} - \tilde{g}\beta u_0^{\beta-1}\right]d\tau \\ &= 2\left[\int_0^{T_0/2} u_0^{\beta-1}\left(\frac{\partial u_0}{\partial \tau}\right)^2 d\tau\right]\left[\int_0^{T_0/2} u_1\left((\beta+\alpha)u_0^{\alpha+\beta-1} - \tilde{g}\beta u_0^{\beta-1}\right)d\tau\right]\end{aligned} \tag{81}$$

In what follows, we will see that the second integral in (81) will become singular at upper-bound, $\frac{T_0}{2}$. Hence, to avoid this singularity, we proceed by integrating the second term up to $\tau_1 = \frac{T_0}{2} - \eta$, with $\eta > 0$. So the integration of the second term up to τ_1 can be performed via integration by parts,

$$\begin{aligned}J &= \int_0^{\tau_1} u_1\left[(\alpha+\beta)u_0^{\alpha+\beta-1} - \tilde{g}\beta u_0^{\beta-1}\right]d\tau \\ &= R(\tau_1) + \int_0^{\tau_1}\left(u_0^{\alpha+\beta} - \tilde{g}u_0^{\beta}\right)\frac{1}{(\partial u_0/\partial\tau)^2}d\tau\end{aligned} \tag{82}$$

where,

$$R(\tau_1) = \frac{u_1(\tau_1)}{\partial u_0/\partial\tau(\tau_1)}u_0^{\beta}(\tau_1)\left(u_0^{\alpha}(\tau_1) - \tilde{g}\right)$$

Next, using (31) for $\gamma = 0$, we can rewrite (82) as,

$$\begin{aligned}J &= R(\tau_1) - \int_0^{\tau_1} u_0^{\beta}\frac{\partial^2 u_0/\partial\tau^2}{(\partial u_0/\partial\tau)^2}d\tau \\ &= R(\tau_1) - \int_0^{\tau_1} u_0^{\beta}\frac{\partial}{\partial\tau}\left(\frac{1}{(\partial u_0/\partial\tau)^2}\right)d\tau \\ &= R(\tau_1) + \frac{u_0^{\beta}(\tau_1)}{\partial u_0/\partial\tau(\tau_1)} - \beta\int_0^{\tau_1} u_0^{\beta-1}d\tau\end{aligned} \tag{83}$$

Since, $\tau_1 = \frac{T_0}{2} - \eta$, the first term in (83) can be evaluated as,

$$\begin{aligned}R(\tau_1) + \frac{u_0^{\beta}(\tau_1)}{\partial u_0/\partial\tau(\tau_1)} &= \frac{u_0^{\beta}(\tau_1)}{\partial u_0/\partial\tau(\tau_1)}\left[u_1(\tau_1)\left(u_0^{\alpha}(\tau_1) - \tilde{g}\right) + 1\right] \\ &= \frac{u_0^{\beta}(\tau_1)}{\partial u_0/\partial\tau(\tau_1)}\left[1 - u_1(\tau_1)\frac{\partial^2 u_0}{\partial\tau}\right]\end{aligned} \tag{84}$$

Note that, given the denominator of $\partial u_0/\partial\tau(\tau_1)$ would cause (84) to be singular, if $\tau_1 \to T_0/2$. Thus, to circumvent this issue, we replace the 1 in (84) with the Wronskian W, (since we had chosen $W = 1$), and then compensate for the singularity to yield,

$$R(\tau_1) + \frac{u_0^{\beta}(\tau_1)}{\partial u_0/\partial\tau(\tau_1)} = \frac{u_0^{\beta}(\tau_1)}{\partial u_0/\partial\tau(\tau_1)}\left[W - u_1(\tau_1)\frac{\partial^2 u_0}{\partial\tau}\right] = -u_0^{\beta}(\tau_1)\frac{\partial u_1}{\partial\tau}(\tau_1) \tag{85}$$

Since, we have the boundary condition $\frac{\partial u_1}{\partial\tau}(T_0/2) = 0$, the right-hand side of the above equation limits to zero,

$$\lim_{\tau_1 \to \frac{T_0}{2}} R(\tau_1) + \frac{u_0^{\beta}(\tau_1)}{\partial u_0/\partial\tau(\tau_1)} = 0 \tag{86}$$

Thus, using the results of (83) and (86) for $\tau_1 \to \frac{T_0}{2}$ in (82) we obtain,

$$J = -\beta\int_0^{T_0/2} u_0^{\beta-1}d\tau \tag{87}$$

Substituting (87) into (81), we get the final expression for $\frac{\partial \mathcal{I}}{\partial \tau}(0,\tilde{g})$,

$$\frac{\partial \mathcal{I}}{\partial \gamma}(0,\tilde{g}) = -2\beta \left[\int_0^{T_0/2} u_0^{\beta-1}\left(\frac{\partial u_0}{\partial \tau}\right)^2 d\tau\right]\left[\int_0^{T_0/2} u_0^{\beta-1} d\tau\right] = -\beta \mathcal{I}(0,\tilde{g}) \int_0^{\tau_1} u_0^{\beta-1} d\tau \tag{88}$$

Now, we can substitute (88) into (35) to obtain an expression for e^2,

$$e^2 = 1 - 2\beta \mathcal{I}(0,\tilde{g})\gamma + 2\beta^2 \mathcal{I}(0,\tilde{g})\mathcal{Q}(0,\tilde{g})\gamma^2 + \mathcal{O}(\gamma^3) \tag{89}$$

with,

$$\mathcal{Q}(0,\tilde{g}) = \int_0^{T_0/2} u_0^{\beta-1} d\tau$$

Using (89) we can obtain the value of CoR as $e = \sqrt{e_+^2}$, where $e_+^2 = \max(0, e^2)$. Note that the evaluating (89) can lead to $e^2 < 0$, therefore the square-root needs to be performed on e_+^2. We may also obtain an approximate expression for e, by using the expansion $(1+\epsilon)^{\frac{1}{2}} = 1 + \frac{\epsilon}{2} - \frac{\epsilon^2}{8} + \mathcal{O}(\epsilon^3)$ on (89),

$$e = 1 - \beta \mathcal{I}(0,\tilde{g})\gamma + \beta^2 \mathcal{I}(0,\tilde{g}) \left[\mathcal{Q}(0,\tilde{g}) - \frac{1}{2}\mathcal{I}(0,\tilde{g})\right]\gamma^2 + \mathcal{O}(\gamma^3) \tag{90}$$

Hence, we have now obtained two approximations for the CoR. The first one depends on computing e^2 using (89) followed by evaluating the CoR as $e = \sqrt{e_+^2}$, where $e_+^2 = \max(0, e^2)$. The second approximation is based on the linearization of e^2 obtained from (89), and is given by (90). Both of these approximations depend on the integral quantities $\mathcal{I}(\tilde{g})$ and $\mathcal{Q}(\tilde{g})$ that do not have explicit solutions when $\tilde{g} \neq 0$. One needs further approximations for the integrals $\mathcal{I}(\tilde{g})$ and $\mathcal{Q}(\tilde{g})$ to be able to analytically evaluate the CoR for a given impact. Appendix C presents further approximations of $\mathcal{I}(\tilde{g})$ and $\mathcal{Q}(\tilde{g})$ that will help us analytically evaluate the value for e. However before proceeding further, since we have obtained two approximations for e in this section, it is important to study the validity of these approximations. Figure 22 presents comparisons for e using the two approximations in (89) and (35) with the *Kuwabara-Kono model* ($\alpha = \beta = 3/2$) for $\tilde{g}$ = 0,0.05,1, and 10. The plots labeled *Num. Integ.* represent the values of e computed via the numerical integration of (4), whereas the plots labeled $e = \sqrt{e_+^2}$, $\mathcal{O}(\gamma^2)$ *(Num. Coeffs.)* and *Lin. e*, $\mathcal{O}(\gamma^2)$ *(Num. Coeffs.)* are the approximations of e using (89) and (35) respectively, with the integrals $\mathcal{I}(\tilde{g})$ and $\mathcal{Q}(\tilde{g})$ computed via numerical integration. Figure 22(a) corresponding to the case when $\tilde{g} = 0$, has the plots labeled $e = \sqrt{e_+^2}$, $\mathcal{O}(\gamma^2)$ *(Exact Coeffs.)* and *Lin. e*, $\mathcal{O}(\gamma^2)$ *(Exact Coeffs.)* instead, denoting that the integrals $\mathcal{I}(\tilde{g}=0)$ and $\mathcal{Q}(\tilde{g}=0)$ can be computed exactly in terms of Euler's Beta function, as shown in (39) and (40). The Fig. 22 also includes the results obtained using the Schwager-Pöschel based approximations, which are labeled as *SP Coeff.*. The absolute errors of all approximations in Fig. 22 with respect to the reference of the values obtained via numerical integration of (4), are reported in Fig. 23.

Examining the results in Fig. 22 and Fig. 23, we can firstly observe that all approximations work well when both γ and $\tilde{g}$ are small. However, as we had observed earlier, the approximation using the Schwager-Pöschel coefficient doesn't work well as γ and $\tilde{g}$ are increased. Among the two approximations derived in this section, it appears that while both approximation appear to work well for small $\tilde{g}$, as $\tilde{g}$ value increase the linearized approximation in (35) performs poorly compared to (89) for high γ values. This shows that the approximation based on $e = \sqrt{e_+^2}$ with (89) is best suited for high $\tilde{g}$. However, careful observation of the absoulte error in Fig. 23 also reveals that the linearized expansion in (35 is slightly more accurate than the approximation using $e = \sqrt{e_+^2}$ for small values of $\tilde{g}$, as can be seen from Fig. 23(a) and Fig. 23(b). Hence, based on these results we can conclude that both these approximations are valid within certain ranges of values of γ and $\tilde{g}$.

We have seen that the linearized expression in (90) is more accurate when $\tilde{g}$ is small, and contrarilty the approximation $e = \sqrt{e_+^2}$ is more accurate when $\tilde{g}$ is large. Therefore, a condition may be used to select between (89) and (90), depending upon the value of $\tilde{g}$ and γ. In numerical computations we observe that the two approximations tend to overestimate the CoR, hence it is interesting to choose the smallest approximation.

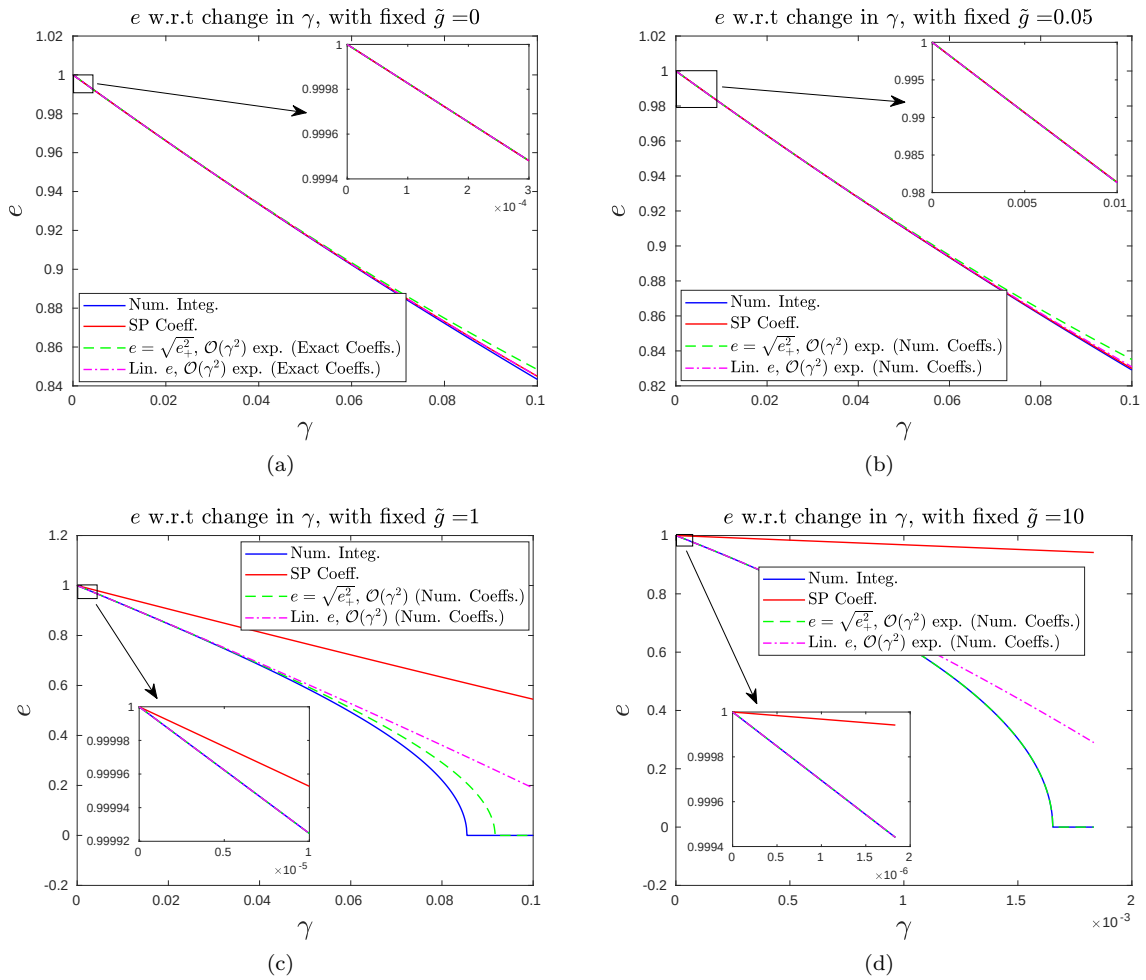

Figure 22: Comparison between the CoR values computed via numerical integration of (4), and the two CoR $\mathcal{O}(\gamma^2)$ approximations presented in (89) (labeled $e = \sqrt{e_+^2},\ \mathcal{O}(\gamma^2)$ *(Num. Coeffs.)*) and (90) (labeled *Lin. e,* $\mathcal{O}(\gamma^2)$ *(Num. Coeffs.)*), with the functions $\mathcal{I}(\tilde{g})$ and $\mathcal{Q}(\tilde{g})$ computed via numerical integration of (41) and (42). In case of $\tilde{g} = 0$, the values of $\mathcal{I}(0)$ and $\mathcal{Q}(0)$ are explicitly calculated using (39) and (40), so the corresponding labels have been replaced by $e = \sqrt{e_+^2},\ \mathcal{O}(\gamma^2)$ *(Exact Coeffs.)* and *Lin. e,* $\mathcal{O}(\gamma^2)$ *(Exact Coeffs.)*. Results are shown for the visco-elastic model with $\alpha = \beta = 3/2$ (*Kuwabara-Kono model*), for the cases: (a) $\tilde{g} = 0$, (b) $\tilde{g} = 0.05$, (c)$\tilde{g} = 1$, and (d) $\tilde{g} = 10$. Additionally the Schwager-Pöschel coefficient based $\mathcal{O}(\gamma^2)$ approximation [using (30)] results are also shown.

C Approximation of $J_{\alpha,\beta}(\theta)$ and $M_{\alpha,\beta}(\theta)$

The goal of the development presented in this appendix is to find approximations for the functions $J_{\alpha,\beta}(\theta)$ and $M_{\alpha,\beta}(\theta)$, which are related to the the integral quantities $\mathcal{I}(\tilde{g}(\theta)) = K(\theta)J_{\alpha,\beta}(\theta)$ and $\mathcal{Q}(\tilde{g}(\theta)) = L(\theta)M_{\alpha,\beta}(\theta)$, which are required for the $\mathcal{O}(\gamma^2)$ expansion of CoR in (36). The parameter θ for these functions maps the value of $\tilde{g}$ such that: $\theta = 1 \implies \tilde{g} = 0$ and $\theta \to 0 \implies \tilde{g} \to \infty$. The functions $J_{\alpha,\beta}(\theta)$ and $M_{\alpha,\beta}(\theta)$ themselves are integrals, and are given by,

$$J_{\alpha,\beta}(\theta) = \int_0^1 \left[\theta + (1-\theta)x - x^{\alpha+1}\right]^{\frac{1}{2}} x^{\beta-1} dx \quad \text{and} \quad M_{\alpha,\beta}(\theta) = \int_0^1 \left[\theta + (1-\theta)x - x^{\alpha+1}\right]^{-\frac{1}{2}} x^{\beta-1} dx \tag{91}$$

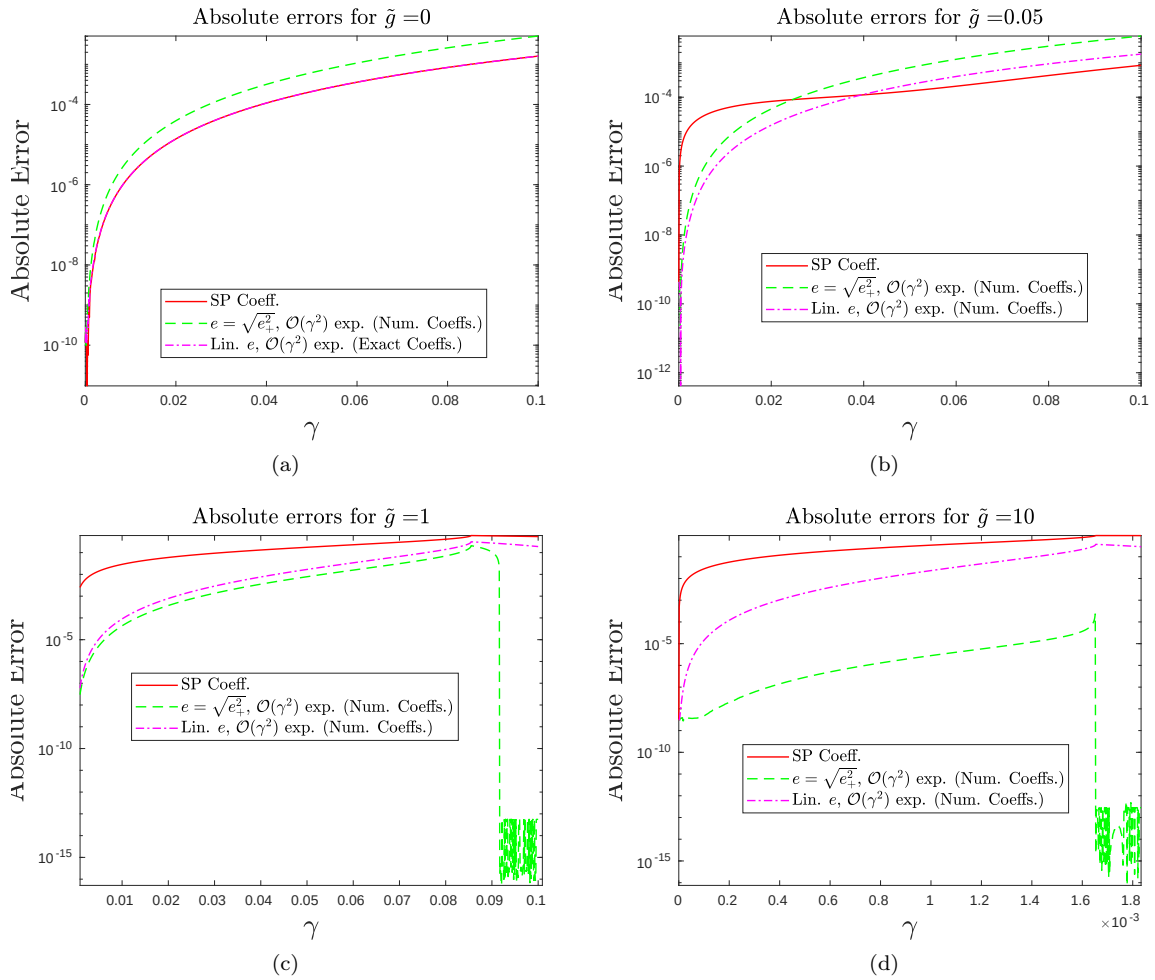

Figure 23: Absolute errors of the two $\mathcal{O}(\gamma^2)$ CoR approximations given in (89) (labeled $e = \sqrt{e_+^2}$, $\mathcal{O}(\gamma^2)$ *(Num. Coeffs.)*) and (90) (labeled *Lin.* e, $\mathcal{O}(\gamma^2)$ *(Num. Coeffs.)*), with the functions $\mathcal{I}(\tilde{g})$ and $\mathcal{Q}(\tilde{g})$ computed via numerical integration of (41) and (42). In case of $\tilde{g} = 0$, the values of $\mathcal{I}(0)$ and $\mathcal{Q}(0)$ are explicitly calculated using (39) and (40), so the corresponding labels have been replaced by $e = \sqrt{e_+^2}$, $\mathcal{O}(\gamma^2)$ *(Exact Coeffs.)* and *Lin.* e, $\mathcal{O}(\gamma^2)$ *(Exact Coeffs.)*. The absolute errors are calculated in reference to CoR values computed through numerical integration of (4). Results are shown for the visco-elastic model with $\alpha = \beta = 3/2$ (*Kuwabara-Kono model*), for the cases: (a) $\tilde{g} = 0$, (b) $\tilde{g} = 0.05$, (c)$\tilde{g} = 1$, and (d) $\tilde{g} = 10$. The absolute errors of Schwager-Pöschel coefficient based $\mathcal{O}(\gamma^2)$ approximation [using (30)] with respect to the numerically integrated CoRs are also included for comparison.

To approximate the integrals $J_{\alpha,\beta}(\theta)$ and $M_{\alpha,\beta}(\theta)$, we will follow the approach of finding equivalent approximations for the integrands of these functions that can be integrated in closed-form.However, observing the structure of the two integrals $J_{\alpha,\beta}(\theta)$ and $M_{\alpha,\beta}(\theta)$, it appears that they can be related to one another. If we multiply $M_{\alpha,\beta}$ with $1-\theta$, we obtain the relationship,

$$
\begin{aligned}
(1-\theta)M_{\alpha,\beta}(\theta) &= \int_0^1 \left[\theta + (1-\theta)x - x^{\alpha+1}\right]^{-\frac{1}{2}} (1-\theta)x^{\beta-1}dx \\
\implies (1-\theta)M_{\alpha,\beta}(\theta) &= \int_0^1 \left[\theta + (1-\theta)x - x^{\alpha+1}\right]^{-\frac{1}{2}} \left[(1-\theta) - (\alpha+1)x^{\alpha} + (\alpha+1)x^{\alpha+1}\right] x^{\beta-1}dx
\end{aligned}
$$

which yields the relationship,

$$(1-\theta)M_{\alpha,\beta}(\theta) = -2(\beta-1)J_{\alpha,\beta-1}(\theta) + (\alpha+1)M_{\alpha,\alpha+\beta}(\theta) \tag{92}$$

Thus, through a substitution of $\beta = \beta + 1$ in the relationship (92), we can obtain a definition of the integral $J_{\alpha,\beta}$ in terms of the integral $M_{\alpha,\beta}(\theta)$,

$$J_{\alpha,\beta}(\theta) = \frac{\alpha+1}{2\beta}M_{\alpha,\alpha+\beta+1}(\theta) + \frac{\theta-1}{2\beta}M_{\alpha,\beta+1}(\theta) \tag{93}$$

Hence, we only need to find the approximation for $M_{\alpha,\beta}(\theta)$ to obtain a complete solution. Let us rewrite the integral $M_{\alpha,\beta}(\theta)$ as,

$$M_{\alpha,\beta}(\theta) = \int_0^1 f_{\alpha,\theta}(x)x^{\beta-1}dx \tag{94}$$

where,

$$f_{\alpha,\beta}(x) = \left[\theta + (1-\theta)x - x^{\alpha+1}\right]^{-\frac{1}{2}} \tag{95}$$

Using Definition 1, the values of $M_{\alpha,\beta}(\theta)$ at $\theta = 0$ and $\theta = 1$, can be directly evaluated as,

$$\begin{aligned} M_{\alpha,\beta}(0) &= \int_0^1 (1-x^{\alpha})^{-1/2}x^{\beta-3/2}dx = \frac{1}{\alpha}B\left(\frac{\beta-1/2}{\alpha}, \frac{1}{2}\right) \\ M_{\alpha,\beta}(1) &= \int_0^1 \left(1-x^{\alpha+1}\right)^{-1/2}x^{\beta-1}dx = \frac{1}{\alpha+1}B\left(\frac{\beta}{\alpha+1}, \frac{1}{2}\right) \end{aligned} \tag{96}$$

Based on the integrand evaluations at the end-points, we can approximate the function $f_{\alpha,\theta}(x)$ in the integral as,

$$f_{\alpha,\theta}(x) = \left[\theta + (1-\theta)x - x^{\alpha+1}\right]^{-\frac{1}{2}} \simeq \left(x^{1-\theta} - x^{\alpha+1}\right)^{-1/2}p_n(x) \tag{97}$$

where $p_n(x)$ is a polynomial of degree n, such that $p_n(x) = 1$ when $\theta = 0$ and $\theta = 1$ to satisfy the end-point integral expressions of $M_{\alpha,\beta}(0)$ and $M_{\alpha,\beta}(1)$. Now to obtain the desired polynomial $p_n(x)$, we rewrite (97) as,

$$h_{\alpha,\theta}(x) = \left(\frac{x^{1-\theta} - x^{\alpha+1}}{\theta + (1-\theta)x - x^{\alpha+1}}\right)^{\frac{1}{2}} \simeq p_n(x) \tag{98}$$

Hence, our goal now is to determine the polynomial $p_n(x)$ that approximates $h_{\alpha,\theta}(x)$ when $\theta \in [0,1]$. We can achieve by interpolating the function $h_{\alpha,\theta}(x)$ at a number of interpolation points in $x \in [0,1]$. However, in order to approximate the function $h_{\alpha,\theta}(x)$ with a polynomial, a finer mesh of interpolation points are required near $x \to 0$, compared to $x \to 1$. Thus, we will use Chebyshev nodes for this interpolation. For this purpose, we will first symmetrize the function over the domain $x \in [0,2]$, by defining,

$$\tilde{h}_{\alpha,\theta}(x) = \begin{cases} h_{\alpha,\theta}(x) & \text{if} \quad x \in [0,1] \\ \\ h_{\alpha,\theta}(2-x) & \text{if} \quad x \in [1,2] \end{cases} \tag{99}$$

The Chebyshev nodes over the range $[0,2]$ are defined as,

$$x_k = \cos\left(\pi\frac{2k+1}{2n+2}\right) + 1, \quad k \in \mathbb{N} \tag{100}$$

Thus, the interpolation points for the polynomial $p_n(x)$ over the domain $[0,1]$ are defined as $\left(x_k, \tilde{h}_{\alpha,\beta}(x_k)\right)$, with $k \in \mathbb{N}$ and $(n+1)/2 \leq k \leq n$ (Assuming n to be an odd number). Our approach would be to define the polynomial $p_n(x)$ using the Chebyshev polynomial basis, and then use some properties of Chebyshev polynomials to obtain a series solution for $M_{\alpha,\beta}(\theta)$. In this approach, we define the polynomial $p_n(x)$ as,

$$p_n(x) = \sum_{j=0}^{n} c_j T_j(x-1) \tag{101}$$

where $T_j(y) = \cos(j \arccos y)$, for $y \in [-1, 1]$ are the Chebyshev polynomials of the first kind. Next using the orthogonality property of Chebyshev polynomials the coefficients c_j can be solved as,

$$\begin{cases} c_0 &= \dfrac{1}{n+1} \displaystyle\sum_{k=0}^{n} \tilde{h}_{\alpha,\theta}(x_k) \\ c_j &= \dfrac{2}{n+1} \displaystyle\sum_{k=0}^{n} \tilde{h}_{\alpha,\theta}(x_k) \cos\left(j\pi \dfrac{2k+1}{2n+2}\right), \qquad 1 \le j \le n \end{cases} \tag{102}$$

Assuming n odd, and using the symmetry of $\tilde{h}_{\alpha,\theta}(x)$ (such that, $x_{n-k} = 2 - x_k$ and $\tilde{h}_{\alpha,\theta}(x_{n-k}) = \tilde{h}_{\alpha,\theta}(x_k)$), the coefficients may be collected as,

$$\begin{cases} c_0 &= \dfrac{2}{n+1} \displaystyle\sum_{k=(n+1)/2}^{n} h_{\alpha,\theta}(x_k) \\ c_j &= \dfrac{4}{n+1} \displaystyle\sum_{k=(n+1)/2}^{n} h_{\alpha,\theta}(x_k) \cos\left(j\pi \dfrac{2k+1}{2n+2}\right), \qquad \text{if} \quad j \ge 2 \text{ and is even} \\ c_j &= 0, \qquad \text{if} \quad j \ge 2 \text{ and is odd} \end{cases} \tag{103}$$

Thus, with the values of c_j we can approximate $h_{\alpha,\beta}(x) \simeq p_n(x)$. The order n used for the polynomial approximation is important. Figures 24 and 25 show the approximations $h_{\alpha,\beta}(x) \simeq p_n(x)$ and their errors for different values of the polynomial order n. As we can note that small values of n lead to larger aggregate errors, whereas large n correspond to small aggregate errors but large local errors between interpolation points. Thus an intermediate value of n is appropriate. Based on the results in Figures 24 and 25 we can conclude that $n = 21$ gives the best overall approximation results. Therefore, we choose $n = 21$ for the remaining of the computations.

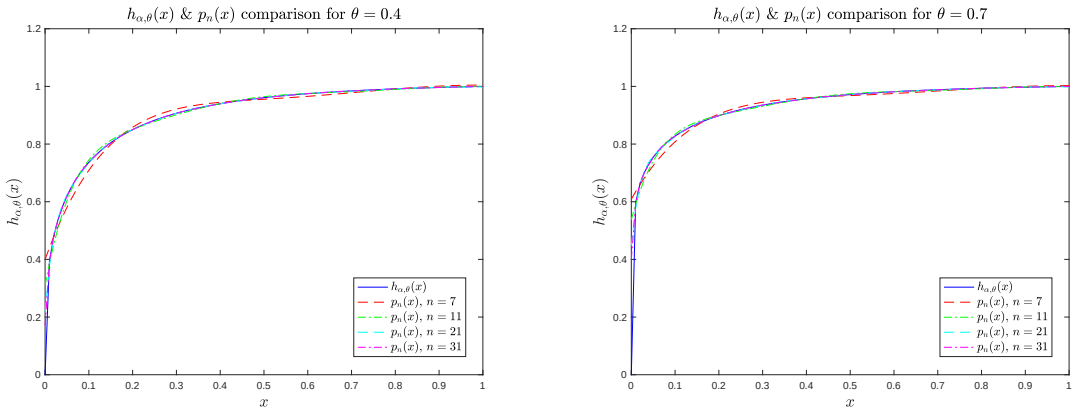

(a) (b)

Figure 24: Polynomial approximation of $h_{\alpha,\theta}(x)$, (a) $\theta = 0.4$ and (b) $\theta = 0.7$

Now having determined the coefficients c_j, we are now ready to derive the approximation for the integral $M_{\alpha,\beta}(\theta)$,

$$M_{\alpha,\beta}(\theta) = \int_0^1 h_{\alpha,\beta}(\theta)\left(x^{1-\theta} - x^{\alpha+1}\right)^{-\frac{1}{2}} x^{\beta-1} dx \simeq \int_0^1 p_n(x)\left(1 - x^{\alpha+\theta}\right)^{-\frac{1}{2}} x^{\beta+\theta/2-3/2} dx \tag{104}$$

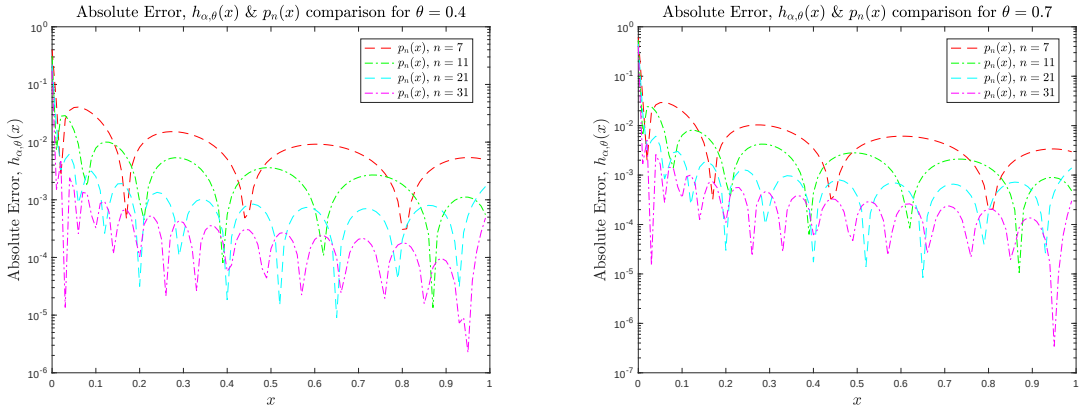

(a) (b)

Figure 25: Errors in Polynomial approximation of $h_{\alpha,\theta}(x)$, (a) $\theta = 0.4$ and (b) $\theta = 0.7$

Thus, using the definition of $p_n(x)$ from (101), we may write the approximation of $M_{\alpha,\beta}(\theta)$ as,

$$\begin{aligned} M_{\alpha,\beta}(\theta) &\simeq \sum_{j=0}^{n-1} c_j a_{j,0} \ , \quad \text{with,} \quad j \text{ even} \\ \text{where,} \quad a_{j,k} &= \int_0^1 T_j(x-1)\big(1-x^{\alpha+\theta}\big)^{-\frac{1}{2}} x^{\beta+\theta/2-3/2+k} dx \end{aligned} \tag{105}$$

Now we can use the recurrence relation properties on the Chebyshev polynomials of the first kind $T_j(x)$ to derive a sequential solution for $a_{j,k}$. The recurrence relation for the Chebyshev polynomials of the first kind is given by,

$$\begin{aligned} T_{j+2} &= 2xT_{j+1}(x) - T_j(x) \quad \text{for} \quad j \geq 0 \\ \text{with,} \quad T_0(x) &= 1 \quad \text{and} \quad T_1(x) = x \end{aligned} \tag{106}$$

Therefore, the recurrence relation of the Chebyshev polynomials in (106) can be used to yield a sequential solution for $a_{j,k}$, when $j \geq 0$

$$\begin{aligned} a_{j+2,k} &= \int_0^1 2(x-1)T_{j+1}(1-x)^{-1/2} x^{\beta+\theta/2-3/2+k} dx - a_{j,k} \\ \implies \qquad a_{j+2,k} &= 2a_{j+1,k+1} - 2a_{j+1,k} - a_{j,k} \end{aligned} \tag{107}$$

Similarly, due to the the first two Chebyshev polynomials $T_1(x) = x$ and $T_0(x) = 1$, we obtain the values,

$$a_{0,k} = \frac{1}{\alpha+\theta} B\left(\frac{\beta+k-1/2+\theta/2}{\alpha+\theta}, \frac{1}{2}\right) \quad \text{and} \quad a_{1,k} = a_{0,k+1} - a_{0,k} \tag{108}$$

Thus, the quantities $a_{j,k}$ can be determined reccurently. After obtaining all values of $a_{j,k}$, one can use the $a_{j,0}$ values and the c_j values to obtain an approximation for $M_{\alpha,\beta}(\theta)$. Again, using the relation (48), $J_{\alpha,\beta}(\theta)$ can also be evaluated by computing $M_{\alpha,\alpha+\beta+1}(\theta)$ and $M_{\alpha,\beta+1}(\theta)$. Thus, both $J_{\alpha,\beta}(\theta)$ and $M_{\alpha,\beta}(\theta)$ approximations are now known and can be easily computed based on the aforementioned reccurence relations. Also, having obtained these approximations the functions $\mathcal{I}(\tilde{g}(\theta))$ and $\mathcal{Q}(\tilde{g}(\theta))$ can be easily computed as well.

We can now check the validity of these approximations by comparing them against numerical integration results of $J_{\alpha,\beta}(\theta)$, $M_{\alpha,\beta}(\theta)$, $\mathcal{I}(g(\theta))$, and $\mathcal{Q}(\tilde{g}(\theta))$. Figure 26 shows the comparison of the approximated and numerically integrated values of $J_{\alpha,\beta}(\theta)$ and $\mathcal{I}(\tilde{g})$. Figure 26(a) compares the approximated and numerically integrated values of $J_{\alpha,\beta}(\theta)$ for the specific parameter values of $\alpha = \beta = 3/2$ (corresponding to Kuwabara-Kono model), and the relative errors for the same is shown in Fig. 26(b). The integral $\mathcal{I}(\tilde{g}(\theta))$ based on the

computation of $J_{\alpha,\beta}(\theta)$ is shown in Fig. 26(c), and their relative errors shown in Fig. 26(d). Lastly, Fig. 26(e) and Fig. 26(d) are showing the maximum relative error of $J_{\alpha,\beta}(\theta)$ and $\mathcal{I}(\tilde{g}(\theta))$ within $\theta \in [0,1]$, for all values of $\beta \in [0,4]$, while keeping α fixed. We note that the maximum value of the relative errors is in the order of 10^{-4} for both $J_{\alpha,\beta}(\theta)$ and $\mathcal{I}(\tilde{g}(\theta))$.

Similarly, Fig. 27 compares the approximated and the numerically integrated results of $M_{\alpha,\beta}(\theta)$ and $\mathcal{Q}(\tilde{g}(\theta))$. Figure 27(a) and Fig. 27(b) show the result comparisons of $M_{\alpha,\beta}(\theta)$ for the Kuwabara-Kono model ($\alpha = \beta = 3/2$). Figure 27(c) and Fig. 27(d) compares the approximated and numerically integrated results of $\mathcal{Q}(\tilde{g}(\theta))$. Lastly, Fig.27(e) and Fig.27(f) show the maximum relative errors of $M_{\alpha,\beta}(\theta)$ and $\mathcal{I}(\tilde{g}(\theta))$, as β is varied in the range $\beta \in [0,4]$. The maximum relative error in these computation is in the order of 10^{-3}. Therefore, we can conclude that the approximations are in good agreement with numerical integration computation results. Hence, we can expect to see good analytical CoR approximation results, if we use the $J_{\alpha,\beta}(\theta)$ and $M_{\alpha,\beta}(\theta)$ integral approximations that we have derived in this section.

D Comparison with known analytical solutions for specific values of α and β

In this final appendix, we will study how well the $\mathcal{O}(\gamma^2)$ CoR approximation presented in this work performs in comparison to known analytical solutions of e for specifice values of α and β. Two of the known solutions of e correspond to the *Linear Spring Dashpot* ($\alpha = \beta = 1$) and the *Tsuji-Tanaka-Ishida* ($\alpha = 3/2$ and $\beta = 5/4$). In both cases the solution is known exactly only when $\tilde{g} = 0$. Nevertheless, in the case of the *Linear Spring Dashpot* with $\tilde{g} \neq 0$, one can use a mixed approach by combining and numerical root-finding approach to obtain e accurate to arbitrary precision. Next, we will derive this (partially) analytical solution for the *Linear Spring Dashpot* model to compare with the predictions from the $\mathcal{O}(\gamma^2)$ CoR approximation presented in Proposition 2.

D.1 Liner Spring-Dashpot Model, $\alpha = \beta = 1$

We consider the scaled dynamics given in (2) with $\alpha = \beta = 1$,

$$\frac{d^2u}{d\tau^2} + \gamma \frac{d}{d\tau}(u_+) + u_+ = \tilde{g}; \qquad u(0) = 0 \ \text{ and } \ u'(0) = 1 \tag{109}$$

The linear non-homogeneous linear ordinary differential equation that governs the dynamics can be solved exactly to yield solutions for the displacement $u(\tau)$ and velocity $u'(\tau)$ (assuming an underdamped response, $0 \leq \gamma \leq 2$),

$$\begin{aligned} u(\tau) &= -\tilde{g}e^{-\xi\tau}\cos(\omega_n\tau) + \left(\tfrac{1-\xi\tilde{g}}{\omega_n}\right)e^{-\xi\tau} + \tilde{g} \\ u'(\tau) &= e^{-\xi\tau}\cos(\omega_n\tau) + \left[\omega_n\tilde{g} - \tfrac{\xi(1-\xi\tilde{g})}{\omega_n}\right]e^{-\xi\tau}\sin(\omega_n\tau) \end{aligned} \tag{110}$$

where,

$$\xi = \tfrac{\gamma}{2} \qquad \text{and} \quad \omega_n = \tfrac{\sqrt{4-\gamma^2}}{2},$$

The CoR e, based on the linear scaled spring-dashpot dynamics from (109) is given by,

$$e = -\frac{u'(T_f)}{u'(0)} = -u'(T_f) \tag{111}$$

where T_f is the final time of impact. The impact ends when $u(\tau = T_f) = 0$, after compression. If there is no external load on the system, $\tilde{g} = 0$, the solutions for the scaled displacement $u(\tau)|_{\tilde{g}=0} \equiv u_{lh}(\tau)$, and velocity $u'(\tau)|_{\tilde{g}=0} \equiv u'_{lh}(\tau)$, are given by,

$$\begin{aligned} u_{lh}(\tau) &= \tfrac{1}{\omega_n}e^{-\xi\tau}\sin(\omega_n\tau) \\ u'_{lh}(\tau) &= e^{-\xi\tau}\cos(\omega_n\tau) - \tfrac{\xi}{\omega_n}e^{-\xi\tau}\sin(\omega_n\tau) \end{aligned} \tag{112}$$

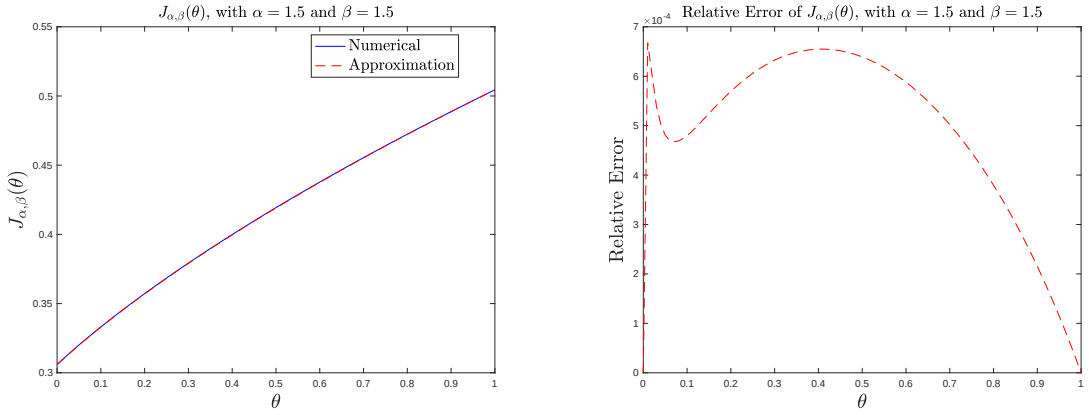

(a)

(b)

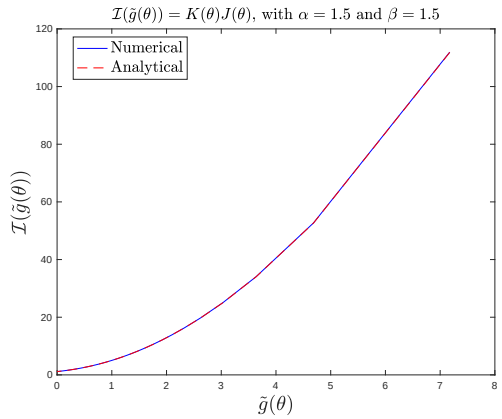

(c)

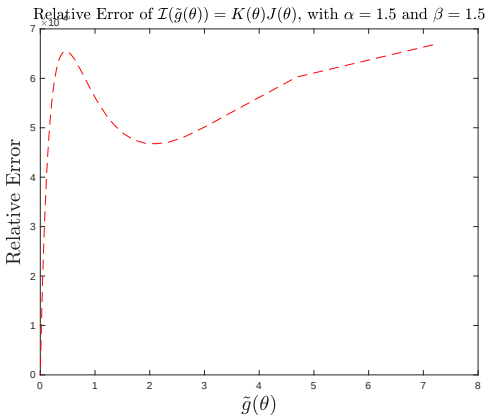

(d)

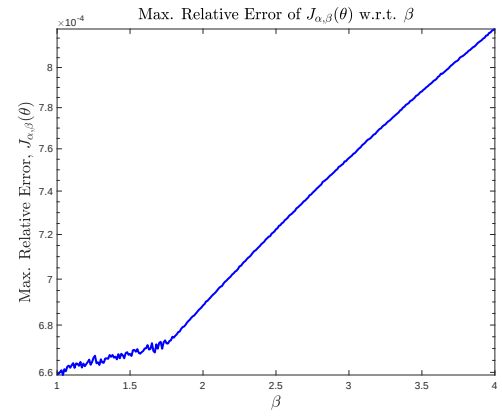

(e)

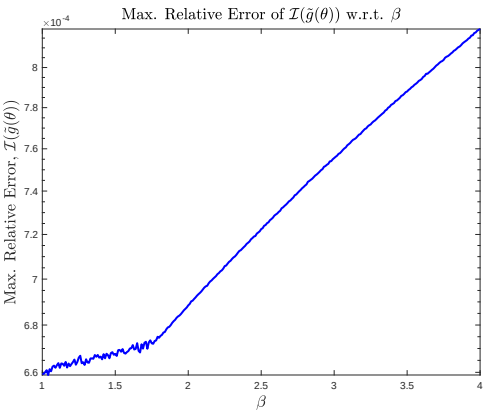

(f)

Figure 26: (a) Comparison between numerical and analytical approximation of $J_{\alpha,\beta}(\theta)$ when, $\alpha = \beta = 3/2$, (b) Relative error of $J_{\alpha,\beta}(\theta)$ approximation when, $\alpha = \beta = 3/2$, (c) Comparison between numerical and analytical approximation of $\mathcal{I}(\tilde{g}(\theta))$, when $\alpha = \beta = 3/2$, (d) Relative error of $\mathcal{I}(\tilde{g}(\theta))$ $\alpha = \beta = 3/2$, (e) Maximum relative error of $J_{\alpha,\beta}(\theta)$ approximation for $\alpha = 3/2$ & $\beta \in [1, 4]$, and (f) Maximum relative error of $\mathcal{I}(\tilde{g}(\theta))$ approximation for $\alpha = 3/2$ & $\beta \in [1, 4]$

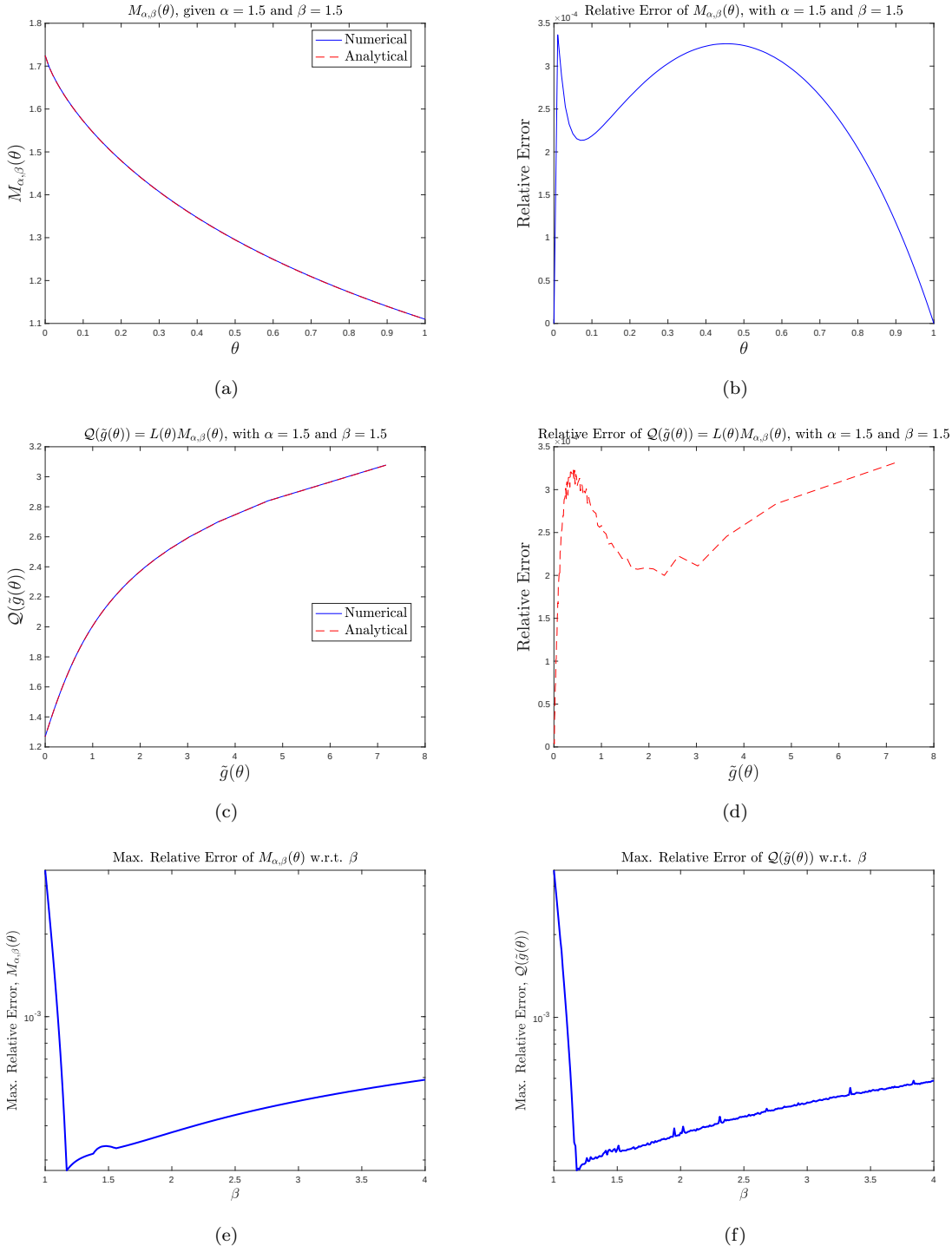

Figure 27: (a) Comparison between numerical and analytical approximation of $M_{\alpha,\beta}(\theta)$ when, $\alpha = \beta = 3/2$, (b) Relative error of $M_{\alpha,\beta}(\theta)$ approximation when, $\alpha = \beta = 3/2$, (c) Comparison between numerical and analytical approximation of $\mathcal{Q}(\tilde{g}(\theta))$, when $\alpha = \beta = 3/2$, (d) Relative error of $\mathcal{Q}(\tilde{g}(\theta))$ $\alpha = \beta = 3/2$, (e) Maximum relative error of $M_{\alpha,\beta}(\theta)$ approximation for $\alpha = 3/2$ & $\beta \in [1, 4]$, and (f) Maximum relative error of $\mathcal{Q}(\tilde{g}(\theta))$ approximation for $\alpha = 3/2$ & $\beta \in [1, 4]$

The time of collision T_f, for the case when $\tilde{g} = 0$, such that $u_{lh}(\tau = T_f) = 0$, can be explicitly calculated as $T_f = \frac{\pi}{\omega_n}$, which also yields the explicit solution for the CoR given by,

$$e = \exp\left(\frac{-\xi\pi}{\omega_n}\right) \tag{113}$$

When $\tilde{g} \neq 0$, the final time of impact T_f, cannot be explicitly solved for using $u(\tau = T_f) = 0$, from (110). Instead, we may proceed by first an approximate value of T_f that is close to the true solution of $u(\tau) = 0$, and then use this approximate value as initial guess for Newton's method to obtain a more accurate value of T_f. The approximate value of T_f close to the solution of $u(\tau) = 0$ can be found by using the symmetric property of the first half-period of the non-dissipative $u(\tau)$ response (γ). The symmetric center of the first half-period, in case of a non-dissipative impact, is at the maximum displacement. The time τ at the maximum displacement can be found by obtaining the stationary points in the response of $u(\tau)$. The set of stationary points τ_{sk} with $k \in \mathbb{Z}$, can be solved for by setting $u'(\tau_{sk}) = 0$,

$$\begin{aligned}
u'(\tau_{sk}) = 0 &= e^{-\xi\tau_{sk}}\cos(\omega_n\tau_{sk}) + \left(\tfrac{\omega_n^2\tilde{g}-\xi(1-\xi\tilde{g})}{\omega_n}\right)e^{-\xi\tau_{sk}}\sin(\omega_n\tau_{sk}) \\
\implies \quad 0 &= e^{-\xi\tau_{sk}}\left(\tfrac{\omega_n^2+(\xi(1-\xi\tilde{g}))^2}{\omega_n}\right)\cos\left(\omega_n\tau_{sk} - \tan^{-1}\left(\tfrac{\omega_n^2\tilde{g}-\xi(1-\xi\tilde{g})}{\omega_n}\right)\right) \\
\implies \quad \tau_{sk} &= \tfrac{1}{\omega_n}\left[\tan^{-1}\left(\tfrac{\omega_n^2\tilde{g}-\xi(1-\xi\tilde{g})}{\omega_n}\right) + \tfrac{2k+1}{2}\pi\right], \text{ for } k \in \mathbb{Z}
\end{aligned} \tag{114}$$

The maximum displacement within the first half-period of the $u(\tau)$ response takes place at $k = 0$, so the time corresponding to the maximum displacement in the first half-period is τ_{s0}. Similarly, the stationary point in the second half-period (trough), is τ_{s1}. The stationary point within the second half-period is important as it could help us determine whether the impact will result in detachment ($0 < e \leq 1$) or sticking ($e = 0$). We can use the criteria,

$$\begin{cases} \text{if} \quad u(\tau_{s1}) < 0 \quad e = -u'(T_f) \quad \text{(Detachment)} \\ \\ \text{if} \quad u(\tau_{s1}) \geq 0 \qquad e = 0 \qquad\quad \text{(Sticking)} \end{cases} \tag{115}$$

to determine if the impact will result in detachment. Lastly, we need the impact time T_f to calculate the CoR, when there is detachment. Since, the first half-period is approximately symmetric about the maximum deformation, when γ is small, the final impact time can be approximated as $T_f \approx 2\tau_{s0}$. Nevertheless, this approximation becomes very inaccurate as γ becomes large. Thus we use Newton's method to obtain better approximation,

$${T_f}^{i+1} = {T_f}^{i} - \frac{u\left({T_f}^{i}\right)}{u'\left({T_f}^{i}\right)} \quad \text{with,} \quad {T_f}^{0} = 2\tau_{s0} \tag{116}$$

where ${T_f}^{i}$ is the value of T_f at an iteration i. Therefore, by combining Newton's method and the analytical solution of $u'(\tau)$ given in (110) , one can obtain the value of e to an arbitrary precision.

Thus, now we can study the $O(\gamma^2)$ CoR approximation in reference to the aforementioned analytical solution of e for the *Linear Spring Dashpot* model. Figure 28 compares the two $\mathcal{O}(\gamma^2)$ approximations and the numerically integrated CoR values to the analytical solution when $\alpha = 1$ and $\beta = 1$. Figures 28(a), 28(b), 28(c), and 28(d) show the results corresponding to $\tilde{g}$ = 0,0.05,1, and 10. In these examples, the known analytical solution of the *Linear Spring Dashpot* model is treated as the reference, while the numerically integrated results are just included for completeness. Hence, the corresponding absolute errors shown in Fig. 29, are calculated with respect to the analytical solutions. We can see from these figures that the $\mathcal{O}(\gamma^2)$ approximations agrees very well with the known analytical solution for small and large $\tilde{g}$, while being slightly inaccurate for intermediate $\tilde{g}$ when γ value is high. Similar to what we have observed for other cases, the $\mathcal{O}(\gamma^2)$ approximation is less accurate for high γ and intermediate values of $\tilde{g}$. As discussed earlier, this is a consequence of the expansion of e around $\gamma \approx 0$ that was used to obtain the $\mathcal{O}(\gamma^2)$ approximation in (36). Nevertheless as we can see, in this case magnitudes of these errors are very small.

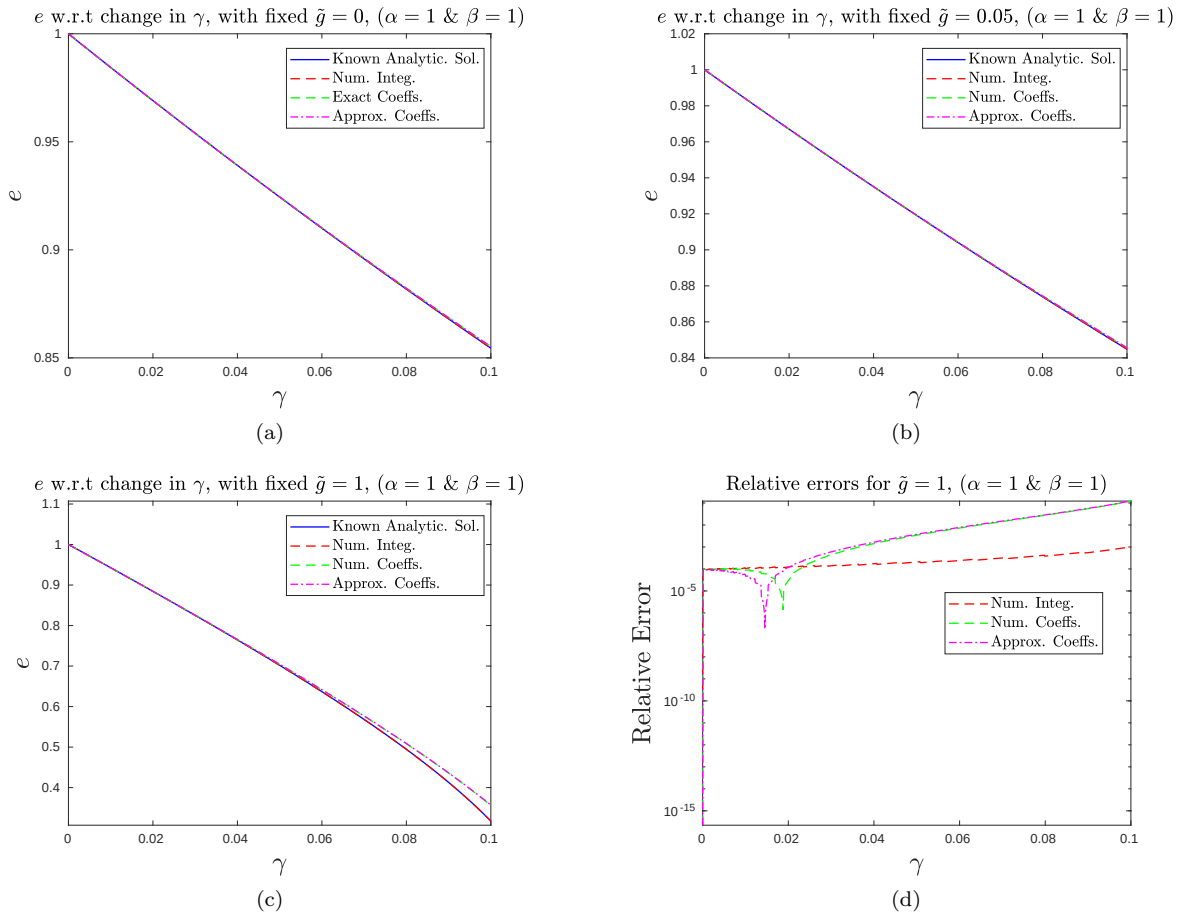

Figure 28: Comparison between the CoR values computed based on the known analytical solution for $\alpha = \beta = 1$ (*Linear Spring-Dashpot model*) given in (110), and the $\mathcal{O}(\gamma^2)$ approximations given by (36), using the numerically integrated functions $\mathcal{I}(\tilde{g})$ and $\mathcal{Q}(\tilde{g})$ from (41) and (42), and the approximated functions $\mathcal{I}(\tilde{g}(\theta)) = K(\theta)J_{\alpha,\beta}(\theta)$ and $\mathcal{Q}(\tilde{g}(\theta)) = L(\theta)M_{\alpha,\beta}(\theta)$ using (48) and (49). Results are shown for the cases: (a) $\tilde{g} = 0$, (b) $\tilde{g} = 0.05$, (c) $\tilde{g} = 1$, and (d) $\tilde{g} = 10$. The CoR results computed via numerical integration of (4) are also included for completeness.

D.2 Antypov-Elliott Solution for $\alpha = 3/2$ & $\beta = 5/4$

Another known analytical solution that exists in the literature, is for the case when $\alpha = 3/2$ & $\beta = 5/4$, which corresponds to the *Tsuji-Tanaka-Ishida* model [9]. Antypov and Elliott presented a mapping between the displacement solutions of *Tsuji-Tanaka-Ishida* model ($\alpha = 3/2$ & $\beta = 5/4$) [39] and *Linear Spring-Dashpot* model ($\alpha = \beta = 1$). However, this mapping is only valid for systems with no external load, which means $\tilde{g} = 0$. The mapping presented by Antypov and Elliot in [39], substitute the displacement δ into the equation of motion, by a function $\delta = Ax^n$. They find that by choosing the parameter values $A = (5/4)^{2/5}$ and $n = 4/5$, the equivalent phase-space equation becomes identical to the differential equation corresponding to linear spring-damper model, with no external load. This leads to a mapping of the solutions with the solutions of a linear-spring damper solution,

$$u(\tau) = \left(\tfrac{5}{4}\right)^{2/5}(u_{lh}(\tau))^{4/5} \qquad \text{and} \quad u'(\tau) = u_{lh}(\tau) \tag{117}$$

where, $u(\tau)$ and $u'(\tau)$ are solutions to the displacement and velocity for the model corresponding to the parameter values $\alpha = 3/2$, $\beta = 5/4$, and $\tilde{g} = 0$, whereas $u_{lh}(\tau)$ and $u'_{lh}(\tau)$ are the velocity solutions for linear spring-damper model, with the parameter values $\alpha = \beta = 1$ and $\tilde{g} = 0$. It can be readily seen from

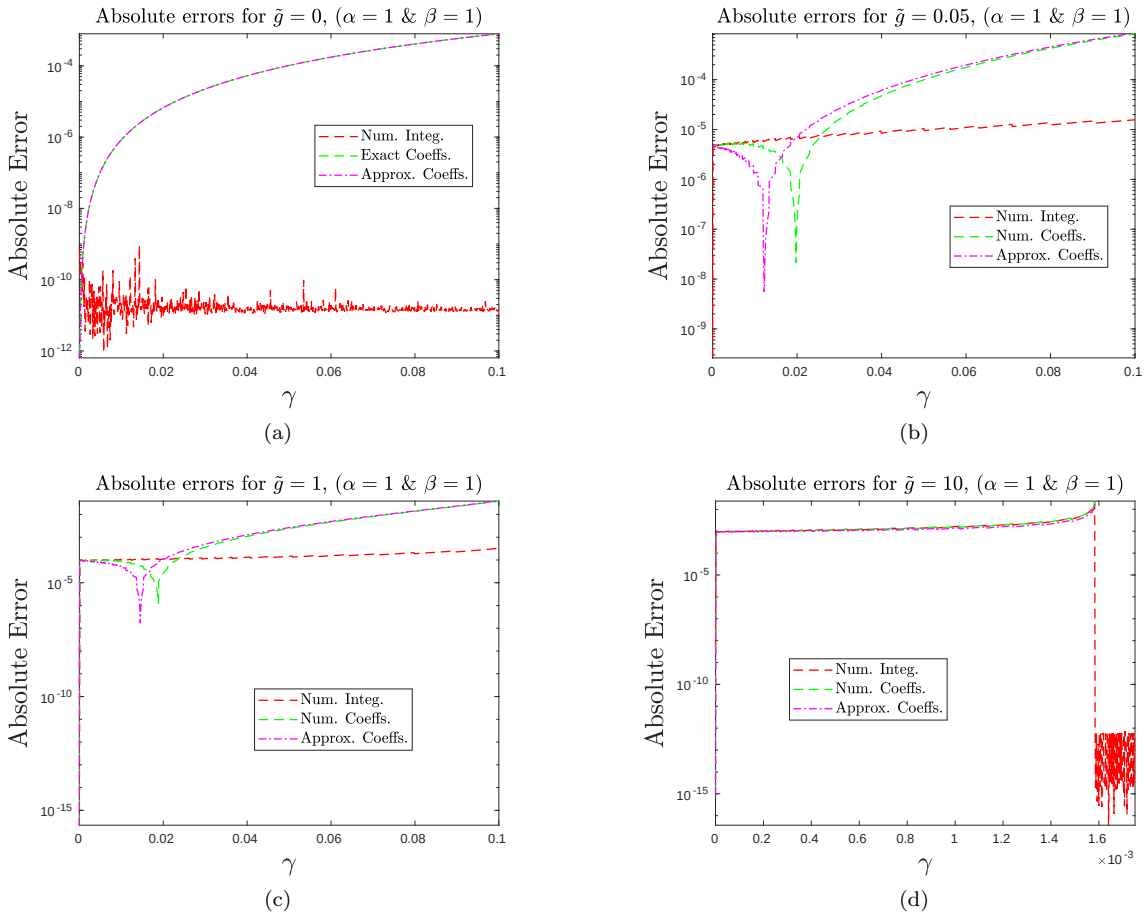

Figure 29: Absolute errors of the $\mathcal{O}(\gamma^2)$ CoR approximations (36), for the case $\alpha = \beta = 1$ (*Linear Spring-Dashpot model*), based on the numerically integrated functions $\mathcal{I}(\tilde{g})$ and $\mathcal{Q}(\tilde{g})$ from (41) and (42), and the approximated functions $\mathcal{I}(\tilde{g}(\theta)) = K(\theta)J_{\alpha,\beta}(\theta)$ and $\mathcal{Q}(\tilde{g}(\theta)) = L(\theta)M_{\alpha,\beta}(\theta)$ from (48) and (49). The absolute errors are computed in reference to the CoR values obtained based on the known analytical solution for the *Linear Spring-Dashpot model* in (110).Results are shown for the cases: (a) $\tilde{g} = 0$, (b) $\tilde{g} = 0.05$, (c)$\tilde{g} = 1$, and (d) $\tilde{g} = 10$. The absolute errors of the numerically integrated CoR results are also shown for completeness.

the mapping in (117), that the root for $u(\tau) = 0$, which gives the value of impact time T_f, is identical to the roots of $u_{lh}(\tau)$. Therefore, the time of impact is given by $T_f = \frac{\pi}{\omega_n}$, and the coefficient of restitution is identical to linear spring-damper model, i.e., $e = \exp(-\xi\pi/\omega_n)$.

Since, the mapping presented by Antypov and Elliott [39] is only valid for $\tilde{g} = 0$, we can only compare the results of the $\mathcal{O}(\gamma^2)$ approximation from (36) with the anlytical solution from (117), for the same case. Figure 30(a) compares the two $\mathcal{O}(\gamma^2)$ approximation (with numerically integrated and approximate analytical coefficients) with the analytical solution using the mapping (117). It also includes a plot corresponding to the numerically integrated value of e. Once again here, the errors assosciated with these results are computed in reference to the known exact analytical solution based on (117). These are presented in Fig. 30(b). As we have seen before, the $\mathcal{O}(\gamma^2)$ CoR approximation tends to be very accurate when $\tilde{g} = 0$, and based on Fig. 30 we can confirm that the same is true for *Tsuji-Tanaka-Ishida* model with $\tilde{g}$ when the $\mathcal{O}(\gamma^2)$ approximations are compared against the exact known analytical solution based on [39].

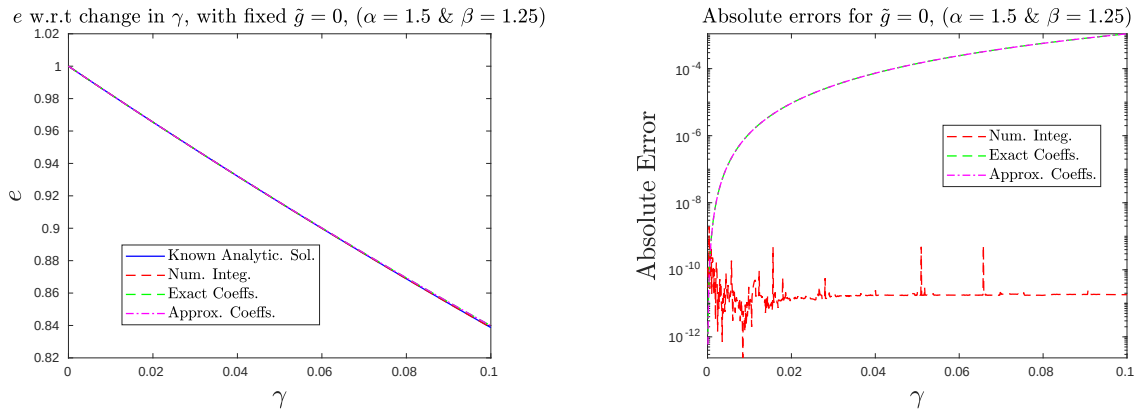

(a) (b)

Figure 30: (a) Comparison of the $\mathcal{O}(\gamma^2)$ CoR approximations for the case $\alpha = 3/2$, $\beta = 5/4$ (*Tsuji-Tanaka-Ishida model*), and $\tilde{g} = 0$ (non-dissipitive impact), with respect to the Antypov-Elliott [39] based analytical solution (117). (b) The corresponding absolute errors with respect to the Antypov-Elliott [39] based analytical solution (117).

References

[1] W. Goldsmith, *Impact: The Theory and Physical Behavior of Colliding Solids*. London: E. Arnold Publishers, 1960.

[2] E. J. Routh, *An Elementary Treatise on the Dynamics of a System of Rigid Bodies*. London: Macmillan, 1877.

[3] G. Darboux, "Mémoire sur la théorie algébrique des forces quadratiques.," *Journal de Mathématiques Pures et Appliquées*, vol. 19, pp. 347–396, 1874.

[4] G. Darboux, "Etude géométrique sur les percussions et le choc des corps," *Bulletin des Sciences Mathématiques et Astronomiques*, vol. 4, no. 1, pp. 126–160, 1880.

[5] B. Brogliato, *Nonsmooth Mechanics. Models, Dynamics and Control*. Switzerland: Springer Int. Pub., 3rd ed., 2016.

[6] N. S. Nguyen and B. Brogliato, *Multiple Impacts in Dissipative Granular Chains*, vol. 72 of *Lecture Notes in Applied and Computational Mechanics*. Berlin Heidelberg: Springer-Verlag, 2014.

[7] J. Alves, N. Peixinho, M. T. da Silva, P. Flores, and H.M.Lankaranic, "A comparative study of the viscoelastic constitutive models for frictionless contact interfaces in solids," *Mechanism and Machine Theory*, vol. 85, pp. 172–188, 2015.

[8] E. Corral, R. G. Moreno, M. G. García, and C. Castejón, "Nonlinear phenomena of contact in multibody systems dynamics: a review.," *Nonlinear Dynamics*, vol. 104, pp. 1269–1295, 2021.

[9] Y. Tsuji, T. Tanaka, and T. Ishida, "Lagrangian numerical simulation of plug flow of cohesionless particles in a horizontal pipe," *Powder Technology*, vol. 71, no. 3, pp. 239–250, 1992.

[10] A. Crook, "A study of some impacts between metal bodies by a piezoelectric method," *Proc. Royal. Soc. A. Math. Phys. Eng. Sci.*, vol. 212, no. 1110, pp. 377–390, 1952.

[11] A. Džiugys and B. Peters, "An approach to simulate the motion of spherical and non-spherical fuel particles in combustion chambers," *Granular Matter*, vol. 3, no. 4, pp. 231–266, 2001.

[12] S. Antonyuk, S. Heinrich, J. Tomas, N. G. Deen, M. S. Van Buijtenen, and J. Kuipers, "Energy absorption during compression and impact of dry elastic-plastic spherical granules," *Granular Matter*, vol. 12, no. 1, pp. 15–47, 2010.

[13] K. L. Johnson, *Contact Mechanics*. Cambridge: Cambridge University Press, 1985.

[14] M. Brake, "An analytical elastic-plastic contact model with strain hardening and frictional effects for normal and oblique impacts," *Int. J. Solids Struct.*, vol. 62, pp. 104–123, 2015.

[15] X. Xiong, R. Kikuuwe, and M. Yamamoto, "A multiscale friction model described by continuous differential equations," *Tribol. Letters*, vol. 51, pp. 513–523, 2013.

[16] J. Bastien and C. Lamarque, "Persoz' gephyroidal model model described by a maximal monotone differential inclusion," *Arch. Appl. Mechanics*, vol. 78, no. 5, pp. 393–407, 2008.

[17] J. Bastien, G. Michon, L. Manin, and R. Dufour, "An analysis of the modified Dahl and Masing models: application to a belt tensioner," *Journal of Sound and Vibration*, vol. 302, pp. 841–864, 2007.

[18] D. Maugis, *Contact, Adhesion and Rupture of Elastic Solids*. Solid-State Sciences, Heidelberg: Springer, 2000.

[19] W. Stronge, "Rigid body collision with friction," *Proc. Royal Soc. Lond. A*, vol. 431, no. 1881, pp. 169–181, 1990.

[20] W. Stronge, "Friction in collisions: Resolution of a paradox," *J. Applied Phys.*, vol. 69, no. 2, pp. 610–612, 1991.

[21] W. Stronge, "Smooth dynamics of oblique impacts with friction," *Int. J. Impact Eng.*, vol. 51, pp. 36–49, 2013.

[22] W. Stronge, "Energetically consistent calculations for oblique impacts in unbalanced systems with friction," *ASME J. Applied Mechanics*, vol. 82, no. 8, p. 081003, 2015.

[23] R. Simon, "The development of a mathematical tool for evaluating golf club performance," *Proceedings of ASME Design Engineering Congress, New York City, USA*, 1967.

[24] K. Hunt and F. Crossley, "Coefficient of restitution interpreted as damping in vibro-impact," *ASME Journal of Applied Mechanics*, vol. 42, no. 2, pp. 440–445, 1975.

[25] G. Kuwabara and K. Kono, "Restitution in a collision between two spheres," *Japan. J. Appl. Phys.*, vol. 26, no. 8, pp. 1230–1233, 1987.

[26] P. Shi, "The restitution coefficient for a linear elastic rod," *Mathematical and Computer Modelling*, vol. 28, no. 4-8, pp. 427–435, 1998.

[27] Y. Shen, D. Xiang, X. Wang, L. Jiang, and Y. Wei, "A contact force model considering constant external forces for impact analysis in multibody dynamics," *Multibody System Dynamics*, vol. 44, no. 4, pp. 397–419, 2018.

[28] A. Carvalho and J. Martins, "Exact restitution and generalizations for the Hunt-Crossley contact model," *Mechanism and Machine Theory*, vol. 139, pp. 174–194, 2019.

[29] P. Müller and T. Pöschel, "Collision of viscoelastic spheres: compact expressions for the coefficient of normal restitution," *Physical Review E*, vol. 84, no. 2, 2011.

[30] R. Ramirez, T. Pöschel, N. Brilliantov, and T. Schwager, "Coefficient of restitution of colliding viscoelastic spheres," *Physical Review E*, vol. 60, no. 4, pp. 4465–4472, 1999.

[31] T. Schwager and T. Pöschel, "Coefficient of restitution for viscoelastic spheres: The effect of delayed recovery," *Physical Review E*, vol. 78, no. 5, p. 051304, 2008.

[32] N. Brilliantov, F. Spahn, J. Hertzsch, and T. Pöschel, "The collision of particles in granular systems," *Phys. A*, vol. 231, pp. 417–424, 1996.

[33] N. Brilliantov, F. Spahn, J. Hertzsch, and T. Pöschel, "Model for collisions in granular gases," *Physical Review E*, vol. 53, no. 5, pp. 5382–5392, 1996.

[34] N. Brilliantov, A. Pimenova, and D. Goldobin, "A dissipative force between colliding viscoelastic bodies: Rigorous approach," *EPL (Europhysics Letters)*, vol. 109, no. 1, 2015.

[35] G. James, K. Vorotnikov, and B. Brogliato, "Kuwabara-Kono numerical dissipation: a new method to simulate granular matter," *IMA Journal of Applied Mathematics*, vol. 85, no. 1, pp. 27–66, 2020.

[36] G. James, "Traveling fronts in dissipative granular chains and nonlinear lattices," *Nonlinearity*, vol. 34, no. 3, p. 1758, 2021.

[37] Z. Zhao, C. Liu, and B. Brogliato, "Energy dissipation and dispersion effects in granular media," *Physical Review E*, vol. 78, no. 3, p. 031307, 2008.

[38] A. Chatterjee, G. James, and B. Brogliato, "Approx-viscoelastic-cor." `https://github.com/ChattAbhi/Approx-ViscoElastic-CoR.git/`, 2021.

[39] D. Antypov and J. Elliott, "On an analytical solution for the damped Hertzian spring," *EPL (Europhysics Letters)*, vol. 94, no. 5, p. 50004, 2011.